Single-Pot Synthesis of Modified SBA-15 NiMo Based Catalysts in Fuel Hydrodesulfurization

BY

Saheed Adewale Ganiyu

A Dissertation Presented to the

DEANSHIP OF GRADUATE STUDIES

KING FAHD UNIVERSITY OF PETROLEUM & MINERALS

DHAHRAN, SAUDI ARABIA

In Partial Fulfillment of the

Requirements for the Degree of

DOCTOR OF PHILOSOPHY

In

CHEMISTRY

May, 2017

KING FAHD UNIVERSITY OF PETROLEUM & MINERALS

DHAHRAN- 31261, SAUDI ARABIA

DEANSHIP OF GRADUATE STUDIES

This thesis, written by **Saheed Adewale Ganiyu** under the direction of his thesis advisor and approved by his thesis committee, has been presented and accepted by the Dean of Graduate Studies, in partial fulfillment of the requirements for the degree of **DOCTOR OF PHILOSOPHY IN CHEMISTRY.**

Dr. Khalid R. Alhooshani
(Advisor)

28/5/2017

Dr. Abdulaziz A. Al-Saadi
Department Chairman

Dr. Mazen M. Khaled
(Co-Advisor)

Dr. Salam A. Zummo
Dean of Graduate Studies

عمادة الدراسات العليا
DEANSHIP OF GRADUATE STUDIES

Dr. Abdalla Abulkibash
(Member)

15/6/17

Date

Dr. Abdulaziz A. Al-Saadi
(Member)

Dr. Basheer Chanbasha
(Member)

Dedication

This thesis is dedicated to loving memory of my late father and the entire family.

ACKNOWLEDGMENTS

All praises and adorations belong to Allah, the Supreme Being, one without the beginning or the end. My prayers, sacrifices, living and the end are to him alone. He (Allah) has thought mankind what he knows not, and Allah is my source of guidance.

My unquantifiable gratitude goes to my advisor, Dr. Khalid R. Alhooshani, whom Allah has used for being there throughout my course of study in KFUPM and his unrelented efforts to support my thesis in all ramifications. In the same vein, I would like to appreciate the supports and professional advices of my thesis committee; Dr. Mazen Khaled (Co-advisor), Dr. Abdallah Abulkibash, Dr. Abdulaziz A. Al-Saadi, and Dr. Basheer Chanbasha throughout my research work.

My inestimable appreciation to Dr. Syed Ahmed Ali of Centre for refining and petrochemicals (CRP) for his supports, technical guidance and positive contributions to my thesis work. Also, the supports and efforts from Dr. Tawfik Saleh are highly appreciated during my thesis work.

To whom much is given, much is expected. On this note, I would like to express my sincere appreciation to Director, Centre of Excellence Nanotechnology (CENT), Dr. Zain H. Yamani for immense contributions and supports to my stay in KFUPM, and for providing me a golden opportunity to conduct effective research works, since my days of research assistant (RA) in CENT to PhD. Thank you for your kind gestures. I would like to acknowledge the efforts of our Lab team, starting from our Lab Manager (Dr. Nasir Zaman, Dr. Abbas Hakeem, Dr. Qasem Drmosh, Muhammad Qamaruddin, Idris A. Bakare, M. Ahmed Ibrar, Muhammad Hassan, Anas k. Jamil, Muhammad Sanhoob, Saleh, Boss Teguh, AKki Zarin (Jiggar), Mansha, Mahmoud, Saheed Lateef, Oluwole Ajumobi, Rashid Bawah) and the senior Research Scientists (Dr. Oki Muraza, Dr. Qamar etc.) in the CENT for their cooperation and technical discussion.

I am indeed grateful and feel honored by the kind gesture of Kingdom of Saudi Arabia, through King Fahd University of Petroleum & Minerals for scholarship opportunity to pursue M.Sc. and PhD degrees.

To the Nigerian community in KFUPM, your valuable supports in different angles are recognized and acknowledged. And to my Gees Aliyu Gbadamosi (Baba Aliy), Dr. Saheed A. Popoola (Popsa), Elder Nurudeen Odewunmi, Sulaimon Amuda (Awowiya), Muyiwa Amuda, Kabir

Adebola Sadiq, Yusuf Taofeek, Hamod Adewale, Inaolaji Olalekan, your brotherhood supports always appreciated.

Lastly, I would like to appreciate the supports and efforts of my family, both the immediate and extended ones, whom Allah have used as the driving force and engine room of my life, when the going was tough. My mother, my lovely wife, son (Abdullah) and my little princesses (Ameenah and Aishah), and to all my siblings (Sekinat A. Akintayo, Rasheedah, Medinat and Taofeek O. Ganiyu (feeky), your patience and perseverance is well acknowledged.

Thank you all for being part of my success.

TABLE OF CONTENTS

LIST OF TABLES

LIST OF FIGURES

LIST OF ABBREVIATIONS

HDS:	Hydrodesulfurization
XRD:	X-ray Diffraction
TPR:	Temperature-Programmed Reduction
TPD:	Temperature-Programmed Desorption
XPS:	X-ray photoelectron spectroscopy
FESEM:	Field Emission Scanning Electron Microscopy
HRTEM:	High Resolution Transmission Electron Microscopy
DBT:	Dibenzothiophene
MDBT:	Methyldibenzothiophene
DMDBT:	Dimethyldibenzothiophene
ICP-OES:	Inductively Coupled Plasma-Optically Emission Spectroscopy
SMSI:	Strong Metal Support Interaction
SE:	Secondary Electron
BSE:	Backscattered Electron
TEOS:	Tetraethylorthosilicate

ABSTRACT

Full Name : Saheed Adewale Ganiyu

Thesis Title : [Single-Pot Synthesis of Modified SBA-15 NiMo Based Catalysts in Fuel Hydrodesulfurization]

Major Field : Chemistry

Date of Degree : May 2017

Mesoporous materials have received much attention due to high surface areas, large pore volumes and are of great interest for adsorption, sensing, and catalysis. The present work focuses on novel hydrothermal development, synthesis and characterization of heteroatoms modified SBA-15 NiMo hydrodesulfurization (HDS) catalysts. Structural and textural properties are characterized by extensive characterization techniques such as Raman, X-ray diffraction (XRD), X-ray photoelectron spectroscopy (XPS), temperature programmed techniques (TPR and TPD), Fourier transformation infrared (FTIR), X-ray fluorescence (XRF), and N_2-physiosorption. The morphology and catalysts compositions are availed by field emission scanning electron microscope (FESEM), high resolution transmission electron microscope (HRTEM) and inductively coupled plasma-optically emission spectroscopy (ICP-OES) to examine and determine the morphology, active phase distribution, metal charge and composition. The as-developed catalysts are tested and evaluated on a simulated fuel containing different organosulfur compounds (dibenzothiophene, methyldibenzothiophene, dimethyldibenzothiophene) in a batch reactor.

ملخص الرسالة

الاسم الكامل: شعيد أدولا. غينو

عنوان الرسالة: التحضير المباشر ذات الخطوة الواحدة المعتمد على إضافات مادة النيكل الموليبدينوم المحسنة لمحفز إس بي أ-15 (SBA-15) و لعملية نزع الكبريت من الوقود

التخصص: الكيمياء

تاريخ الدرجة العلمية: مايو 2017

لقد تلقت المواد ذات المسامية العالية الكثير من الاهتمام بسبب مساحة السطح العالية، وحجم المسام الكبير و التي تعد ذات أهمية كبيرة لعملية الامتزاز، والاستشعار، والحفز. و يركز العمل الحالي على الوسيلة الحديثة من التطوير الحراري، والتوليف و التوصيف الحديث المعتمد على الإضافات مادة النيكل الموليبدينوم المحسنة لمحفز إس بي أ-15 (SBA-15) و التي تم تطويرها لعملية نزع الكبريت بالهيدروجين (HDS). وتم توصيف و تمييز الخصائص الهيكلية والنسيجية بتقنيات توصيف واسعة النطاق مثل رامان، و حيود الأشعة السينية (XRD)، و التحليل الطيفي الضوئي بالأشعة السينية (XPS)، و تقنيات خواص المواد عند درجة الحرارة مختلفة (TPD &TPR)، و الأشعة تحت الحمراء (FTIR)، و الأشعة السينية (XRF)،و عملية خواص أسطح المواد (N_2- physiosorption). يتم توصيف تشكل المركبات المحفزة من قبل المجهر الإلكتروني، و المجهر النافذ وبالاقتران الطيفي للبلازما البصري (ICP-OES) لفحص وتحديد التشكل، وتحديد المواقع النشطة ومستوى الأيوني و نسبة التراكيب. يتم اختبار وتقييم المحفزات المحسنة على وقود محاكي يحتوي على مركبات مختلفة من الكبريت العضوي (dibenzothiophene, methyldibenzothiophene, dimethyldibenzothiophene) في مفاعل ثابت (Batch reactor).

Chapter 1
Introduction

1.1 Background Information

Refinery operation becomes more challenging due to increasing stringent environmental regulations, which made it imperative to produce ultra-clean low sulfur content for transportation fuels. Recently, the maximum sulfur content of 500 ppmw is to be reduced to 15 ppmw and 10 ppmw, in the US and EU respectively, while the future global goal is sulfur free for transportation fuels [1]. Industrially, catalytic hydrotreating is the major petroleum refinery technology employed to reduce the sulfur and the nitrogen content of the heavy gas oil [2]. These heavy oils contain high content of sulfur, nitrogen, metals and asphatenes that are difficult to process [3, 4]. Since the quality of these products has to be improved to satisfy stringent environmental regulations [5], many efforts are aimed at development of novel catalysts with improved selectivity and activity for catalytic hydrotreating of heavy gas oil. The catalysts used for residue hydroprocessing are sulfides of Co, Ni, W and Mo supported catalysts, which have a variety of pore structure and active metal dispersion (active sites).

γ-Al_2O_3 has been widely used as an effective support material for hydrotreating catalysts due to its good mechanical and textural properties, better dispersion for active metals, and low cost, but it suffers from strong metal support interaction (SMSI) with most of the active metals such as Mo and Ni [6]. In addition, commercial sulfided-Co(Ni)Mo(W)/alumina catalysts lack the capacity to achieve deep HDS of present fuel feedstocks, and urgent alternative to develop a novel, stable and high catalytic activities catalysts is required to deal with the present sulfur regulations. Therefore, the use of novel mesostructured materials, such as MCM-41, SBA-15 and KIT-6 as supports has different advantages in comparison with alumina [7, 8]. They possess appropriate physicochemical properties, large surface area, tunable pore size, good thermal and mechanical [8]. However, poor dispersion and hydrothermal stability of amorphous silica walls limited their industrial applications such as catalysis in petrochemicals, sensors, adsorption of heavy metals, enzymes immobilization and energy storage. To overcome these limitations, different scientific approaches have been employed to obtain significant improvements in HDS activities of silica-based catalysts. These modifications include addition of chelating agents, additives (phosphorous), incorporation of transition metals and organic functional groups [9-11]. Our main task will involve developing

hierarchical multifunctional HDS catalysts, by adopting a facile and economical approaches by incorporation of metals and/or bi-metals with or without complexing agent to achieve better activities and selective. Extensive characterization techniques will be employed on the newly developed catalysts, to study any structural, textural and chemical change. Finally, catalytic evaluation of as-developed HDS catalysts will be conducted on batch reactor with different organosulfur compounds.

1.2 Hydrodesulfurization and Classification of Sulfur in Fuel

Hydrodesulfurization (HDS) is an important aspect of hydroprocessing technology for removal of sulfur in naphtha, kerosene, diesel, and heavy crude oil, other than nitrogen, oxygen, metal contaminations via denitrogenation, deoxygenation and demetallization, respectively, with the aid of hydrogen [12]. This process is dated more than decades and usually conducted at high temperature (200-450 ^{o}C) and pressure (5-300 bar) [12]. The sulfur in fuel can be classified according to their sources; mercaptans, sulfides, disulfides, thiophene, benzothiophenes and dibenzothiophene. The acyclic, and saturated cyclic sulfur compounds can be easily desulfurized under mild conditions, while the aromatic organosulfur compounds (benzothiophenes, BT and dibenzothiophene, DBT), especially their alkylated derivates require harsh operating processing conditions to desulfurize [13].

1.3 HDS Catalysts Composition and Preparation

HDS active catalysts are usually Mo(W)S_2 promoted with transition metals Ni(Co) in bimetallic or trimetallic form such as, Ni(Co)Mo(W), Co(Ni)Mo(W), NiCoMo or NiMo-CoMo [13]. These catalysts can be unsupported or supported on different mixed oxides (Al_2O_3, TiO_2, ZrO_2), acidic supports (Zeolites and amorphous Silica-alumina) and mesoporous silicas (SBA-15, MCM-41, FDU-12, SBA-16 etc.). NEBULA® unsupported catalysts that was jointly by Akzo Nobel, Nippon Ketjen and Exxon Mobil in 2001, possessed high catalytic efficiency for deep HDS than traditional catalysts, however, its cost is a serious concern [14, 15]. Other the other hand, supported catalysts proffers some solution to cost implication of NEBULA catalysts by depositing active species on high surface area support via impregnation either in one step always referred as co-impregnation or two steps, called sequential impregnation. Also, the dispersion of active species

which are controlled by several factors such as method of impregnation, nature of support, solution concentration, pH, calcination and drying temperatures etc., is challenging.

1.4 HDS catalysts requirements

The choice of HDS catalysts as described in section 1.3 is subject to meeting certain requirements for efficient catalytic performance. For example, the surface area is an important physical characteristic that must be high enough (150- 400 m^2/g) to disperse the active species with high active sites. In addition, the pore-size distribution (PSD) and pore volume should be (7-13 nm) and less than 0.7 cm^3, respectively, for better diffusion of reactants within the pores of the catalysts [12]. Mechanical strength and thermal stability of the catalysts for attrition and abrasion is necessary to prevent pressure drop and maldistribution of active species due to structural collapse.

1.5 Research Motivation

HDS catalyst preparation is usually carried out by impregnation and coprecipitation of solution or precursor of active species onto γ-Al_2O_3 support. These approaches are disadvantageous in one way or the other. Coprecipitation as a method of catalyst preparation ensures good distribution of active phases on the support, however, strong interaction of Ni(Co)Mo(W) active species that are difficult to sulfide is prominent. Whilst impregnation approach seems to be alternative for prevention of crystalline phase during preparation stage, multiple heat treatment during drying and calcination resulted in loss of special characteristics and catalyst quality. In addition, temperature programmed reduction analysis revealed the existence of strong metal support interaction of active metals with alumina, and consequently resulted in low catalytic activity. With mesoporous silica supports, poor dispersion of active species is the major problem, while employing impregnation approach to deposit Ni(Co)Mo(W) on support surface. Therefore, there is a research gap to be filled by employing a new strategy for introduction of active species on the support.

1.6 Research Objectives

The current research trend to achieve ultradeep HDS of crude sources with high sulfur content requires highly stable, efficient and low-cost catalysts. Therefore, the use of high surface area support to maximize the dispersion of active species is inevitable. In addition, the method of

preparation to aid better dispersion and distribution of active metals compared to existing approaches is necessary. This thesis focusses on a single-pot attempt to synthesis highly dispersed active species (NiMo) on a mesoporous SBA-15 support modified with heteroatom (Ti) for efficient HDS catalytic activity. This approach will reduce multi-steps and excessive calcination and drying involved by impregnation approach, and ultimately lower the cost of catalyst preparation. The catalysts' physico-chemical properties are supported by different characterization techniques such as; X-ray diffraction (XRD), Raman spectroscopy, N_2-physisorption, temperature-programmed techniques by desorption and reduction (TPR and TPD), Fourier transform infra-red (FTIR) and FTIR-pyridine, X-ray photoelectron spectroscopy (XPS), Scanning electron microscopy (SEM), and high resolution transmission electron microscopy (HRTEM) The following objectives are studied and reported under each chapter of this thesis write-up;

Chapter 3: Single-Pot Synthesis of Ti-SBA-15-NiMo Hydrodesulfurization Catalysts: Role of Calcination Temperature on Dispersion and Activity.

Chapter 4: Hydrodesulfurization activity controlled by hydrothermal synthesis temperature and molybdenum loading of NiMo active phase supported over SBA-15.

Chapter 5: Simultaneous HDS of DBT and 4,6-DMDBT Over Single-Pot Ti-SBA-15-NiMo Catalysts: Influence of Si/Ti Ratio on the Structural Properties, Dispersion and Catalytic Activity.

Chapter 6: Dependence of HDS activity on Nickel promoter and its deposition strategy: New catalyst synthesis approach for highly efficient Ultra-HDS of fuel.

Chapter 2

Literature Reviews

2.1 Mesoporous SBA-15 Supported Hydrodesulfurization (HDS) catalysts

Hydrodesulfurization (HDS) of fuel is an important aspect of hydroprocessing technology for Clean fuel production and other applications involving catalytic converters [1]. The prevailing stringent environmental regulations, as well as the future development of sulfur-free fuel cells, have put the HDS of transportation fuels as urgent necessity amongst the industrial processes in the petroleum refining [16, 17]. The combustion of sulfur compounds in fuel gives SO_x, which is capable of causing acid rain, as well as poisoning catalysts for reducing CO_x and NO_x in automobile catalytic converters. [17, 18]. Therefore, research attention or focus has been shifted towards the synthesis of highly active and stable HDS catalyst to meet this regulation requirement. Recently, several research efforts such as changing or modifying the type or nature of support, active metals, synthesis routes and the use of organic or inorganic additives, aim to improve the HDS activities have been employed. γ-Al_2O_3 is the most popular industrial hydrotreating support, however, it strongly interacts with active phase metal (MoO_3) in a monolayered tetrahedral coordination form [19]. This interaction leads to resistance towards active phase reduction, which in turn lowers the activities during operation as compared to Mo in octahedral geometry [19]. Hence, a novel catalyst support is required to deal with ever-growing stringent environmental regulation. Recently, modified class of mesoporous supports such as silicas, zeolites, carbon, titania, and mixed metal-oxides have been reported as alternatives to alumina support for HDS, with significant improvement [20-25].

After the discovery of mesoporous silicas in early 90's, SBA-15 is the most studied mesoporous silica, owing to its high surface to volume ratio, high pore size, highly ordered 2D hexagonal structure, good mechanical property and thick pore wall, responsible for hydrothermal stability. It has been reported that combined micro and mesoporous materials are advantageous over exclusively microporous or mesoporous materials, for better catalytic activities. SBA-15 is a porous material with combination of micropores (0.5-3.0 nm) and mesopores (4-14 nm) of uniform hexagonal tunable mesoporous [26], as shown in **Figure 2-1** or scheme below.

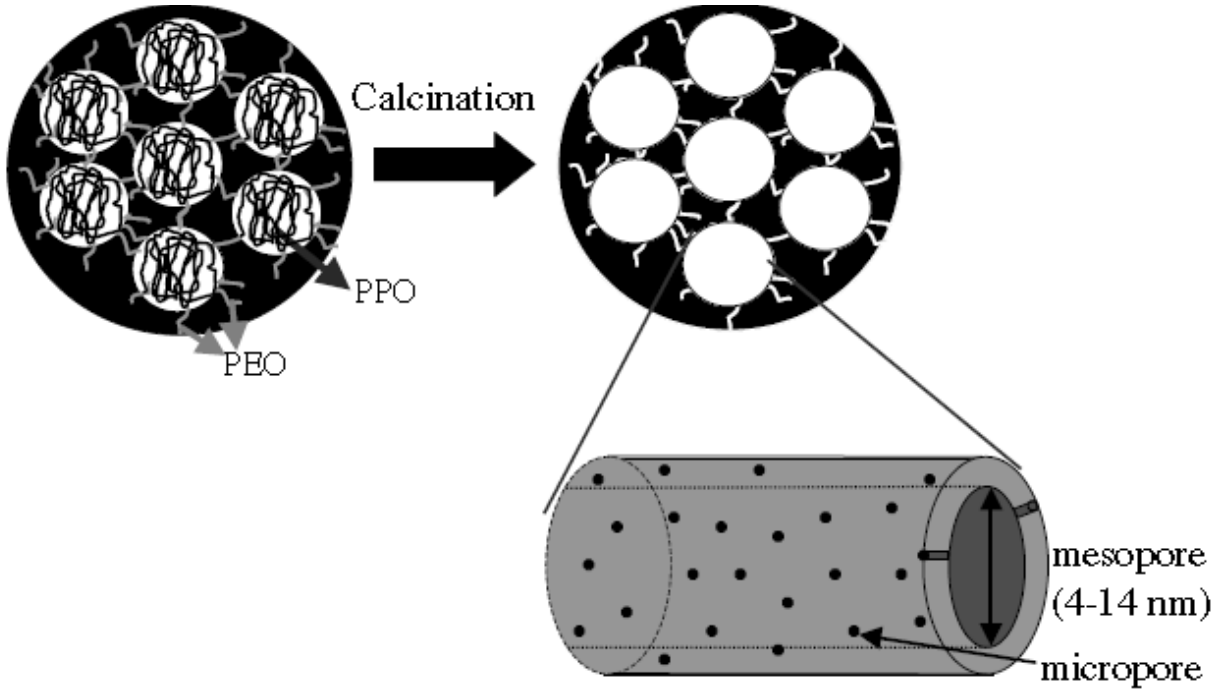

Figure 2-1 Schematic representation of SBA-15 showing micro and mesopores before and after calcination [26].

Recently, there has been tremendous increase in the use of SBA-15 as HDS supports, because of aforementioned catalytic properties possessed. However, poor dispersion of active phase(s) and hydrothermal stability, resulted from amorphous silica wall hinders the full catalytic potential of SBA-15 material. In lieu of this, different modification approaches such as incorporation of transition metals, addition of chelating agents, the use of additives, have been used to overcome this barrier. Chelating agents such as nitriloacetic acid (NTA), ethylenediaminetetraacetic acid (EDTA), cyclohexanediaminetetraacetic acid (CyDTA), citric acid (CA), have been used to improve significantly the characteristics of HDS catalysts [27-30]. Addition of chelating agents renders soluble β-$CoMoO_4$ phase by increasing the dispersion of CoMo without blockage of the active sites [31]. Synthesis routes and conditions of support are another option to improve the catalytic activity of the HDS catalysts, by improving the textural properties. Although the adoption of microwave oven in preparing mesoporous support usually takes very much lesser time than using conventional hydrothermal method, yet the additional step of magnetic stirring during the microwave treatment enhances formation of more uniform structure, and thus producing better ordered support materials [32, 33]. In fact, the formation of uniform nucleation centers followed by crystallization is promoted by the rapid and uniform heating [34]. Furthermore, incorporation of heteroatoms (Ti, Zr, and Al) and organic functional group, either by direct or post synthesis approach has been reported to improve the stability and activity of SBA-15 HDS catalyst, because of its lack of functionality [35]. Heteroatoms are Lewis acids, and can improve poor dispersion of active phase by increasing the support-metal interaction (MSI) from low to moderate. Combined effect of heteroatoms and complexing agent was recently studied by Sandeep *et. al.* In their study, direct synthesis of M-SBA-15 (Ti, Zr and Al) was used to incorporate heteroatoms on the support, followed by dispersion of active phase with the aid of EDTA via impregnation method. Better HDS activities are associated with increase in surface acidity and MSI for NiMo/Ti-SBA-15 and NiMo/Ti-SBA-15/2EDTA by 12 % and 18 %, respectively [6]. Lara *et. al*, reported the significance of complexing agents (EDTA and citric acid) with respect to HDS catalytic activity enhancement (91.6 % at 8 h of reaction) of DBT. They claimed that the use of chelating agents avoid the formation of crystalline ($CoMoO_4$) phase, and resulted in better dispersion of MoO_3, as confirmed by the XRD and HRTEM [36]. Miguel *et. al*, studied the amount of citric acid required to achieve higher activity and selectivity of NiMo/SBA-15 in deep HDS. Their result showed that addition of citric acid at optimum ratio of 1 (CA:Mo), resulted in increase in the degree of

sulfidation and dispersion catalytically active phase (MoS_2), which in turn improve the HDS performance of DBT and DMDBT significantly than reference NiMo/SBA-15 [4]. Having established the correlation between the concentration of Mo and Ni on the edges of sulfide particles and the catalytic HDS activities, Oliver *et. al* highlighted the influence of the nature of the support on the dispersion of non-promoted catalysts and the decoration degree of Ni on the edges of Ni-Mo-S phase [37].

In addition, the use of additives such as fluorine and phosphorus has also been reported. There are few literature reports on the use transition metals phosphides with SBA-15 as HDS catalyst with non-noble metals, in spite of their excellent activities towards HDS reaction than sulfided counterparts [38]. In addition, metal carbides SBA-15 (Mo_2C/SBA-15) has been rarely studied, and applied as commercial HDS catalysts, even though, it was claimed to possess high HDS activity [39]. Furthermore, supported noble metals are known for their excellent activities in hydrotreating processes, but their susceptibility to poisoning by sulfur, associated from strong interaction with H_2S is a major drawback [40].

Despite all aforementioned research efforts to improve the catalytic activities of SBA-15, deposition of active metals has been achieved via equilibrium adsorption, sequential and co-impregnation, mechanical mixing, sol-gel approach and grating, and there is little or no details report on the single-pot synthesis of NiMo/Ti-SBA-15 with or without complexing agent in the same reaction mixture. Therefore, the objective of the present work is to adopt a facile approach in the development of HDS catalyst via single-pot (SP) synthesis of modified mesoporous SBA-15 support and active phase(s) with or without complexing agent to promote dispersion, by conventional hydrothermal (HT) method. This approach (SP) will present new simple and easy steps in catalyst design and preparation, avoids significant loss of active surface area, affords low cost of catalyst design and incorporation of active phase within the mesoporous framework and ultimately resulted in enhanced HDS performance.

Chapter 3

Single-Pot Synthesis of Ti-SBA-15-NiMo Hydrodesulfurization Catalysts: Role of Calcination Temperature on Dispersion and Activity

ABSTRACT

A novel approach was systematically investigated for developing single-pot (SP) NiMo-supported Ti-SBA-15 catalysts for hydrodesulfurization (HDS). The technical challenge associated with the SP approach is the formation of crystalline $NiMoO_4$, and this was avoided by reducing the calcination temperature of the oxide catalyst from 550°C to 300°C to form a highly dispersed and efficient HDS catalyst. The dispersion, textural properties, surface acidity, oxide reducibility and surface chemical composition of developed catalysts were measured by XRD, Raman spectroscopy, N_2-physisorption, and temperature-programmed techniques (TPR and TPD) and X-ray photoelectron spectroscopy (XPS). Scanning electron microscopy (SEM), and transmission electron microscopy (TEM) were employed as additional characterization methods to investigate the catalysts' morphology and microstructure. Catalyst performance was evaluated in a batch autoclave reactor using a simulated feed containing 2,500 parts per million sulfur (ppm-S) (dibenzothiophene, DBT) in dodecane. The catalyst prepared by the SP approach and calcined at a lower temperature (300°C) showed significantly improved HDS activity and direct desulfurization selectivity compared to the catalyst prepared by the conventional impregnation approach. An increase in the calcination temperature to 550°C, however, resulted in a decrease in the HDS activity of the catalysts prepared by both methods. The dispersion, surface acidity, and textural properties of the catalysts prepared using the SP method combine to improve the catalytic efficiency. The use of a complexing agent to aid the dispersion of the active phase was unnecessary when the SP method was used for catalyst preparation.

3.1 Introduction

Stringent environmentally driven regulations limiting the sulfur content in transportation fuels and the development of sulfur-free fuel cells continue to challenge researchers to develop highly active and stable hydrodesulfurization (HDS) catalysts. Several research efforts toward improving HDS catalysis have been reported, such as changing or modifying the type or nature of the support, the active metals, the synthesis routes, and the use of organic or inorganic additives [16, 17].

γ-Al_2O_3 has been the most widely used support for hydrotreating catalysts, but it interacts strongly with the active phase metal (MoO_3) in a monolayered tetrahedral coordination. This interaction inhibits active phase reduction, which in turn decreases catalytic activity compared to octahedral Mo [19]. Mesoporous supports, such as silica, novel zeolites, carbon, titania, and mixed metal oxides, are reported to provide significant improvements compared to γ-Al_2O_3 [23, 41-45].

SBA-15 is one of the most studied mesoporous silica materials due to its high surface: volume ratio, high pore size, highly ordered 2D hexagonal structure, good mechanical strength, and thick pore wall, which is responsible for hydrothermal stability among other silicas. SBA-15 possesses a combination of micropores (0.5-3.0 nm) and mesopores (4-14 nm) in a uniform hexagonal tunable pore structure [26]. Recently, the use of SBA-15 as an HDS support has tremendously increased because of its catalytic properties; however, poor dispersion of the active phase(s) hindered its full catalytic potential.

To overcome this limitation, different modification approaches, such as the incorporation of transition metals, the addition of chelating agents, and the use of additives, have been reported. For example, chelating agents, such as nitriloacetic acid (NTA), ethylenediaminetetraacetic acid (EDTA), cyclohexanediaminetetraacetic acid (CyDTA), and citric acid (CA), have been shown to improve the performance of SBA-based HDS catalysts [27-30]. The addition of chelating agents renders β-$CoMoO_4$ or $NiMoO_4$ soluble by increasing the dispersion of Co or Mo without blocking active sites [31]. Moreover, the incorporation of heteroatoms (Ti, Zr, and Al) and organic functional groups, either by a direct or post-synthesis approach, have reportedly improved the stability and activity of SBA-15 HDS catalysts [35]. The heteroatoms are Lewis acids and can improve the dispersion of the active phase by increasing the metal-support interaction (MSI) from low to moderate.

Badoga et al. [6] studied the combined effect of heteroatoms and complexing agents in the direct synthesis of M-SBA-15 (Ti, Zr, and Al) followed by the dispersion of the active phase with the aid of EDTA via the impregnation method. The HDS activities for NiMo/Ti-SBA-15 and NiMo/Ti-SBA-15/2EDTA were improved by 12% and 18%, respectively, as a result of the increased surface acidity and MSI.

Pena et al. [46] reported the significance of EDTA and CA in enhancing the HDS catalytic activity (91.6% after 8 h of reaction) of DBT. They claimed that the use of chelating agents avoided the formation of a crystalline ($CoMoO_4$) phase and resulted in better dispersion of MoO_3, as confirmed by XRD and HRTEM. Valencia and Klimova [47] studied the effect of citric acid (CA) loading on the sulfided NiMo supported on SBA-15 for HDS of DBT. Their investigation revealed that increase in the amount of CA resulted in better dispersion of active metals (Ni and Mo) as confirmed by XRD and DRS, and consequently on the selectivity of the catalysts towards direct desulfurization (DDS) route. In addition, they showed that all catalysts prepared with CA have higher activity than without CA, but the increase in the amount of CA beyond (2.7) decreases the activity. By establishing the correlation between the concentration of Mo and Ni on the edges of sulfide particles and the catalytic HDS activities, Gutiérrez et al. [37] highlighted the influence of the nature of the support on the dispersion of non-promoted catalysts and the degree of Ni decoration on the edges of the Ni-Mo-S phase.

The use of additives such as fluorine and phosphorus has been reported, but non-noble metal-based HDS catalysts, such as transition metal phosphides with SBA-15 and molybdenum carbide-SBA-15, have not been extensively studied, despite their excellent HDS activities [38, 39]. However, supported noble metals are susceptible to sulfur poisoning due to the strong interaction with H_2S, which limits their use in hydrotreating processes [40]. The synthesis routes and conditions of the support, which can improve textural properties, provide alternative ways to improve the catalytic activity of HDS catalysts.

Despite research efforts to improve the catalytic activities of SBA-15, including the deposition of active metals via equilibrium adsorption, sequential and co-impregnation, mechanical mixing, sol-gel approach, and grafting, there are no extensive literature reports on the single-pot synthesis of Ti-SBA-15-NiMo with or without a complexing agent in the same mixture for the HDS reaction.

Therefore, the present work adopts a facile approach in the development of an HDS catalyst via the single-pot (SP) synthesis of a modified mesoporous SBA-15 support and active phase(s) with or without a complexing agent by the hydrothermal (HT) method. The SP approach presents new, simple, and easy steps in catalyst design and preparation, which allows low-cost catalyst design and active phase incorporation within the mesoporous framework. In addition, effect of calcination temperature was studied as a function of catalysts dispersion and activity, and catalysts were characterized by X-ray diffraction (XRD), N_2- physisorption, Raman spectroscopy, Fourier transform Infra-red (FTIR), temperature programmed analysis by desorption and reduction (TPD and TPR), scanning and transmission electron microscope (SEM and TEM), and X-ray photoelectron spectroscopy (XPS).

3.2 Experimental Section

3.2.1 Materials

Tetraethylorthosilicate (TEOS) $(C_2H_5O)_4Si$ as the silica source, pluronic P123 PEO_{20}-PPO_{70}-PEO_{20} triblock copolymer as the structural directing agent, nickel nitrate hexahydrate (99%) as the nickel precursor, titanium isopropoxide (97%) as the titanium source, citric acid (99.7%), dibenzothiophene (DBT) (98%), and dodecane were purchased from Sigma-Aldrich. Ammonium molybdate (VI) tetrahydrate (99%) was obtained from ACROS organics. High-purity deionized water (18 μS/cm) was produced in-house using *Thermo Scientific Barnstead NANOPURE* after distillation with a *Labstrong FiSTREEM^{TM} II 2S Glass Still* distiller.

3.2.2 Synthesis of SBA-15 and Titanium-Modified SBA-15 Support

Mesoporous SBA-15 and Ti-SBA-15 (Si/Ti = 10) were prepared using procedures described by Zhao et al. [48] via the hydrothermal (HT) synthesis method. Typically, SBA-15 was prepared from a reaction mixture of 60 g of 2 M HCl, 4.16 g of TEOS, 2 g of P123, and 15 g of deionized water stirred at 500 rpm for 24 h at 40°C. The mixture was transferred into a Teflon-lined autoclave and then heated for 24 h according to the HT method at 100 ^{o}C. The synthesized SBA-15 was calcined at 550°C for 6 h (ramp rate of 10°C/min) for template removal. For Ti-SBA-15, the same procedure was followed but with the incorporation of an equivalent amount of titanium isopropoxide to the mixture after stirring the TEOS-surfactant mixture for 90 min.

3.2.3 Single-Pot (SP) Synthesis of Ti-SBA-15-NiMo Catalyst

The single-pot (SP) synthesis of HDS catalyst was accomplished by modifying the sol-gel preparation route for SBA-15, as illustrated in Figure 3-1. This method involves the addition of approximately 4.16 g TEOS to a mixture containing a well-dispersed 2 g (P123) in 60 g of 2 M HCl and 15 g of deionized water, which was stirred for 30 min. The titanium precursor in a 10:1 (Si:Ti) molar ratio was added before the hydrolysis of TEOS and stirred continuously for 20 h. A mixture of the Mo and Ni (13 wt. % and 3 wt. %, respectively) precursors without or with citric acid (CA:Mo ratio of (1:1)) [4], which were previously mixed at room temperature (RT) for 1 h, was added to the synthesis pot and stirred vigorously for 3 h at RT without pH adjustment (pH < 1). The mixture was transferred to a Teflon-lined autoclave for hydrothermal (HT) synthesis at

100°C for 24 h. The solid product was then centrifuged and washed with deionized water before drying at 100°C for 12 h and subjected to final calcination at either 300°C or 550°C for 6 h in a muffle furnace. The heating rate during calcination was maintained at 10°C/min.

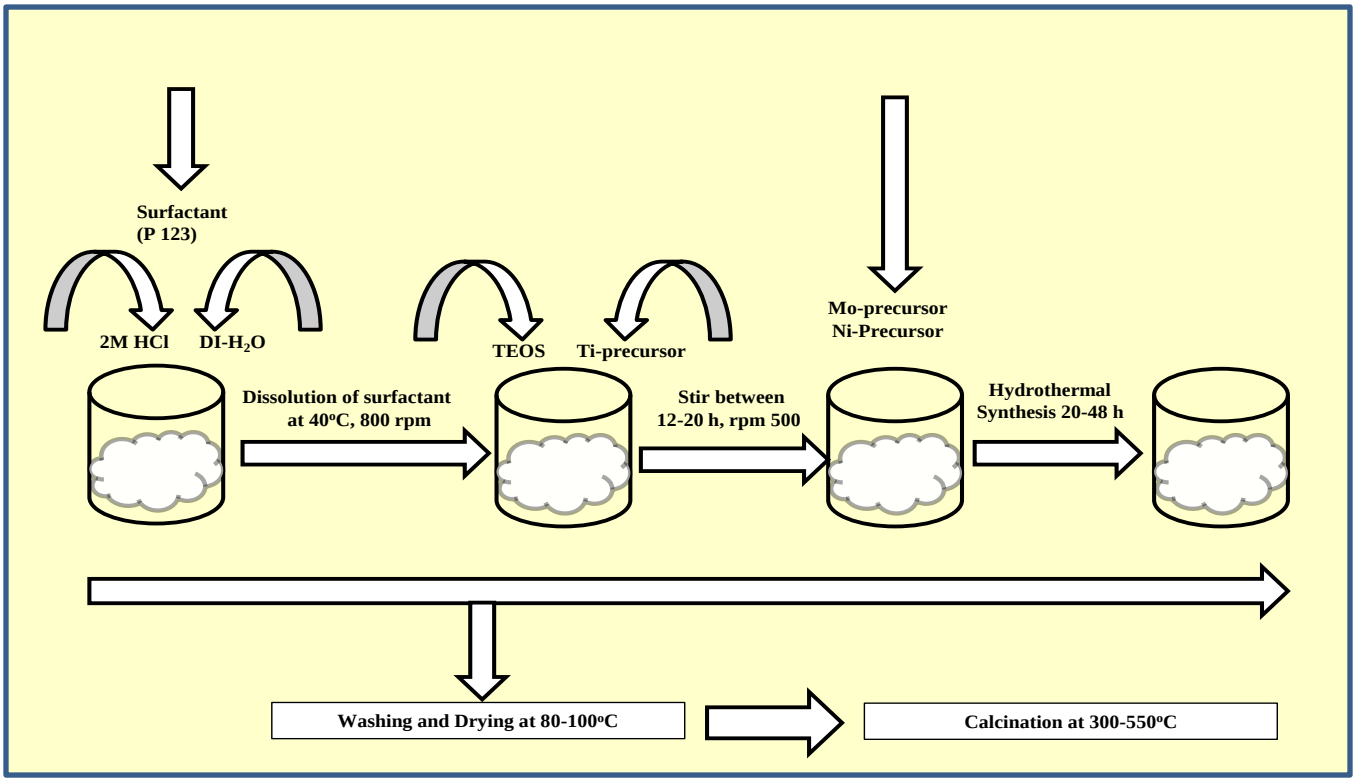

Figure 3-1 Schematic representation of Single-Pot (SP) Synthesis of NiMo Supported on Metal-Modified SBA-15 Catalysts.

3.2.4 Impregnation of NiMo Active Phase on the Support

The impregnation of NiMo active phase on the support was performed by the excess wet solution method in deionized water. The procedure involves stirring equivalent amounts of nickel and molybdenum precursors (to obtain 3 wt.% and 13 wt.% of metal, respectively, in the catalyst) at room temperature for 3 h without or with citric acid (CA: Mo ratio of 1:1), followed by the addition of 1 g Ti-SBA-15 to the mixture without pH adjustment (pH 4-5). This mixture was stirred for 2 h and then dried by slow evaporation at 60-70°C. Prior to final calcination at 300 or 550°C, the catalyst was dried at 100°C for 12 h.

Table 3-1 lists the supports and catalysts prepared and investigated in this study along with their codes and descriptions. The Ti-SBA-15-NiMo catalysts prepared by the single-pot method with and without a complexing agent are denoted as TSMN(CA)-SP(*x*) and TSMN-SP(*x*), respectively, where *x* represents the calcination temperature. The Ti-SBA-15/NiMo catalysts prepared by the impregnation method with and without a complexing agent are denoted as TSMN(CA)-Imp(*x*) and TSMN-Imp(*x*), respectively, where *x* represents the calcination temperature.

Table 3-1 Description of Catalysts

Sample Code	Description	Catalyst Preparation Method	Calcination Temperature (°C)
SBA-15	Template-free SBA-15	-	550
Ti-SBA-15	Titanium-modified SBA-15	-	550
TSMN-Imp300	NiMo/Ti-SBA-15	Impregnation	300
TSMN-Imp550	NiMo/Ti-SBA-15	Impregnation	550
TSMN-SP300	NiMo-Ti-SBA-15	Single-Pot	300
TSMN-SP550	NiMo-Ti-SBA-15	Single-Pot	550
TSMN(CA)-Imp300	NiMo/Ti-SBA-15 with citric acid	Impregnation	300
TSMN(CA)-Imp550	NiMo/Ti-SBA-15 with citric acid	Impregnation	550
TSMN(CA)-SP300	NiMo-Ti-SBA-15 with citric acid	Single-Pot	300
TSMN(CA)-SP550	NiMo-Ti-SBA-15 with citric acid	Single-Pot	550

3.2.5 Characterization of Supports and Catalysts

3.2.5.1. Textural Properties

The BET surface area, pore size, and pore volumes were measured on a Micromeritics ASAP 2020 using N_2 adsorption-desorption at -196°C. Prior to measurement, the samples were degassed at 250°C for 3 h to remove impurities or moisture. The Brunauer, Emmett, and Teller (BET) method was used to calculate the surface area, and the adsorption part of Barrett, Joyner, and Halenda (BJH) method was used to calculate the pore size distribution and pore volume.

3.2.5.2 Thermogravimetric Analysis

Thermal analysis of the prepared catalysts was performed on an SDTQ600 TGA in high-purity zero air. The furnace temperature was increased from 30°C to 1000°C at a rate of 10°C/min, whereas the cooling rate was 30°C/min.

3.2.5.3 X-ray Diffraction

X-ray diffraction (XRD) at a wide angle using Cu anode (9 kV) at Kα = 1.5405 (Rigaku miniflex-bench top X-ray powder) was used to determine the crystallinity of the prepared catalysts. The samples were scanned between 20° and 80° at 3°/min.

3.2.5.4 Raman Spectroscopy

A Raman spectroscope (HORIBA, iHR320 with CCD detector) with a laser wavelength of 532 nm (300 mW, green laser) was used to characterize the MoO_3 and TiO_2 phases.

3.2.5.5 Fourier Transformation Infrared (FTIR) Spectroscopy

FTIR was used to identify the functional groups present in the developed supports and catalysts. The (IR) absorption spectra of SBA-15, Ti-SBA-15, and NiMo-supported catalysts were recorded on a Thermo Scientific Nicolet 6700 FT-IR spectrometer with a scanning range of 400-4000 cm^{-1}. The samples for FTIR analysis were prepared using KBr powder mixed with the support/catalyst in a ratio of 100:1 to form pellet-like translucent discs.

3.2.5.6 Temperature-Programmed Desorption of Ammonia (NH_3-TPD)

Surface acidity measurement was conducted on a Micromeritics Chemisorb 2750 (pulse chemisorption system) using 10 wt. % NH_3 by temperature-programmed desorption (TPD). Approximately 100 mg of non-sulfided catalyst was loaded into a quartz tube and covered with

quartz. The sample was purged with high purity helium at 600°C and held for 30 min before being cooled to 100°C. The probe molecule (NH_3) was adsorbed on the sample at 100°C for 30 min, which was followed by helium purging for 60 min to remove any physisorbed ammonia. NH_3 desorption was accomplished by heating the furnace at 10°C/min to 800°C, and the data were recorded with a thermal conductivity detector (TCD).

3.2.5.7 Temperature-Programmed Reduction by Hydrogen (TPR-H_2)

The reducibility potential of metal oxides supported on Ti-SBA-15 was determined by temperature-programmed reduction with hydrogen as the probe molecule using a Micromeritics (Autochem II-2920) chemisorption analyzer. Approximately 50 mg of the prepared catalyst previously calcined at 300°C or 550°C was pre-treated for one hour in high-purity helium at 500°C and then cooled to ambient temperature before being heated to 1000°C at 10°C/min under a steady flow (20 ml/min) of 10% H_2 in helium. The consumption of H_2 at the reducible temperature(s) was recorded on a thermal conductivity detector (TCD).

3.2.5.8 Field Emission Scanning Electron Microscopy (FE-SEM)

The TESCAN LYRA 3 unit was used to examine the morphology of SBA-15 and modified SBA-15-NiMo catalysts using secondary electron (SE) and backscattered electron (BSE) modes at an accelerating voltage of 30 kV. The unit was equipped with an energy-dispersive X-ray spectrometer (EDS, Oxford, Inc.) detector for elemental analysis.

3.2.5.9 Transmission Electron Microscopy (TEM)

Microstructural and morphological analysis of sulfided NiMo HDS catalysts was performed on FEI Titan 300, high resolution transmission electron microscope (HRTEM), operated at 120kV. The sample preparation was performed by dispersing sulfided catalysts powder in ethanol until total dissolution, which was followed by deposition of an air-dried sample on a carbon coated grid for TEM analysis.

3.2.5.10 X-ray Photoelectron Spectroscopy (XPS)

The bonding state and chemical composition of sulfided HDS catalysts were determined by X-ray photoelectron spectroscope (PHI 5000 Versa Probe II, ULVAC-PHI Inc.). The sample preparation was done by making a few centimeters pelletized disc and subjected to high vacuum before XPS analysis.

3.2.5.11 Elemental Analysis by ICP-OES

The elemental composition of the bulk catalysts for Si, Ti, Mo and Ni were determined by inductively coupled plasma (ICP) attached with optical emission spectrometer (Ultima 2, Horiba Scientific). Typical sample preparation procedure involves fusing a 50 mg of catalyst sample with 350 mg of lithium metaborate in a muffle furnace at 1000◦C for 20 min. The fused product was dissolved in10 ml of 10% HNO_3 and diluted with deionized water to make a total volume of 50 ml. The solution thus obtained was analyzed by ICP-OES.

3.2.6 Presulfiding and Performance Evaluation of Catalysts

Samples of prepared catalysts were pelletized, crushed, and sieved into 300-500 micron sizes. Each sample was reduced under a flow of 5% H_2/He (60 ml/min) at 400°C (ramp rate of 10°C/min) for 2 h to convert Ni and Mo to metallic forms. Presulfidation was performed using a solution containing 2 wt.% CS_2 in a quartz tube at 350°C overnight.

The HDS performance of prepared catalysts was evaluated in a high-pressure batch reactor (model: Parr 4576B) at 350°C under 5 MPa of H_2 pressure and constant 300 rpm stirring. Approximately 0.25 g of catalyst was added to 100 ml of the simulated feed containing DBT (2500 ppm-S) in dodecane. Each test was conducted for 4 h after the target process conditions were achieved. Product samples were collected every hour during this period.

The sulfur content in the feed and products was quantified using a gas chromatography sulfur chemiluminiscence detector (GC-SCD), and product identification was achieved with gas chromatography mass spectrometry (GC-MS). Hydrocarbon analysis was performed with a gas chromatography flame ionization detector (GC-FID).

3.3 Results and Discussion

3.3.1 Textural Properties

The textural properties of synthesized supports (SBA-15 and Ti-modified SBA-15) and NiMo catalysts without sulfidation are presented in **Table 3-2,** and the adsorption-desorption isotherms are presented in **Figure 3-2**. The parent SBA-15 exhibits a high specific surface area (643 m^2/g) and large pore volume (1.25 cm^3/g), with an average pore diameter of 7.9 nm. It exhibits a type-IV isotherm showing an H1 hysteresis loop, which is a typical characteristic of mesoporous SBA-15 silica according to IUPAC [26]. Notably, the incorporation of titanium into SBA-15 improves its textural properties (for instance, the surface area is increased to 679 m^2/g). The introduction of Ni and Mo onto Ti-SBA-15 either by impregnation or through the single-pot approach, however, reduces the pore size due to surface and void blockage. Nitrogen adsorption and desorption isotherms (**Figure 3-2**) provide the evidence of particles plugged within the support matrix. The catalysts prepared by the SP approach exhibit higher surface areas than those prepared by the impregnation method. The relative preservation of textural properties by the SP approach is likely due to the ability of the active metal-oxides to be embedded into the support matrix without total surface coverage. It can thus be expected that the SP approach will create a highly dispersed active phase for efficient catalytic performance.

Table 3-2 Textural Properties of Supports and Catalysts

Sample Code	BET Surface Area (m^2/g)	Microporous Surface Area (m^2/g)	Macroporous Surface Area (m^2/g)	Microporous Pore Volume (cm^3/g)	Total Pore Volume (cm^3/g)	Average Pore Size (nm)
SBA-15	643	47	595	0.023	1.25	7.9
Ti-SBA-15	679	81	596	0.040	1.39	8.3
TSMN-Imp300	146	21	125	0.011	0.16	6.1
TSMN-Imp550	145	21	125	0.010	0.33	8.8
TSMN-SP300	403	30	374	0.014	0.66	6.5
TSMN-SP550	260	17	244	0.008	0.45	6.6
TSMN(CA)-Imp300	160	14	146	0.007	0.19	5.5
TSMN(CA)-Imp550	103	11	92	0.005	0.21	7.6
TSMN(CA)-SP300	352	28	324	0.013	0.51	6.3
TSMN(CA)-SP550	155	18	137	0.009	0.77	6.9

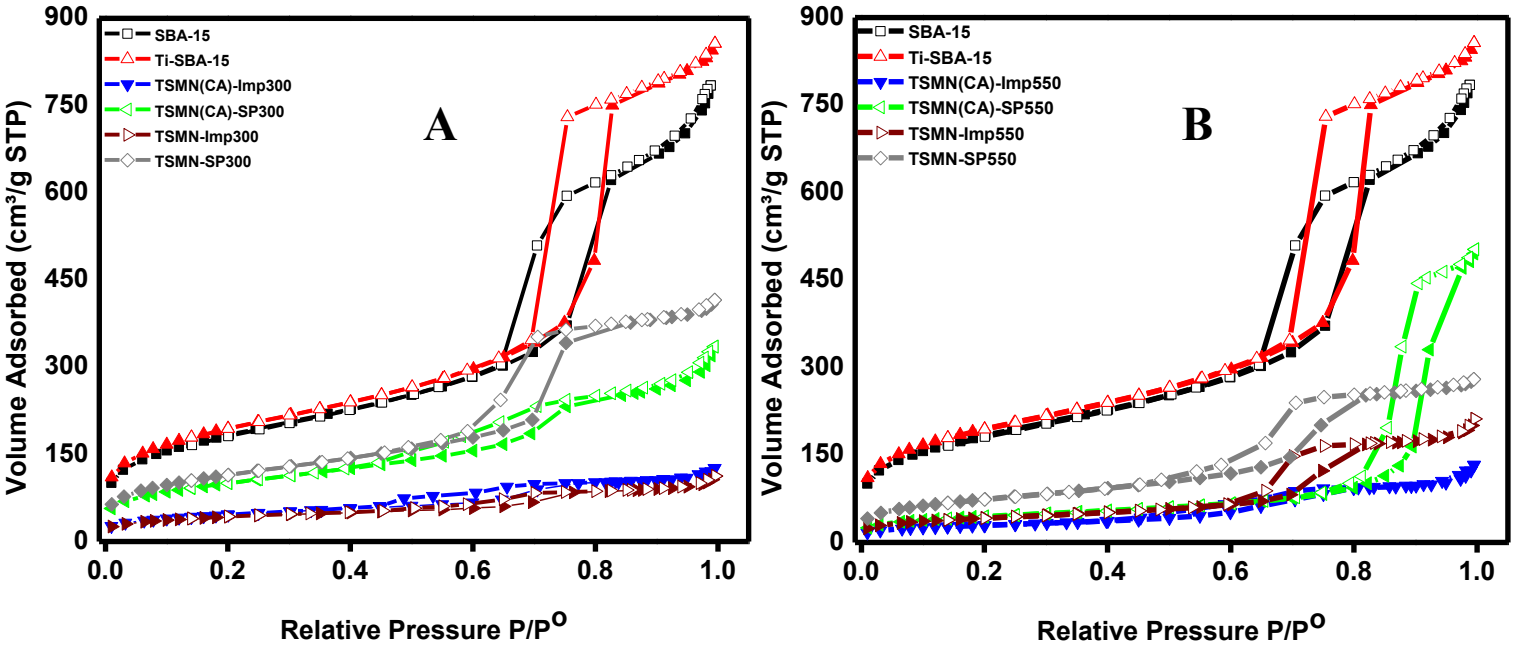

Figure 3-2 Nitrogen Adsorption-Desorption Isotherms of Catalysts Calcined at [A] 300°C and [B] 550°C.

3.3.2 Thermogravimetric Analysis

The thermal stability of the synthesized catalysts was evaluated by thermogravimetric analysis (TGA) in which weight loss or phase change is observed upon heating the catalyst samples to 1000°C. SBA-15 has been reported to possess higher hydrothermal stability due to the thick microporous silica pore wall (3-6 nm) compared to MCM-41, MCM-48, and HMS [49].

TGA of the TSMN catalyst sample without calcination reveals that the major weight loss occurs below 300°C due to the loss of surfactants and adsorbed water, as shown in **Figure 3**. When the catalysts that were calcined at different temperatures between 300°C and 550°C were subjected to TGA, the results show similar trends in the thermal stability up to 700°C, as shown in ***Figure 3-3***A Therefore, a calcination temperature of 300°C is sufficient to remove surfactants and adsorbed water from the catalysts synthesized by the SP method with or without complexing agent. (***Figure 3-3*B**)

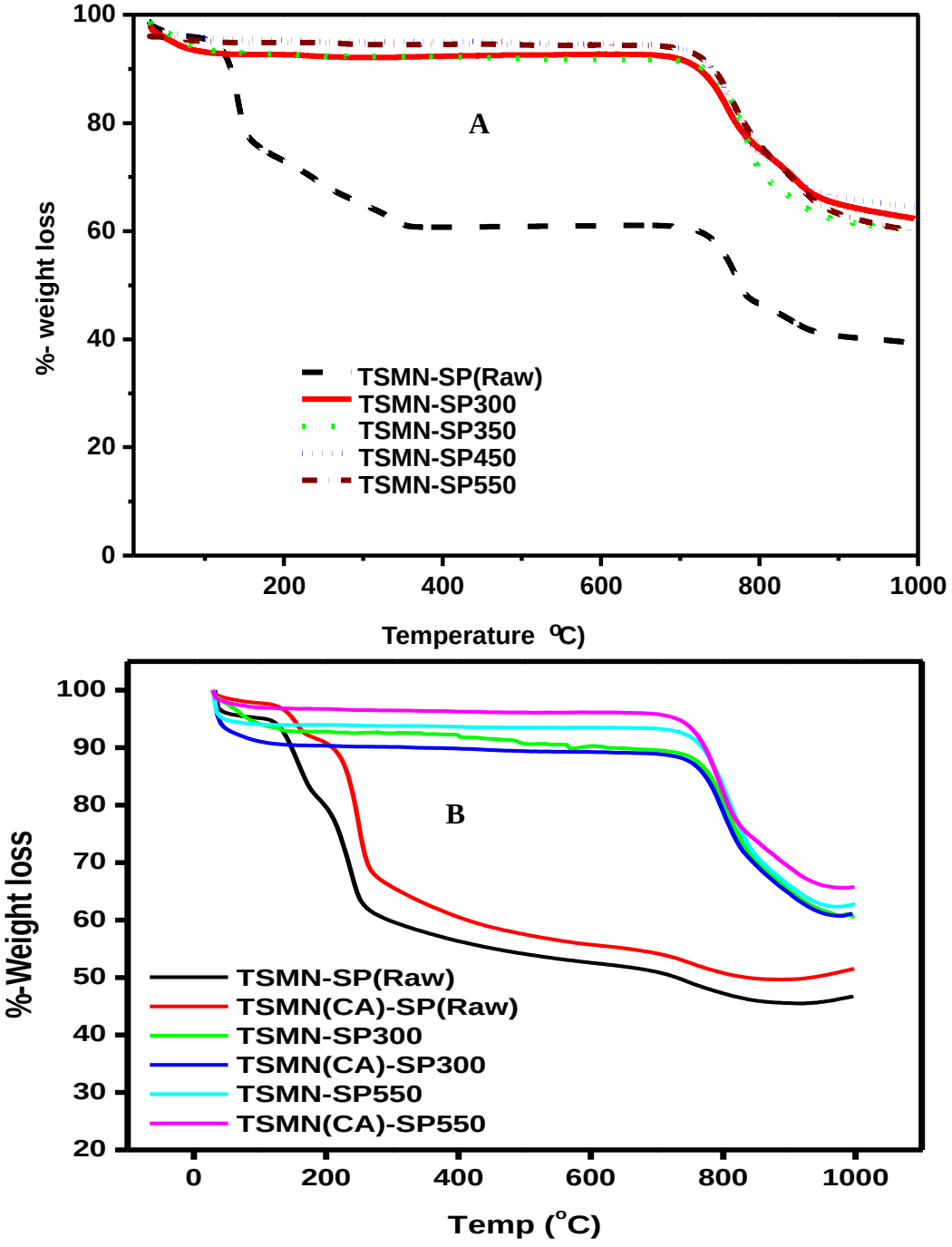

Figure 3-3 Thermogravimetric Analysis of Catalysts Prepared by the SP Method and Calcined at Different Temperatures.

3.3.3 X-Ray Diffraction

X-ray powder diffraction (XRD) analysis enabled the determination of the crystallinity and different phases of the synthesized supports (SBA-15 and Ti-SBA-15) and the NiMo catalysts supported on Ti-SBA-15. The structure of SBA-15 in low-angle XRD exhibits three characteristic diffraction peaks of silica and, these peaks are associated with p6mm ordered hexagonal symmetry, indexed as (100), (110), and (200) [50]. Additionally, as shown in ***Figure 3-4*** from wide-angle XRD, the MoO_3 characteristic peaks are identified at different peak positions. The major peaks at 2-theta of 13, 23.42, 26, 27.52, and 39 degrees are due to the orthorhombic MoO_3 crystalline phase [51], whereas peaks at 2-theta of 26, 39, and 67, which mostly coincide with and are overlaid by MoO_3, indicate TiO_2 anatase [52]. The diffraction peak associated with nickel could not be identified due to concentration limitations in XRD for the metal oxides. The molybdena present in all catalysts subjected to high temperature calcination can be indexed to orthorhombic MoO_3 (JCPDS card no. 05-0508) with the space group Pbnm of octahedral form. As shown in ***Figure 3-4*****B**, the catalyst prepared by impregnation with a complexing agent (TSMN(CA)-Imp550) at a higher calcination temperature shows exceptional characteristics of MoO_3 reflections unlike others, due to high intensity of the peak centered at $2\Theta = 26$ degrees. In general, the catalysts calcined at 300°C show better dispersion on the support with broadened peaks and low intensities of the (020), (040), and (060) phases corresponding to MoO_3 particles, which signifies the presence of small crystallites [53].

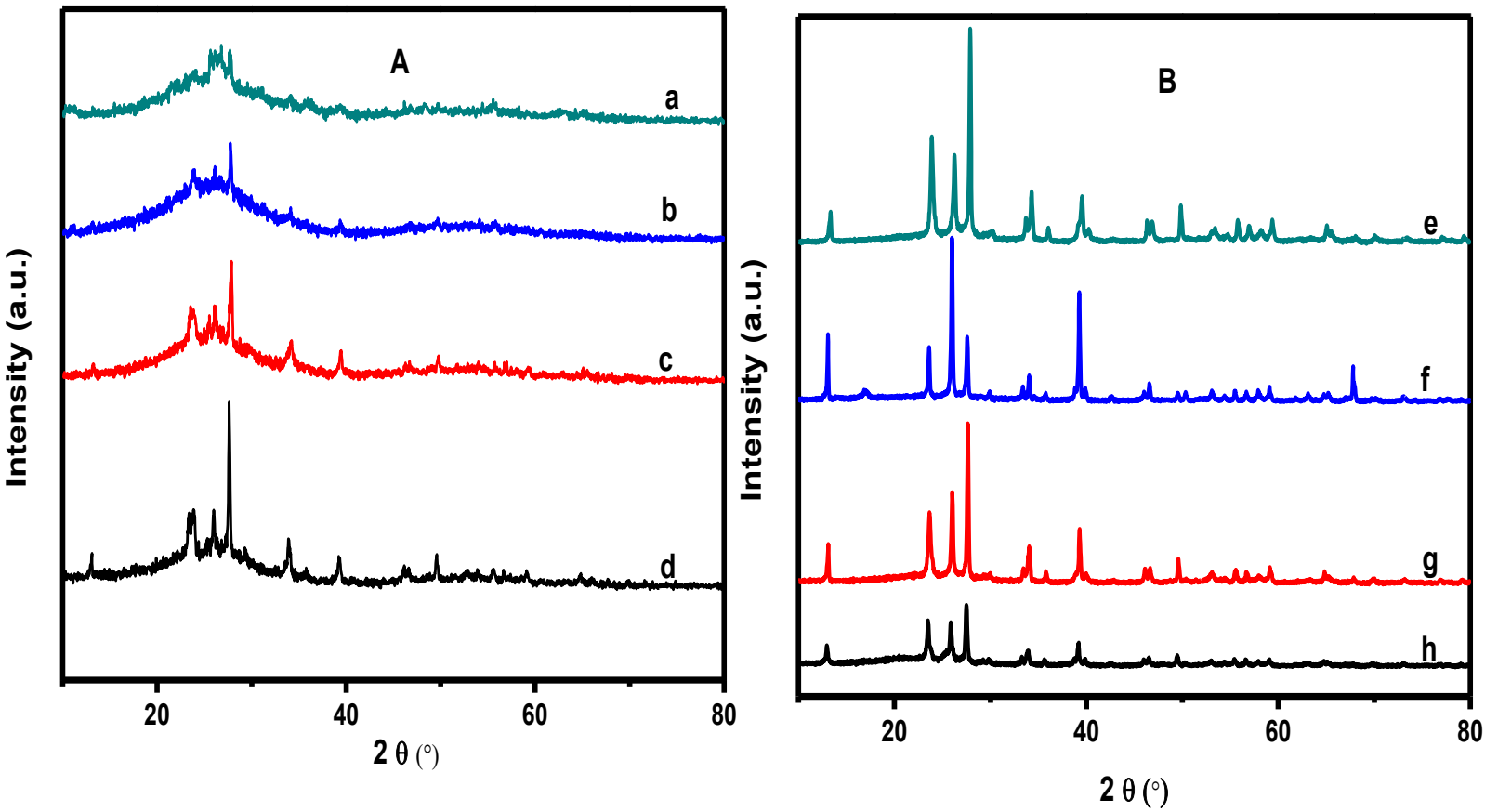

Figure 3-4 X-ray Diffraction Analysis of HDS Catalysts. [(A) (a) TSMN-Imp300, (b) TSMN(CA)-Imp300, (c) TSMN-SP300, (d) TSMN(CA)-SP300], and [(B) (e) TSMN-Imp550, (f) TSMN(CA)-Imp550, (g) TSMN-SP550, (h) TSMN(CA)-SP550].

3.3.4 Raman Spectroscopy

Raman spectroscopy is a non-destructive method for characterizing the dispersion of active metal on the support [54]. Molybdenum oxide and titanium oxide phases for the HDS NiMo catalysts were examined using a laser Raman spectroscope, with the crystalline molybdena existing either in the tetrahedral (tet) or octahedral (oct) form [55]. For pure MoO_3 crystallites, the peaks at 819 and 665 cm^{-1} are characteristic of the Mo-O-Mo bridge stretching mode, whereas symmetric stretching of the Mo=O terminal oxygen is observed at 994 cm^{-1} [56, 57]. The bands at 336 and 375 cm^{-1} could be assigned to the bending and deformation modes of vibrations of O=Mo=O and O-Mo-O, and the Mo=O wagging mode of vibration is observed at 290-280 cm^{-1} [58, 59]. As shown in **Figure 3-5**, the characteristic MoO_3 peaks are observed in all NiMo catalysts prepared at the higher calcination temperature (550 °C), with differences in their peak intensities and positions due to different degrees of interaction with the supports (related to the degree of crystallinity and/or dispersion). The dominant molybdena species due to the interaction on SBA-15 may exist in the form of tetrahedral $(Si\text{-}O\text{-})_2Mo(=O)_2$ di-oxo species, due to the presence of bands at 970 and 355 cm^{-1} [60]. However, good dispersion is achieved for the NiMo oxide catalysts subjected to a lower calcination temperature, as evidenced by the presence of amorphous peaks at 950 cm^{-1} [61].

Notably, Ti-SBA-15 synthesized by the direct approach before the addition of NiMo for the HDS oxide catalysts exhibits five peaks corresponding to the anatase phase of titania. Peak analysis reveals that the stretching (E_g) mode of vibrations in O-Ti-O is observed at 144, 197, and 630 cm^{-1}, whereas the symmetric (B_{1g}) and asymmetric (A_{1g}) bending vibrations are at 395 and 520 cm^{-1}, respectively [62]. However, upon the introduction of Mo into the matrix support, all modes of vibrations assigned to titania (anatase) become unobservable, perhaps due to the dominance of Mo **(**see **Appendix A1).** Therefore, the observed peaks shown in **Figure 3-5** are assigned only to MoO_x phases of either crystalline SP or impregnation HDS catalysts.

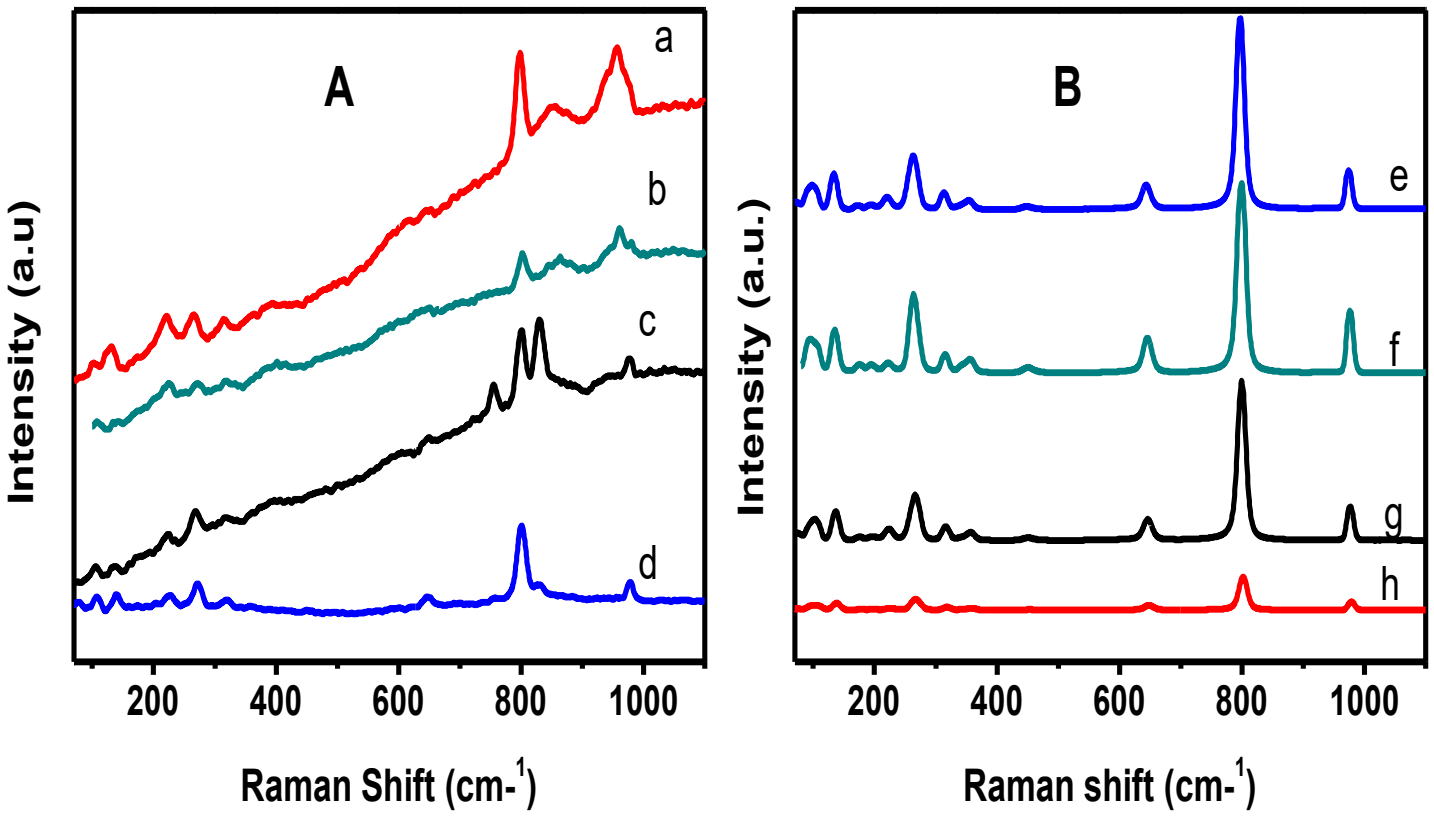

Figure 3-5 Raman Analysis of HDS Catalysts. [(A) (a) TSMN-Imp300, (b) TSMN(CA)-Imp300, (c) TSMN-SP300, (d) TSMN(CA)-SP300], and [(B) (e) TSMN-Imp550, (f) TSMN(CA)-Imp550, (g) TSMN-SP550, (h) TSMN(CA)-SP550].

3.3.5 FTIR Spectroscopy

FTIR spectroscopy was employed to gain insight into the functional groups of SBA-15, Ti-SBA-15, and NiMo-modified Ti-SBA-15 catalysts. As shown in **Figure 3-6**, SBA-15 shows a strong intensity band at approximately 1,218 cm^{-1}, corresponding to the asymmetric stretching modes of Si-O-Si, along with a broad absorption band at 1,628 cm^{-1}, which is characteristic of the -OH stretching of an absorbed water molecule [63]. The band at 3,500 cm^{-1} can be associated with the silanol end group (Si–OH) and Si_3–O–Ti–OH due to Brønsted acid sites. The incorporation of Ti into the SBA-15 mesoporous silica network results in bands at 800 and 950 cm^{-1} due to the Ti–O symmetric stretching mode and Ti–O–Si bending modes, respectively [6]. For NiMo-supported SBA-15, the Mo-O-Mo stretching mode is observed at approximately 620 and 850 cm^{-1}, and the band at 797 cm^{-1} corresponds to the presence of polymolybdate (Mo_{36}) [64]. The intensity of this band is more pronounced for the catalysts synthesized with a complexing agent and calcined at 300°C, indicating better dispersion of the active metals. These results are in agreement with those obtained with Raman spectroscopy and XRD.

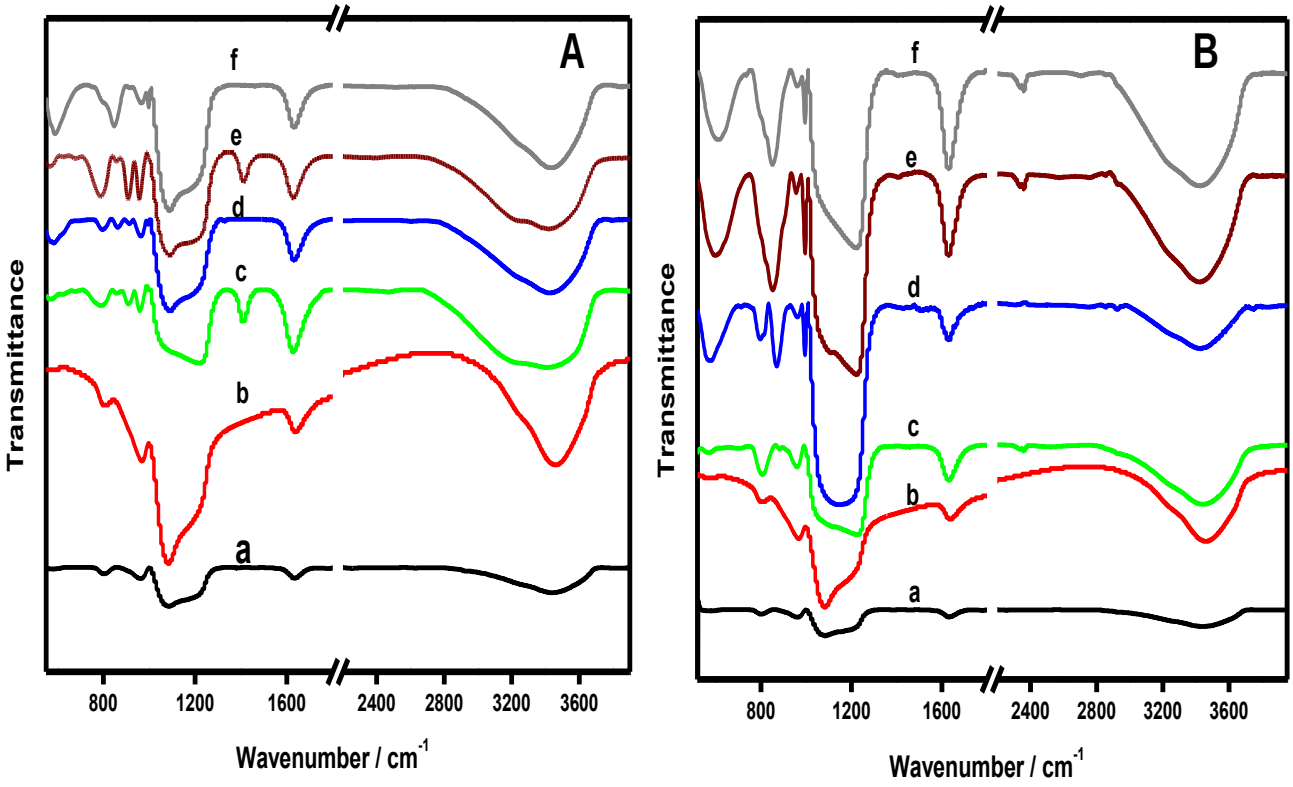

Figure 3-6 FTIR Results of Supports and Catalysts. [A] (a) SBA-15; (b) Ti-SBA-15; (c) TSMN(CA)-Imp300; (d) TSMN(CA)-SP300; (e) TSMN-Imp300; (f) TSMN-SP300, and [B] (a) SBA-15; (b) Ti-SBA-15; (c) TSMN(CA)-Imp550; (d) TSMN(CA)-SP550; (e) TSMN-Imp550; (f) TSMN-SP550

3.3.6 Temperature-Programmed Desorption

The surface acidity characteristics of non-sulfided HDS catalysts were determined by NH_3-TPD. Ti, which is a tetravalent element, incorporates into the silica framework easily with improves surface acidity (see Figure SI-3 and Table SI-1), and the nature of the acidity observed in all prepared catalysts is mostly weak and/or moderate, characterized by Lewis acid sites in the temperature range between 195° and 220°C (**Table 3-3**) [65]. In all cases, the acidic strength of catalysts calcined at 300°C is higher than the catalysts calcined at 550°C. In addition, the catalysts prepared by the SP approach with or without citric acid [TSMN(CA)-SP300 and TSMN-SP300] have more surface acidity than the others. It seems that the incorporation of active metals at the beginning of catalyst preparation in the SP approach improves the acidity considerably. In addition, the surface acidity of Ti-modified SBA-15-NiMo HDS catalysts prepared by SP method at both calcination temperatures is higher than the unmodified SBA-15-NiMo catalysts prepared by the same approach.

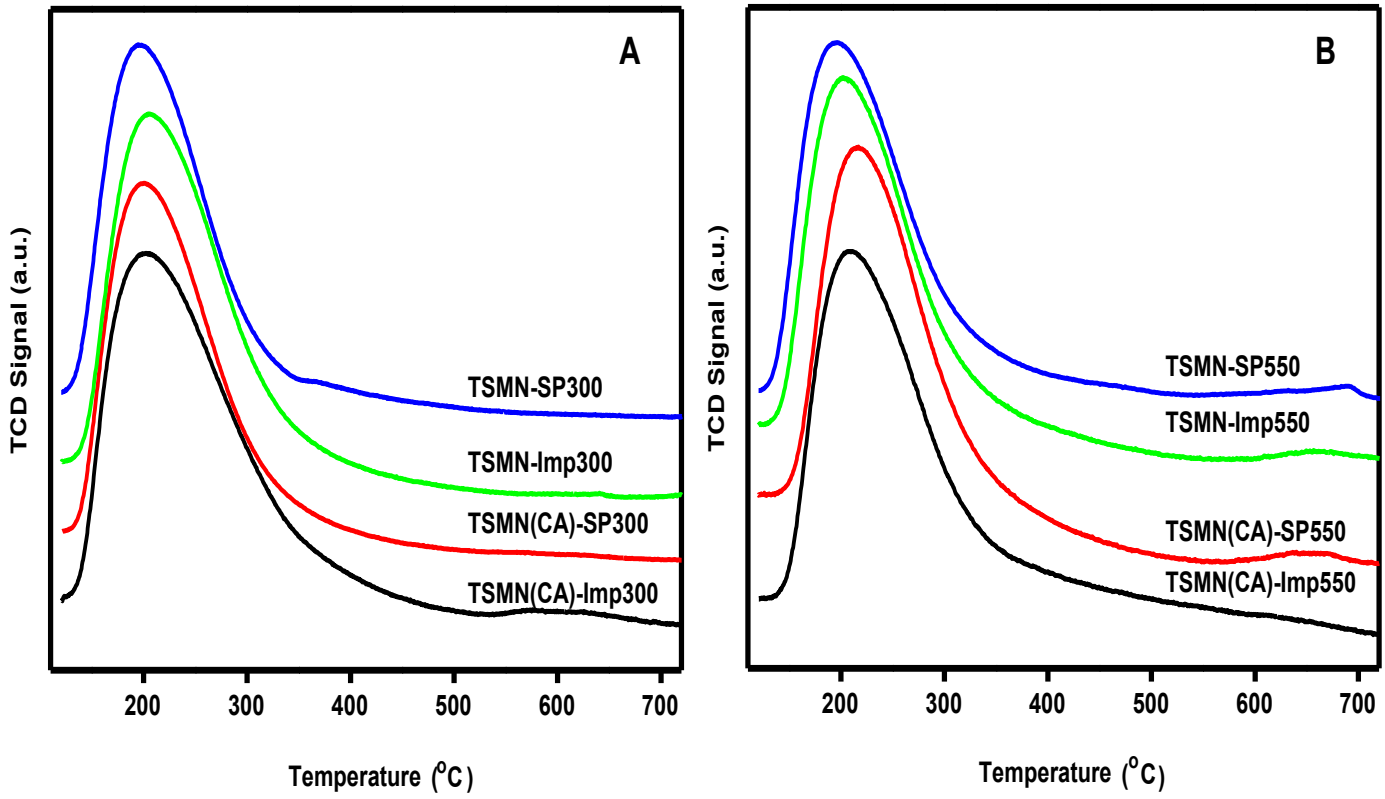

Figure 3-7 NH3-TPD Results of HDS Catalysts (in the Oxide Form) Calcined at [A] 300°C and [B] 550°C.

Table 3-3 TPD and TPR Results of Catalysts (in the Oxide Form).

Catalysts	TPD: NH_3 desorbed		TPR: H_2-consumption	
	Peak Temperature(s) (°C)	**Amount (mmol/g)**	**Peak Temperature(s) (°C)**	**Amount (mmol/g)**
TSMN-Imp300	206	0.158	640.57	29.49
TSMN-Imp550	202	0.085	720, 1000	66.43
TSMN-SP300	195	0.198	571, 950	44.22
TSMN-SP550	196, 686	0.179	516, 888	27.34
TSMN(CA)-Imp300	200	0.138	608, 1000	44.14
TSMN(CA)-Imp550	207	0.100	590	45.44
TSMN(CA)-SP300	202	0.235	471.47	43.74
TSMN(CA)-SP550	218, 670	0.099	573, 1000	46.69

3.3.7 Temperature-Programmed Reduction

The H_2-TPR profiles of catalysts prepared by the SP and impregnation approaches are shown in **Figure 3-8**. A variation is noticed in the reduction temperature of the active metals (NiMo) due to either the active phase deposition method or calcination temperature. At relatively low temperature (410-560°C), the main H_2 consumption temperature corresponding to the reduction of Mo polymeric octahedral (Mo^{6+} to Mo^{4+}) is observed, while the reduction temperature of H_2 between (700-770°C) could be attributed to (Mo^{4+} to Mo^{0}) of polymeric octahedral, tetrahedral and bulk molybdena species [4]. The reduction temperatures for the catalysts prepared at low calcination temperature (300°C) are lower than those at high temperature (550°C) in both cases of Mo reduction (Mo^{6+} to Mo^{4+} and Mo^{4+} to Mo^{0}) (Table 3). It has been reported that the increase in the reduction temperature is related to a strong metal support interaction, which decreases dispersion and in turn affects the catalytic performance. It is noteworthy that the use of citric acid (as a complexing agent) aids the dispersion of the active phase, as observed in the XRD and Raman spectroscopy results; this was further established by the lower reduction temperature in the H_2-TPR analysis. These results are in good agreement with the report by Badoga et al. [6], who used EDTA as a complexing agent.

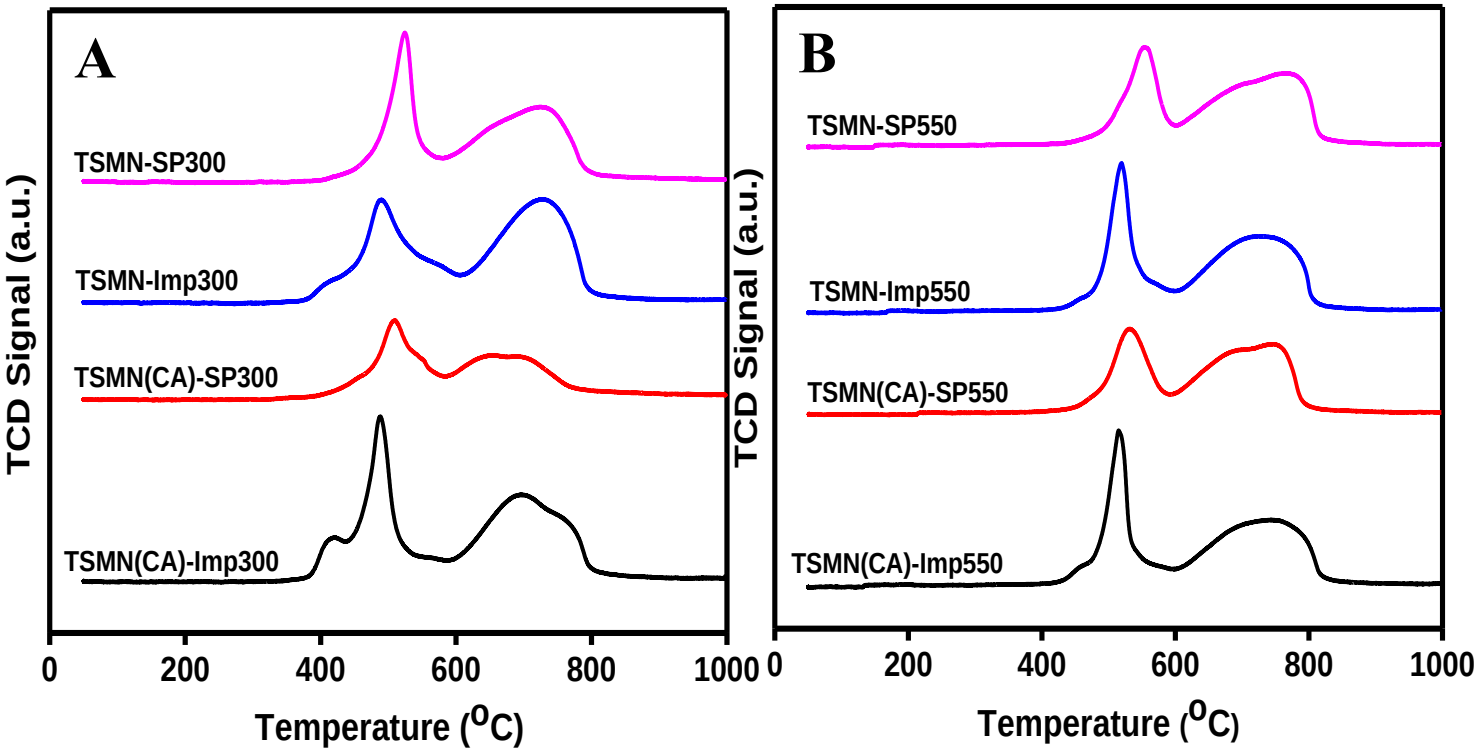

Figure 3-8 H2-TPR Results of HDS Catalysts (in the Oxide Form) Calcined at [A] 300°C and [B] 550°C.

3.3.8 Scanning Electron Microscopy

Images captured by scanning electron microscopy for non-sulfided HDS catalysts are presented in **Figure 3-9**. For catalysts prepared by the SP approach (with or without CA) subjected to a low calcination temperature (300°C), a unique nano-cubical flat-sheet morphology of Mo is observed, and this morphology is grown alongside the rod-like morphology of heteroatom modified-SBA-15. However, the low calcination temperature catalysts obtained by the impregnation method show little or no NiMo particles on the surface of the support, which indicates that the active metals are preferably embedded in the SBA-15 structural unit. For all non-sulfided catalysts obtained at a high calcination temperature (550°C), there are long rectangular rods of Mo on the support, which is responsible for the observed high-intensity crystalline phases of MoO_3. These results are in agreement with those obtained by Raman spectroscopy and XRD.

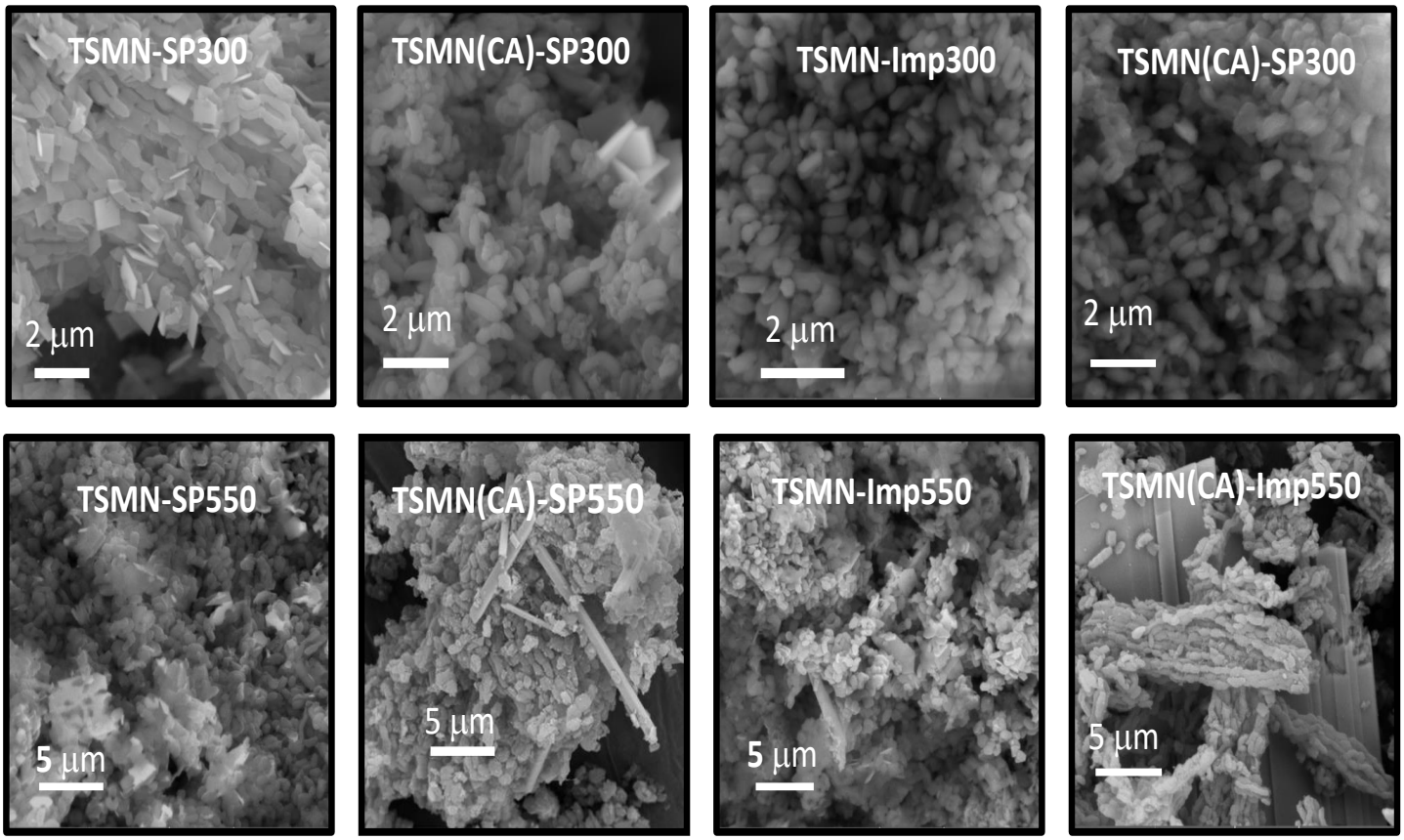

Figure 3-9 SEM Results of the Synthesized Catalysts.

3.3.9 Transmission Electron Microscopy

Better understanding of active phase (MoS_2) distribution and dispersion of sulfided HDS catalysts, as a function of calcination temperature, addition of complexing agent and preparation method was obtained by HRTEM. The selected representative micrographs (as shown in **Figure 3-10**) showed the morphological and microstructural changes of NiMo supported on Ti-SBA-15 by impregnation and SP-approach. The arrows are pointed to the MoS_2 crystallites with measured interplanar distance of 0.61 nm. The MoS_2 crystallite lengths of the catalyst prepared by impregnation approach without citric acid (TSMN-Imp300) is found between 2 and 4.4 nm, and the stacking degree of 1-2 layers, while the catalyst prepared by impregnation approach with citric acid exhibits slightly different MoS_2 crystallite lengths between 2 and 4.8 nm, and the same stacking layers with TSMN-Imp300. The crystallite lengths and stacking degree observed for TSMN(CA)-SP300 is similar to both catalysts prepared by impregnation approach at low calcination temperature. There is a slight variation in the distribution and morphology of TSMN-SP300 catalyst prepared by SP-approach at low calcination temperature, this catalyst exhibits longer MoS_2 crystallites between 2.5-5.0 nm, with layer stacking of 2-4 layers compared to other counterparts at low calcination temperature. On the other hand, the catalysts calcined at high temperature showed different active phase distributions and morphologies, with longer MoS_2 slab length and higher stacking degrees. As observed for non-sulfided oxide NiMo catalysts, the dispersion of low temperature catalysts is better than the corresponding high calcination temperature catalysts and thus expected to favor catalytic activities. However, there is little distinction that can be deduced within the catalysts of the same group, with the exception of TSMN-Imp550 exhibiting better slab length and stacking degree than others at high calcination temperature. The details of crystallite lengths and stacking degrees are summarized in **Table 3-4**.

Table 3-4 MoS_2 crystallites length and stacking degree distribution and elemental compositions by ICP-OES

Catalysts	HRTEM morphology				Elements		
	Length distribution (nm)	Average length (nm)	Stacking distribution (layers number)	Average stacking (layers number)	Mo (%)	Ni (%)	Si/Ti
TSMN-Imp300	2 – 4.4	3.3	1 – 2	2	12.9	2.95	9.98
TSMN-Imp550	2 – 6.6	4.8	2 – 4	4.5	13.18	3.02	9.92
TSMN-SP300	2.5 – 5.0	3.8	2 – 4	3.1	12.46	1.63	10.04
TSMN-SP550	3 – 7.6	5.5	2 – 10	6.2	12.98	1.84	10.15
TSMN(CA)-Imp300	2 – 4.8	3.2	1 – 2	2.5	13.01	2.96	9.97
TSMN(CA)-Imp550	4 – 7.8	6.2	2 – 10	6.5	11.18	2.99	10.01
TSMN(CA)-SP300	2 – 4.4	3.3	1 – 2	2.5	11.92	1.39	10.12
TSMN(CA)-SP550	4 – 6.1	5.3	2 – 8	5	13.31	1.26	10.26

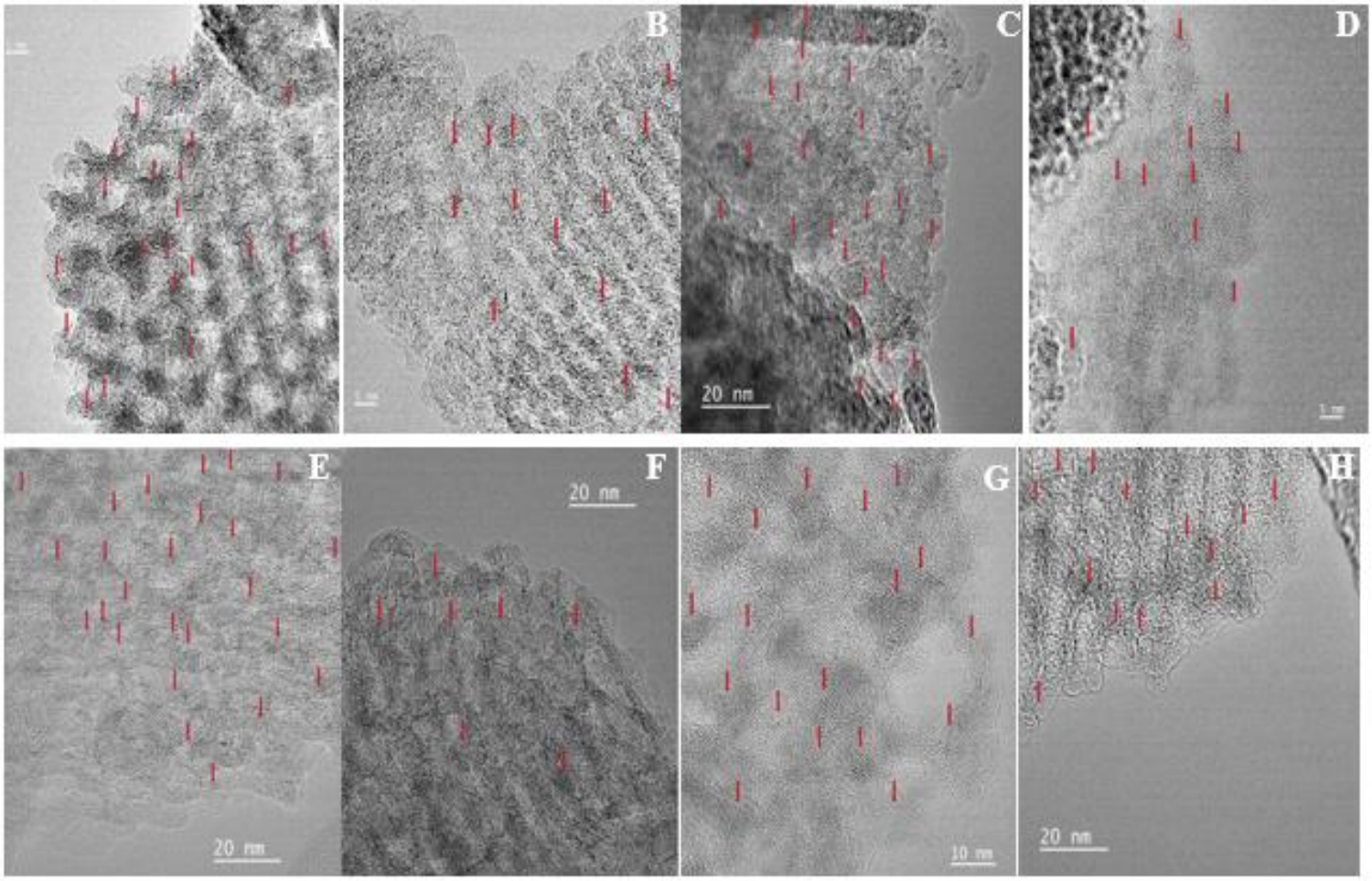

Figure 3-10 HRTEM analysis of sulfided HDS catalysts (A) TSMN-Imp300, (B) TSMN(CA)-Imp300, (C) TSMN-SP300, (D) TSMN(CA)-SP300, (E) TSMN-Imp550, (F) TSMN(CA)-Imp550, (G) TSMN-SP550 and (H) TSMN(CA)-SP550

3.3.10 Chemical compositions of HDS catalysts

The chemical compositions of bulk catalysts prepared both SP and impregnation approach was investigated by ICP-OES analysis. It is observed that main active element (molybdenum) is well attached to the support (Ti-SBA-15) by both deposition methods, and all the catalysts possessed reasonable amount of the ca. 13 wt. %. However, there is a disparity in the amount of nickel observed in both active phase deposition approaches. In the case of impregnation approach, nickel is well attached to the support irrespective of the calcination temperature, while the SP-approach suffers significant loss in the amount of nickel present in the final HDS catalysts **(Table 3-4)**. This observation is due to the presence of soluble nickel in the solution that could be not completely anchored to the support under synthesis parameters and method [66].

3.3.11 X-ray Photoelectron Spectroscopy (XPS)

The surface composition and bonding state of representative sulfided HDS catalysts were analyzed by XPS. The spectra for Mo and S states are presented in (**Figure 3-11A and B**), respectively and the atomic weight of all elements are summarized in (**Table SI-2**). Being a surface analysis technique, the distribution and degree of sulfidation can be explained to some extent. As observed from Mo spectra, all catalysts possessed significant amount of Mo^{6+} ($d_{5/2}$) oxidation state between 232 and 232.8 eV, while the bonding state of molybdenum corresponding to Mo^{4+} (as in MoS_2) is observed between 229 and 229.8 eV. In addition, we observed contribution of sulfur around 226.6 eV, corresponding to 2S line, and this is subtracted from molybdenum composition [67]. As shown in **Figure 3-11B**, the XPS peak attributed to sulfide in MoS_2 form is between 161 and 163.8, which is present for all catalysts in different degrees**.** In addition to MoS_2 peak, a peak corresponding to oxy-sulfide is present (168-170 eV). We observed from atomic weight percent calculation (**Table SI-2**) different degree of sulfidation among the HDS catalysts, with the highest for TSMN-Imp300 and the lowest for TSMN-SP550. This result confirms that the low calcination temperature catalysts are relatively more dispersed than high calcination temperature counterparts.

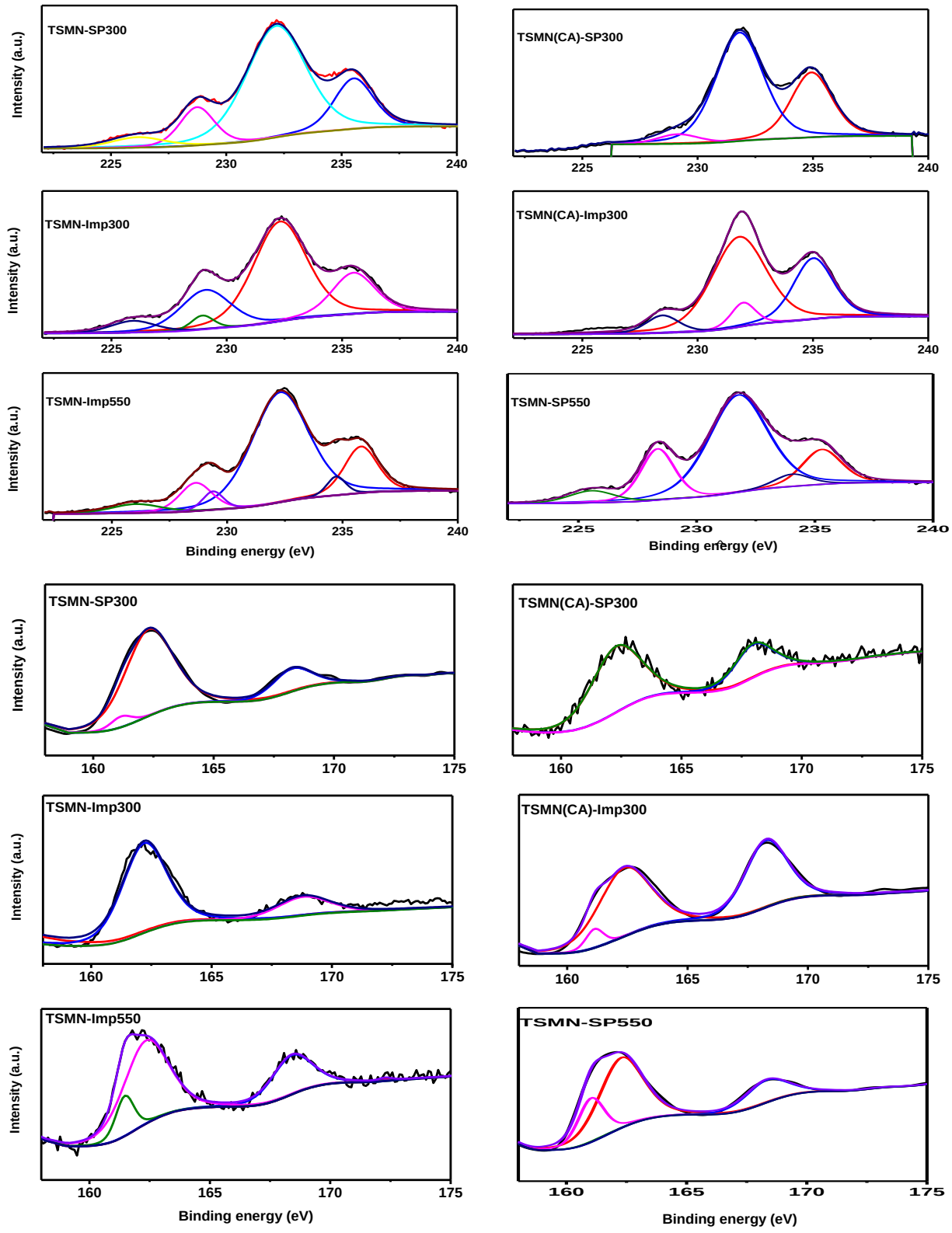

Figure 3-11 X-ray Photoelectron Spectroscopy Analysis of Sulfided HDS Catalysts Showing (A) Molybdenum bonding states, and (B) Sulfur bonding states

3.3.12 HDS Activities of Synthesized Catalysts

The sulfur contents of the products at different reaction times are presented in **Table 3-5**. The results show a significant variation in the performance of the synthesized catalysts, which indicates the influence of the preparation method (SP versus impregnation), calcination temperature (300°C versus 550°C), and complexing agent. In terms of initial activity, which can be estimated by the product sulfur content after one hour, catalysts calcined at 300°C perform better than those calcined at 500°C, irrespective of the preparation method or the use of a complexing agent. When the complexing agent is not used, the performance of the catalyst prepared by the SP method (TSMN-SP300) is significantly better than the catalyst prepared by the conventional impregnation method (TSMN-Imp 300). The trend of the initial activity is observed to be TSMN-SP300 > TSMN-Imp300 > TSMN-Imp550 > TSMNSP550. This trend continues with increased reaction time, as shown in **Figure 3-12A**.

For the catalysts prepared using the complexing agent, the influence of the preparation method (SP versus impregnation) is modest, but impregnation is better. However, the influence of calcination temperature remains significant. Thus, the trend in the initial activity is found to be TSMN(CA)-Imp300 > TSMN(CA)-SP300 > TSMN(CA)-Imp550 ~ TSMN(CA)-SP550. With the increase in reaction time, however, the influence of calcination temperature also diminishes, as shown in **Figure 3-12B**.

In addition, the significant effect of citric acid at the end of reaction time (4 h) is noticeable as shown in **Table 3-5**, especially for the catalyst prepared by impregnation approach. It is observed that the catalyst prepared by impregnation approach with CA at low and high calcination temperatures, showed higher activity of sulfur removal by (98.92% against 98.36%) and (98.52% against 93.28%), respectively, than without CA.

Table 3-5 Catalyst Performance Test Results: Product Sulfur Content.

Catalysts	Product Sulfur Content (ppm)			
	1 h	2 h	3 h	4 h
TSMN-Imp300	1,038	562	327	41
TSMN-Imp550	1,411	1,046	600	168
TSMN-SP300	494	139	90	25
TSMN-SP550	1,600	1,300	700	238
TSMN(CA)-Imp300	639	343	164	27
TSMN(CA)-Imp550	1,349	702	443	37
TSMN(CA)-SP300	763	600	295	34
TSMN(CA)-SP550	1,377	889	529	247

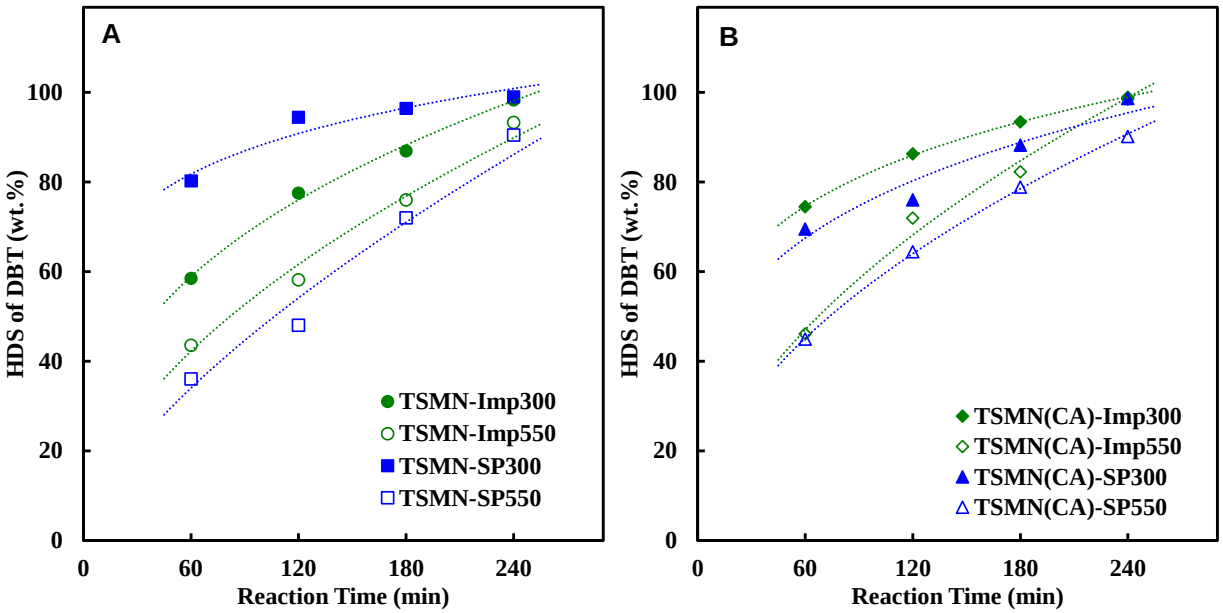

Figure 3-12 Activities of Synthesized Catalysts for the HDS of DBT at Different Contact Times.

3.3.12.1 Reaction Pathways

The HDS of DBT occurs via two parallel pathways as illustrated in **Figure 3-13**: (i) direct desulfurization (DDS) or hydrogenolysis by C-S bond cleavage in a single step; or (ii) hydrogenation (HYD) in 2-3 steps through the hydrogenation of one of the phenyl rings followed by C-S bond cleavage [68]. The HDS of DBT via the DDS pathway yields biphenyl (BP) and H_2S as final products. However, the HYD pathway results in the formation of intermediates, such as tetrahydro dibenzothiophene (THDBT) and hexahydro dibenzothiophene (HHDBT), followed by fast desulfurization to form cyclohexyl benzene (CHB). Because the DDS pathway consumes substantially less hydrogen, it is the preferred route.

The analysis of hydrocarbon products obtained after one hour of reaction time over different synthesized catalysts is presented in **Table 3-6**. BP is the predominant compound in all products, indicating that DDS is the generally preferred route. However, there are significant differences in the preference for DDS among the synthesized catalysts as revealed by the BP/CHB ratio in the products. When a complexing agent is not used, the catalysts calcined at 300°C exhibit approximately twice the BP/CHB ratio of catalysts calcined at 550°C. The catalysts prepared by the SP method and calcined at 300°C show exceptional preference for the DDS route with a BP/CHB ratio of approximately 10. The use of a complexing agent significantly reduces the BP/CHB ratio, which indicates that the direct scission of the C-S bond is not effective and that the hydrogenation reaction is also enhanced. The effect of calcination temperature on the BP/CHB ratio is not significant when complexing is used.

The 4-HDBT intermediate is detected only in products obtained from TSMN-Imp550, TSMN-SP550, and TSMN(CA)-SP550. These are low-activity catalysts, which also result in higher sulfur contents (>150 ppm) in the products even after a contact time of 4 h (**Table 3-5**).

Table 3-6 Catalyst Performance Test Results: Product Distribution.

Catalysts	Product Distribution (wt.%)			BP/CHB
	CHB	BP	4HDBT	
TSMN-Imp300	19.91	80.09	-	4.02
TSMN-Imp550	31.61	61.72	6.67	1.95
TSMN-SP300	9.12	90.89	-	9.97
TSMN-SP550	14.63	76.42	8.95	5.22
TSMN(CA)-Imp300	32.13	67.87	-	2.11
TSMN(CA)-Imp550	28.52	71.48	-	2.51
TSMN(CA)-SP300	14.70	85.30	-	5.80
TSMN(CA)-SP550	14.94	76.49	8.57	5.12

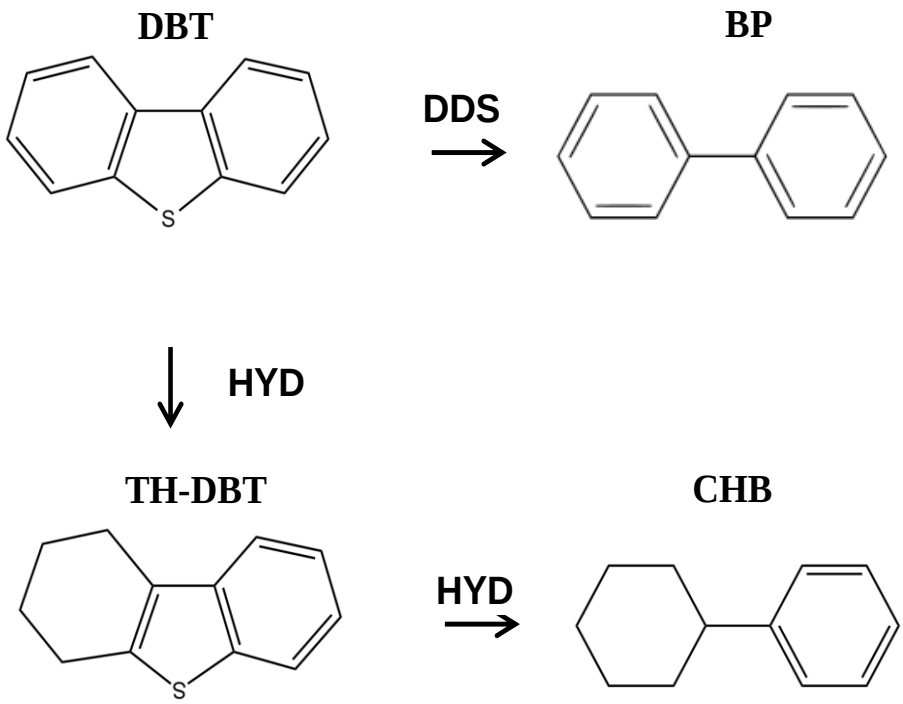

Figure 3-13 Reaction Pathways for the HDS of DBT.

3.3.12.2 HDS kinetics

The HDS rates were calculated assuming pseudo-first order kinetics, and the values of the reaction constant, k (min^{-1}), were determined using the initial conversion values – those obtained after the first hour of the reaction. The results presented in **Table 3-7** show that the value of the HDS rate constant is 13.5×10^{-3} min^{-1} for the TSMN-Imp300 catalyst. This value compares well with the reported rate constant of 18.3×10^{-3} min^{-1} for the HDS of DBT at 350°C over a $CoMo/Al_2O_3$ catalyst [44].

3.3.13 Effect of Calcination Temperature:

The decrease in the calcination temperature from 550°C to 300°C results in consistently higher HDS rates. The catalyst prepared by the impregnation method without the complexing agent (TSMN-Imp550) exhibits an HDS rate of 8.4×10^{-3} min^{-1}, which is increased by approximately 61% to 13.5×10^{-3} min^{-1} when the calcination temperature is reduced (TSMN-Imp300). The catalyst prepared by the SP method and calcined at 300°C (TSMN-SP300) exhibits the highest rate constant of 25.6×10^{-3} min^{-1}, which is approximately four times the rate obtained with TSMN-SP550. The trend of a higher HDS rate for the catalysts calcined at 300°C is also observed for the catalysts prepared using a complexing agent. However, the increase is moderately higher for the catalysts prepared by the impregnation method (47%) compared with those prepared by the SP method (41%). It seems that the addition of a complexing agent offsets some of the benefits of a lower calcination temperature.

The rate constants for the DDS and HYD pathways are presented in Table 3-7 as k_{DDS} and k_{HYD}, respectively. In addition to the significant increase in the HDS rates, a lower calcination temperature is effective in promoting HDS by the DDS pathway. The catalyst prepared by the impregnation method without the complexing agent (TSMN-Imp550) exhibits a k_{DDS}/k_{HYD} ratio of 1.7, which is increased by three times when the calcination temperature is reduced (TSMN-Imp300). The catalyst prepared by the SP method and calcined at 300°C (TSMN-SP300) exhibits the highest k_{DDS}/k_{HYD} ratio of 17.2, which is approximately five times the rate obtained with TSMN-SP550. It should be noted that while k_{DDS} increases four times due to a reduction in the calcination temperature, k_{HYD} remains unchanged. This observation indicates that the active sites for DDS may be different from those in the HYD pathway.

The trend of a higher HDS rate for the catalysts calcined at 300°C is also observed for the catalysts prepared by the SP method using a complexing agent. However, the increase is not as drastic as that observed with the catalysts prepared without the complexing agent.

As shown in Section 3.1, the catalyst prepared by the SP method and calcined at 300°C (TSMN-SP300) possesses a significantly higher surface area (460 m^2/g) and pore volume (0.66 cm^3/g) compared to the catalyst calcined at 550°C (TSMN-SP550). This method provides a much better dispersion of active metals and better accessibility to reactants. TSMN-SP300 also exhibits the highest surface acidity among the catalysts prepared without the addition of a complexing agent. XRD results also show that the catalysts calcined at 300°C exhibit better dispersion of active metals on the support and the presence of small crystallites. Similar trends are observed by Raman spectroscopy and FTIR spectroscopy. These factors can be attributed to the highest overall HDS rate of TSMN-SP300 as well as the increased DDS activity.

3.3.14 Effect of Preparation Method:

Comparison of the HDS rates exhibited by catalysts prepared by the two methods investigated in this study, i.e., impregnation and SP, provides insight into the efficacy of each method. The SP approach presents new, simple, and easy steps in catalyst design and preparation, which leads to low-cost catalyst design and the incorporation of the active phase within the mesoporous framework. The catalyst prepared by the SP method exhibits higher HDS activity compared to catalyst prepared by impregnation when the calcination temperature is 300°C. The overall HDS rate constant of TSMN-SP300 is approximately 90% higher than the rate constant of TSMN-Imp300. Moreover, HDS by DDS is significantly enhanced by TSMN-SP300, resulting in a 3.5-fold increase in the $\boldsymbol{k}_{DDS}/\boldsymbol{k}_{HYD}$ ratio. However, when the calcination temperature is increased to 550°C, the catalyst prepared by the SP method exhibits lower activity, and the benefits of the SP method in terms of the $\boldsymbol{k}_{DDS}/\boldsymbol{k}_{HYD}$ ratio are drastically reduced.

The main differences in the characteristics of the catalysts prepared by the SP and impregnation methods are the significantly higher surface area (especially the external surface area) and pore volume for SP catalysts. The catalysts prepared by the SP method also possess higher surface acidity, which can enhance C-S bond scission and result in higher DDS.

The use of a complexing agent improves the performance of catalysts prepared by the impregnation method. The increase in the HDS rate from TSMN-Imp 300 to TSMN(CA)-Imp300 is 46%. However, this improvement is reduced to only 24% when the calcination temperature is increased to 550°C. The use of a complexing agent affected the performance of catalysts prepared by the SP method in a different manner. Although the complexing agent is beneficial for the overall HDS rate when the calcination temperature is 550°C, it exhibits a negative impact at the calcination temperature of 300°C. However, the $\boldsymbol{k}_{DDS}/\boldsymbol{k}_{HYD}$ ratio of 8.3 for TSMN(CA)-SP300 is the highest among all catalysts prepared using a complexing agent.

The incorporation of a complexing agent improves the dispersion of active metals as observed by XRD and Raman spectroscopy. The impact of better dispersion is evident from the improved HDS activity of catalysts prepared by the impregnation method, i.e., by comparing TSMN(CA)-Imp300 and TSMN(CA)-Imp550 to TSMN-Imp300 and TSMN-Imp550, respectively. However, the catalysts prepared by the SP method are negatively affected by the complexing agent.

In general, the HDS activities of the SP-approach catalysts at a low calcination temperature are better than the other catalysts within the series, and it is noteworthy that better performance could be achieved without the use of a complexing agent to aid the dispersion of active metals. Therefore, the preparation of supported HDS catalysts at a low calcination temperature leads to deep desulfurization within a short period of time could be attributed to high dispersion of the active phase, as indicated by the absence of crystalline phases in Raman spectroscopy and XRD analyses.

Table 3-7 First-Order Rate Constants for HDS of DBT at 350°C.

Catalysts	k_{HDS} x 10^3 (min^{-1})	k_{DDS} x 10^3 (min^{-1})	k_{HYD} x 10^3 (min^{-1})	k_{DDS}/k_{HYD}
TSMN-Imp300	13.6	10.5	2.1	5.1
TSMN-Imp550	8.4	5.2	3.0	1.7
TSMN-SP300	25.6	21.8	1.4	17.2
TSMN-SP550	6.5	5.4	1.5	3.6
TSMN(CA)-Imp300	19.7	11.7	4.6	2.6
TSMN(CA)-Imp550	10.4	6.7	2.4	2.8
TSMN(CA)-SP300	15.8	15.0	1.8	8.3
TSMN(CA)-SP550	9.3	7.0	1.9	3.8

3.4 Conclusions

The single-pot (SP) synthesis of NiMo-supported Ti-SBA-15 HDS catalyst was successfully developed, and the catalyst was evaluated for the HDS of dibenzothiophene. The results with this catalyst were compared with those using the established impregnation approach. The catalyst from the SP approach exhibited a great potential to minimize the time involved in catalyst design and preparation. Furthermore, the use of a complexing agent to improve dispersion and prevent the formation of crystalline $NiMoO_4$ was unnecessary. Overall, the SP catalyst formed at a low calcination temperature (TSMN-SP300) possessed superior catalytic performance and selectivity for direct desulfurization compared with the other studied catalysts. The dispersion, surface acidity, and textural properties were contributing factors that improved catalytic efficiency.

ACKNOWLEDGMENTS

The authors acknowledged the support provided by King Fahd University of Petroleum & Minerals (KFUPM) for funding this work through project No. DSR NUS15105. Authors would like to acknowledge the efforts of Dr. Osama Shekhah of Advanced Membranes and Porous Materials center (AMPM), King Abdullah University of Science and Technology (KAUST) for HRTEM analysis.

Chapter 4

Hydrodesulfurization activity controlled by hydrothermal synthesis temperature and molybdenum loading of NiMo active phase supported over SBA-15

ABSTRACT

We report herein the investigation of catalytic activity on the hydrothermal synthesis temperature (60 – 120 ^{o}C) and molybdenum loading (5 -13 wt. %) of NiMo catalyst supported over titanium-modified mesoporous silica (Ti-SBA-15) for simultaneous hydrodesulfurization (HDS) of dibenzothiophene (DBT) and methyldibenzothiophene (MDBT) in dodecane. It was found that the dispersion of NiMo active phase in one-pot synthesis is size-dependent and mostly controlled by hydrothermal synthesis temperature for efficient HDS catalytic performance. The as-developed catalysts were characterized by N_2-physiosorption, X-ray diffraction (XRD), temperature programmed techniques and scanning electron microscope. The XRD analysis revealed that MoO_3 particles agglomerate to form high crystalline phase, as a function of hydrothermal temperature and Mo-loading, which in turn affects the textural properties, number of active sites and reduction temperature. The catalytic performance for simultaneous HDS of dibenzothiophene and 4-methyldibenzothiophene was evaluated at 350 ^{o}C and 5 MPa in a batch autoclave reactor. Results show that hydrothermal synthesis temperature of Ti-SBA-15-NiMo catalyst above 100 ^{o}C leads to marked decrease in catalytic performance. The effect of Mo loading on catalytic performance was also influenced by the hydrothermal synthesis temperature. Hydrothermal temperature of 80 ^{o}C and 13 wt. % Mo loading resulted in improved overall HDS rate as well as HDS by direct desulfurization (DDS) route.

4.1 Introduction

Sulfur content in transportation fuels must be as low as 10-15 ppm to meet the environment-driven regulations promulgated by many industrially developed countries. It is expected that the future catalytic converters application in automobiles requires sulfur-free fuels [3, 16]. In view of such stringent sulfur level requirements, more robust and efficient catalysts are necessary for ultra-deep hydrodesulfurization (UD-HDS) of transportation fuels. Hence, research is focused on designing novel supported hydrotreating catalysts [14, 15]. Several published articles have reported the use of composite supports, such as SiO_2-Al_2O_3, ZrO_2, ZrO_2-Al_2O_3, TiO_2-ZrO_2, TiO_2-SiO_2, TiO_2-Al_2O_3. However, their low surface area and support-metal interactions limit their catalytic performance [69-75].

One of the promising approaches is to employ high surface area mesoporous silica in the synthesis of HDS catalysts as an alternative to γ-alumina and composite supports [35]. This approach involves incorporation of metals (Al, Ti, Zr) and complexing agents, with a view to overcome the amorphous nature of the silica and facilitate dispersion of active metals and surface modification to improve acidity [6]. We have recently developed and reported a new systematic single-pot (SP) approach which improves the dispersion of active metals on a porous support, reduce the steps in catalysts preparation, and prevent the loss of textural properties that are necessary for catalytic efficiency of HDS catalysts [76]. However, one of the technical challenges associated with SP synthesis approach of metal modified SBA-15 NiMo catalysts is the formation of crystalline NiMo phase.

Due to its flexibility to control size, morphology and surface chemistry of material by changing the synthesis parameters (temperature, solvent, pH, synthesis aging time etc.), hydrothermal synthesis method has been adopted for synthesis of various supports (Al_2O_3, SiO_2) [48, 77, 78], solid catalysts (zeolites) [79, 80] and metal oxides (ZnO, MoO_3, WO_3, NiO, TiO_2, MgO, etc.) [81-86]. Hydrothermal synthesis temperature (HTsynT) is considered as a key factor controlling the nucleation and crystallization growth of as-synthesized catalyst material [87].

Systematic approach of changing the hydrothermal synthesis temperature (HT-synT), in addition to calcination temperature, can prevent the formation of crystalline phase, and in essence prevent blockage of micropores within the mesopores of SBA-15. Such an approach is expected to result

in better catalytic performance compared to impregnation via fast diffusion of reactant molecules through mesopores and adsorption on the active sites embedded within the micropores of the catalyst [88, 89]. It seems there exist an optimum hydrothermal synthesis temperature (HTsynT) that prevents formation of agglomerated MoO_3 and/or $NiMoO_4$ particles in HDS catalysts. Hydrothermally synthesized crystalline unsupported MoS_2 catalysts have been reported, and the effect of HTsynT with respect to crystallization, morphology and activity is highlighted [87, 90, 91], but this approach is rarely reported for supported Ni(Co)Mo(W) catalysts, especially for (un)modified-SBA-15 HDS catalysts. It has been reported that hydrothermally synthesized NiW/γ-Al_2O_3 catalyst achieved the same HDS activity as a commercial NiW/γ-Al_2O_3 catalyst containing higher loading of active species [92].

To the best of our knowledge, the effect of hydrothermal synthesis temperature on NiMo supported on Ti-SBA-15 prepared by single-pot (SP) approach has not been reported. This study aims at finding optimum hydrothermal synthesis temperature to obtain highly dispersed NiMo HDS catalyst and prevention of agglomerated active species for efficient desulfurization of refractory organosulfur compounds in single-pot approach recently reported by our group [76].

4.2 Experimental Section

4.2.1 Materials

Tetraethylorthosilicate (TEOS) $(C_2H_5O)_4Si$ as silica source, pluronic P123 PEO_{20}-PPO_{70}-PEO_{20} triblock copolymer as structural directing agent, nickel nitrate hexahydrate (99 %) as nickel precursor, and titanium isopropoxide (97 %) as titanium source were purchased from Sigma-Aldrich. Ammonium molybdate (V1) tetrahydrate (99 %) was obtained from ACROS organics. High-purity deionized water (18 μS/cm) was produced in-house using *Thermo Scientific Barnstead NANOPURE* after distillation with a *Labstrong FiSTREEM^{TM} II 2S Glass Still* distiller.

4.2.2 Synthesis of Ti-SBA-15-NiMo

NiMo supported on Ti-SBA-15 catalyst by single-pot approach is obtained as described in our previous work [14]. The typical synthesis procedure involves dissolution of 1g of (P123) triblock copolymer in 30 g of 2M HCl and 7.5g DI-H_2O and stirred vigorously for 1 h before addition of TEOS (2.08 g) and equivalent amount of Ti-precursor, respectively, to obtain Si/Ti ratio (10). The above mixture was stirred between 18h and 20 h before addition of molybdenum and nickel with their respective precursors, and continued to stir for additional 4 h. The mixture obtained after 24 h of stirring was transferred into teflon autoclave and subjected into hydrothermal (HT) synthesis between 60 ^oC and 120 ^oC for another 24 h. The light-yellow solid was centrifuged once without further washing, to avoid leaching of active phase(s) into solvent, and dried in oven at 100 ^oC for 12 h, before final calcination at 300 ^oC. The obtained non-sulfided HDS catalyst was denoted as HTy*(x)*, where y represents HT-temperature, and *x* in parenthesis denotes Mo loading in weight percent. The nickel content in all the synthesized catalysts is maintained at about *Ca*. 3 wt. %. A series of seven formulations were prepared as listed in **Table 1**.

4.2.3 Catalyst Characterization

The textural properties were determined using Micromeritics ASAP 2020 analyzer. The samples were degassed at 250 ^oC for 3 h under vacuum to remove traces of adsorbed moisture and impurities, prior to N_2-physisorption measurement. Crystallinity of the active phase was examined by Rigaku X-ray diffraction (XRD) using CuKα 3 ^oC/min scan rate using 0.03 width.

The active sites and surface acidity characteristics were determined by temperature programmed desorption (TPD) using 10 wt. % ammonia (NH_3) as adsorbate molecules on a Micromeritics Chemisorb 2750. Approximately 50 mg of NiMo-oxide Ti-SBA-15 catalyst was loaded into a quartz tube, and was purged with high purity helium at 600°C for 30 min before cooling to 100°C. Ammonia was adsorbed on the catalyst at 100°C for a period of 30 min, followed by purging by helium for 60 min to remove any physisorbed adsorbate. Desorption of NH_3 was accomplished by heating the furnace up to 800°C at 10°C/min. The amount of NH_3 adsorbed and desorbed was recorded with a thermal conductivity detector (TCD).

The reducible temperature of the catalysts was determined by temperature-programmed reduction with hydrogen as the adsorbate using Micromeritics (Autochem II-2920) chemisorption analyzer. About 50 mg of the prepared catalyst previously calcined at 300°C was pre-treated for one hour in high-purity helium at 400°C and then cooled to ambient temperature. The reduction temperature was measured by linearly increasing the furnace temperature to 1000°C at 10°C/min under a steady flow (50 ml/min) of 10% H_2 in helium. The consumption of H_2 at the reducible temperature(s) was recorded by a TCD.

Morphology examination of the Ti-SBA-15-NiMo catalysts was conducted on the TESCAN LYRA 3, using secondary electron (SE) and backscattered electron (BSE) modes at an accelerating voltage of 30 kV. The unit was equipped with an energy-dispersive X-ray spectrometer (Oxford Instruments) detector for elemental analysis.

4.2.4 Activity Measurement

The pelletized and sized (300-500 µm) catalyst samples were reduced in a constant flow of 10% H_2/He at 400^{o}C for 2.5 h to ensure conversion of active metals to metallic form. The presulfiding was carried out using 2 wt.% CS_2 solution in *n*-hexane at 350^{o}C for 6 h. The catalytic activity was measured at 350 ^{o}C in a batch reactor (Parr 4576B) under initial hydrogen pressure of 5 MPa. About 250 mg of sulfided catalyst was added into 100 ml of a simulated fuel containing 1000 ppm-S each of dibenzothiophene (DBT) and 4-methyldibenzothiophene (4-MDBT) in dodecane. Each test was conducted for four hours and aliquots were withdrawn at one hour intervals for quantification and qualification by gas chromatograph sulfur chemiluminiscence detector (GC-SCD) and mass spectrometer (GC-MS), respectively.

4.3 Results and Discussion

4.3.1 Textural Properties

The textural properties of different HTsynT and Mo-loading catalysts were estimated by Brunauer, Emmett, and Teller (BET) and the Barrett, Joyner, and Halenda (BJH-adsorption) methods. The results are presented in **Table 4-1**. Ti-SBA-15 support exhibited high surface area and pore volume, with 6.2 nm pore size. Incorporation of NiMo active phase precursor alongside the support in a single-pot (SP) synthesis changed the textural properties as a function of HTsynT and Mo loading concentrations. At a Mo loading of 8 wt.%, the increase in HTsynT from 60^{o}C to 120 ^{o}C caused a significant loss of surface area with increase in average pore size. The effect is more pronounced when the HTsynT is between 100 ^{o}C and 120 ^{o}C. Compared to Ti-SBA-15, the loss in surface was more than 65% for HT120(*8*). This observation can be related to the formation of aggregated particles of active phase on the support, which in turn covered the surface and block the pores, because the particles gained more energy to fuse and become larger particles at higher temperatures.

Furthermore, a change in Mo concentration on the support affected the textural properties significantly. The surface area of HT80 catalysts were reduced by more than 30% when the Mo loading content was increased from 5 wt.% to 13 wt.%. Similar trend was observed with other HTsynT cases, with certain loss of surface area and pore volume. However, the reduction in surface area for HT(100) catalysts was less than HT(80) catalysts. This phenomenon can be attributed to the ability of MoO_3 particles to grow inside and/or outside the support matrix, and at higher Mo concentration the tendency for agglomeration is higher due to particles' proximity and surface density.

As shown in **Figure 4-1**, the isotherms obtained represents type IV of mesoporous material, with two desorption steps, which is typical of SBA-15 and presence of plugged nanoparticles on the NiMo supported on Ti-SBA-15 [26]. The isotherms at higher and lower Mo wt. % loading other than 8 wt. % are presented in **Figure 4-2.**

Table 4-1 Textural properties of supports and catalysts.

Sample Code	**BET Surface Area (m^2/g)**	**Microporous Surface Area (m^2/g)**	**External Surface Area (m^2/g)**	**Total Pore Volume (cm^3/g)**	**Average Pore Size (nm)**
Ti-SBA-15	903	174	729	1.10	6.2
HT60*(8)*	667	105	562	0.83	6.2
HT80*(8)*	496	54	442	0.77	6.8
HT100*(8)*	421	39	382	0.86	8.1
HT120*(8)*	282	30	252	0.71	10.7
HT80*(5)*	611	114	497	0.76	6.2
HT80*(13)*	406	40	366	0.72	7.3
HT100*(13)*	398	29	369	0.66	6.5

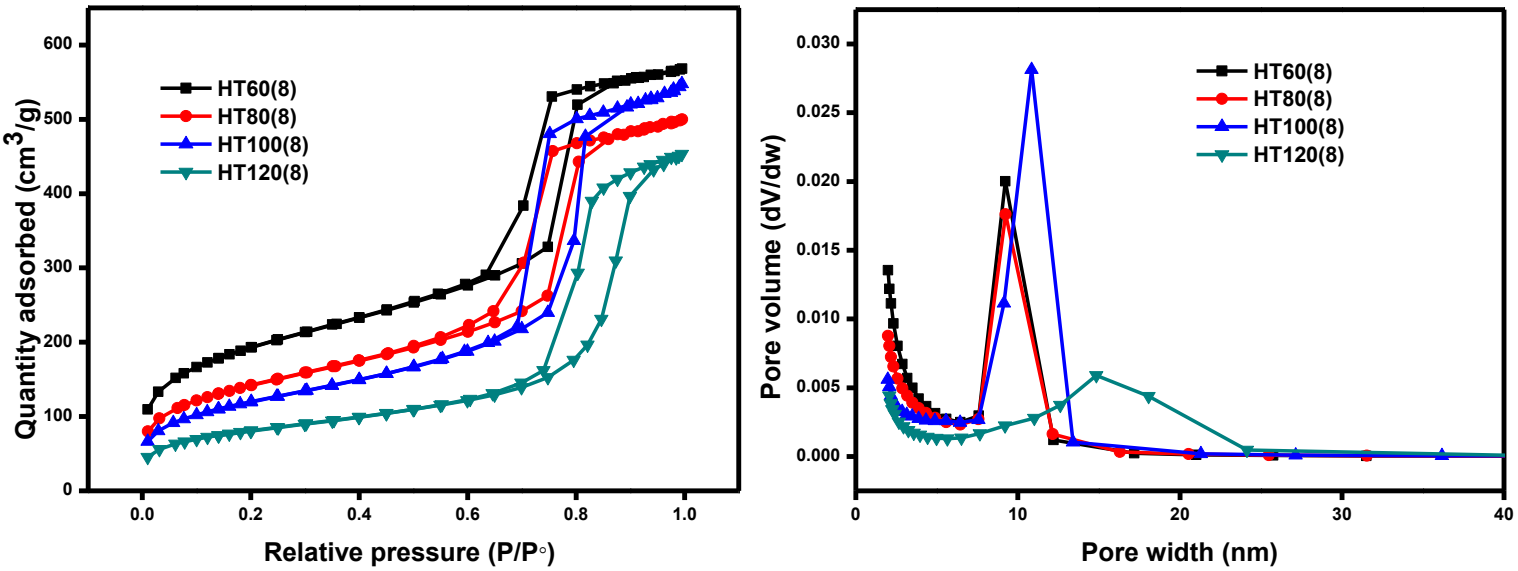

Figure 4-1 Nitrogen adsorption isotherms by BET (left) and pore-volume-size isotherms by BJH (right) for Ti-SBA-15-NiMo catalysts with 8 wt.% Mo loading at different hydrothermal temperatures.

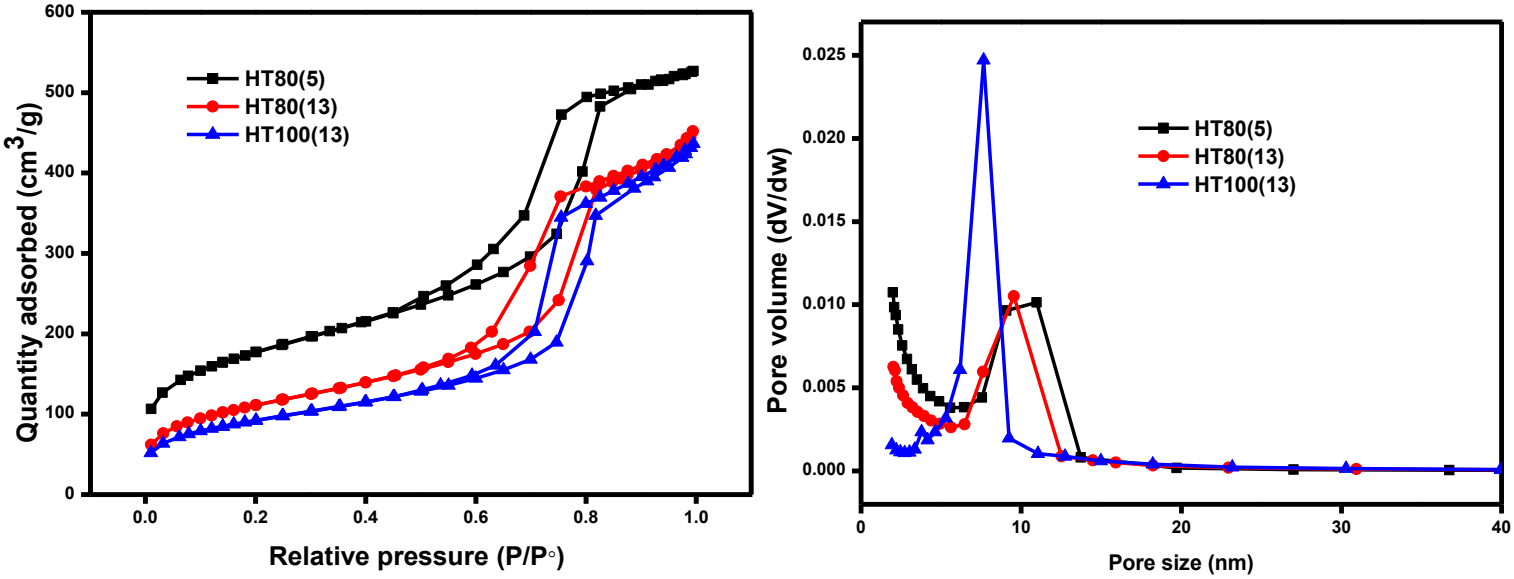

Figure 4-2 Surface area analysis isotherms by BET (left) and pore-volume-size isotherms by BJH (right) for Ti-SBA-15-NiMo catalysts at 5 and 13 wt.% molybdenum.

4.3.2 X-Ray Diffraction (XRD) Analysis of Oxide Catalysts

Dispersion of active phase(s) of Ti-SBA-NiMo catalysts is determined by wide angle powder X-ray diffraction (XRD). As shown in **Figure 4-3**, the diffractograms reflect the effect of HT-synT on the crystallite size of MoO_3 on the Ti-SBA-15. Crystalline phase of MoO_3 was observed at 8 wt. % even when the catalysts were calcined at lower temperature (300 ^oC) for 6 h. This result is in contrast to that reported by Huang *et al.* [93] which claimed that no reflection of crystalline MoO_3 occur below 13 wt.% (i.e. at 8%), although, the difference in results might be due to longer calcination hours (6 h) used in our study, despite being low (300 ^oC) compared to 500 ^oC at 3 h reported by the group.

The crystallinity and crystallite size is increased as the HT-synT increases. Therefore, the degree of dispersion, which is a measure of number of active sites, is not favored by high synthesis temperature. The XRD analysis reveals that the small crystallite size of active phase at 8 wt.% Mo loading was obtained between 60^oC and 80 ^oC , and beyond this temperature the particle size becomes larger due to aggregation of MoO_3 particles. In addition, increase in Mo loading on the support is another factor that forms agglomerated MoO_3 particles irrespective of hydrothermal synthesis temperature, but at different degrees **Figure 4-4**.

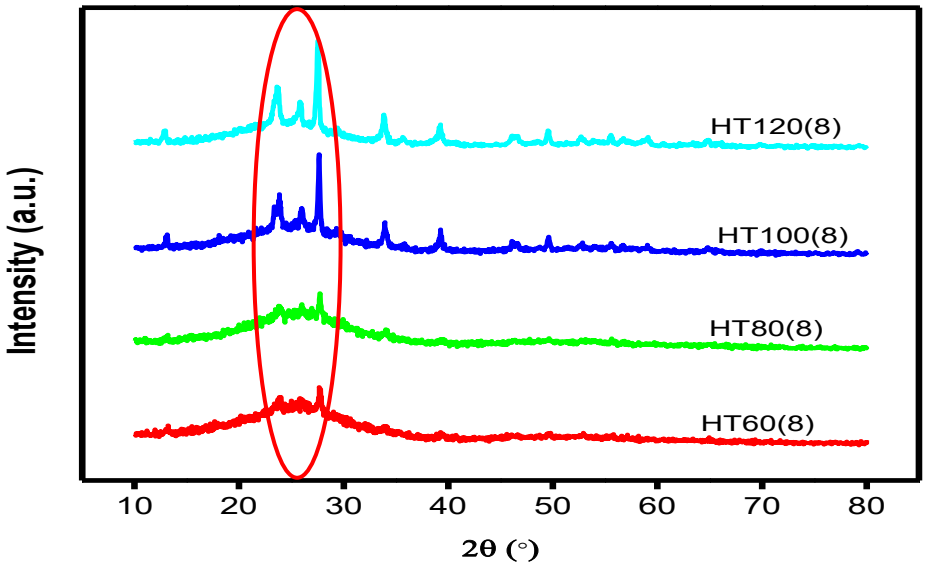

Figure 4-3 X-ray diffraction (XRD) analysis of hydrothermally synthesized HDS catalysts with 8 wt.% Mo loading at different hydrothermal temperatures.

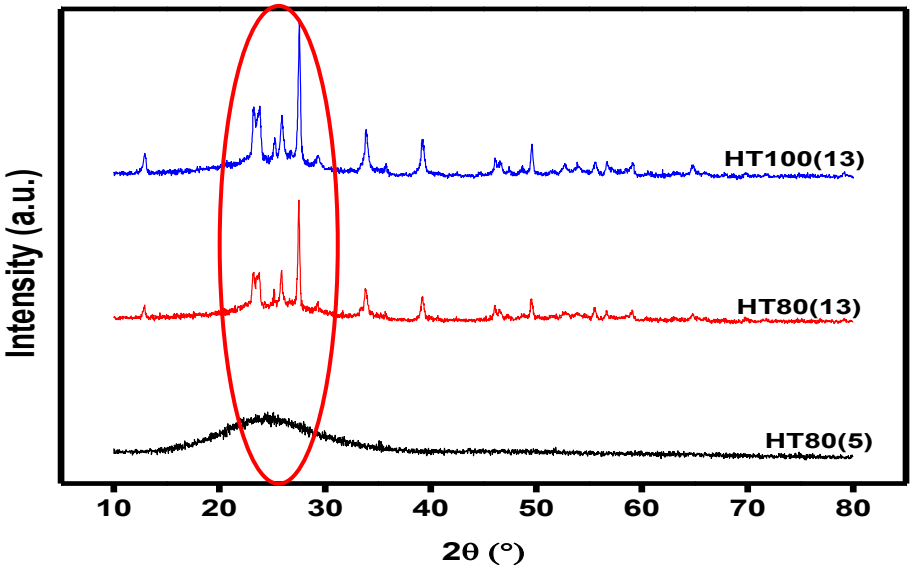

Figure 4-4 X-ray diffraction (XRD) analysis of hydrothermally synthesized HDS catalysts at 5 and 13 wt.% molybdenum.

4.3.3 Temperature Programmed Desorption

TPD analysis was carried out to quantitatively determine the strength, the number and the type of active sites using NH_3 as probe molecules. The surface acidity can be categorized into weak (< 200 ^oC), moderate (200-350 ^oC) and strong acidity (> 350 ^oC) [41]. The results, presented in **Table 4-2 and Figure 4-5,** revealed that the catalysts possessed moderate acidity with peaks between 227 ^oC and 246 ^oC. In addition, a strong acidity character with lesser intensity was observed at higher temperatures (650-770 ^oC). With 8 wt.% Mo loading, the total acidity increased with HT-SynT up to 80^oC followed a drop with further increase in HT-SynT. Hence, the impact of HT-SynT on the dispersion and active sites of NiMo supported Ti-SBA-15 catalysts was established from XRD results as well as from TPD data.

The effect of Mo-loading is used to establish the optimum loading content for maximum active phase dispersion with higher number of active sites. Comparison of TPD results of HT80 with different Mo loading indicates that HT80*(8)* possess highest total acidity. Similar trend was observed for HT100*(8)* as compared to HT100*(13)*. Analysis of these results along with XRD data show that at low concentration of active species better dispersion may be obtained with low surface acidity, and optimum balance must be achieved to obtain high dispersion and surface acidity, for better catalytic performance. Furthermore, the HT80*(13)* with high XRD peak intensities as a measure of poor dispersion, shows lower surface acidity, which can be correlated to lower number of active sites. In this case, there is a direct relationship between the dispersion of active phase and the number of active sites available for catalytic activities (See supporting **Figure 4-6**). In essence, the HTsynT of 80 ^oC seems most suitable to form highly dispersed NiMo phase with high number of active sites.

The TPD data presented in **Table 4-2** can be used to correlate the amount NH_3 of ammonia desorbed at respective temperature to catalysts' dispersion and number of active sites provided by surface acidity. Based on the results, HT80*(8)* possessed high significant surface acidity character than others, and the surface acidity in decreasing order when the effect of HTsynT was varied follows: HT80*(8)* > HT60*(8)* > HT100*(8)* > HT120*(8*). When the amount of Mo-loading content was varied, the trend in surface acidity was as follows: HT80*(8)* > HT80*(5)* > HT80*(13)*. Generally, the increase in HTsynT favors active phase agglomeration as observed between 100 ^oC

and 120 ºC, and the optimum temperature that forms metastable hexagonal active phase was between 60 and 80 ºC [93]. Therefore, HT80*(8)* is expected to have better catalytic activity and selectivity as compared to others.

Table 4-2 Temperature programmed desorption by ammonia.

Catalysts	TPD: NH_3 desorbed				
	Peak Temperature (200-350 °C)	**Amount (mmol/g)**	**Peak Temperature (> 350 °C)**	**Amount (mmol/g)**	**Total (mmol/g)**
HT60*(8)*	233	0.336	707	0.022	0.358
HT80*(8)*	230	0.348	713	0.018	0.366
HT100*(8)*	235	0.290	698	0.020	0.310
HT120*(8)*	246	0.142	673	0.012	0.154
HT80*(5)*	238	0.110	770	0.220	0.330
HT80*(13)*	228	0.115	654	0.004	0.119
HT100*(13)*	227	0.133	670	0.011	0.144

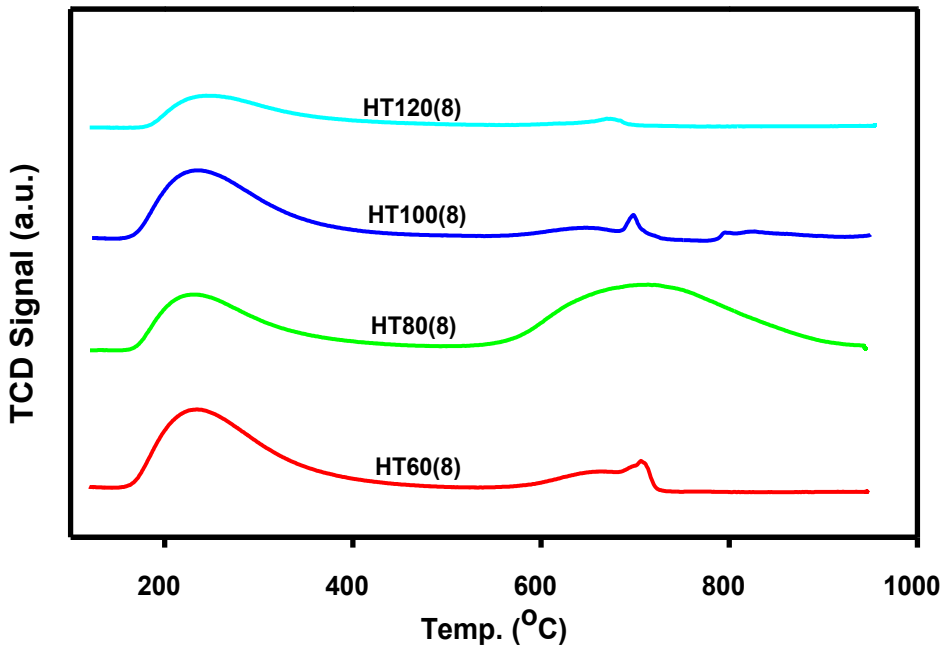

Figure 4-5 Temperature programmed desorption analysis by ammonia of HDS catalysts with 8 wt.% Mo loading at different hydrothermal temperatures.

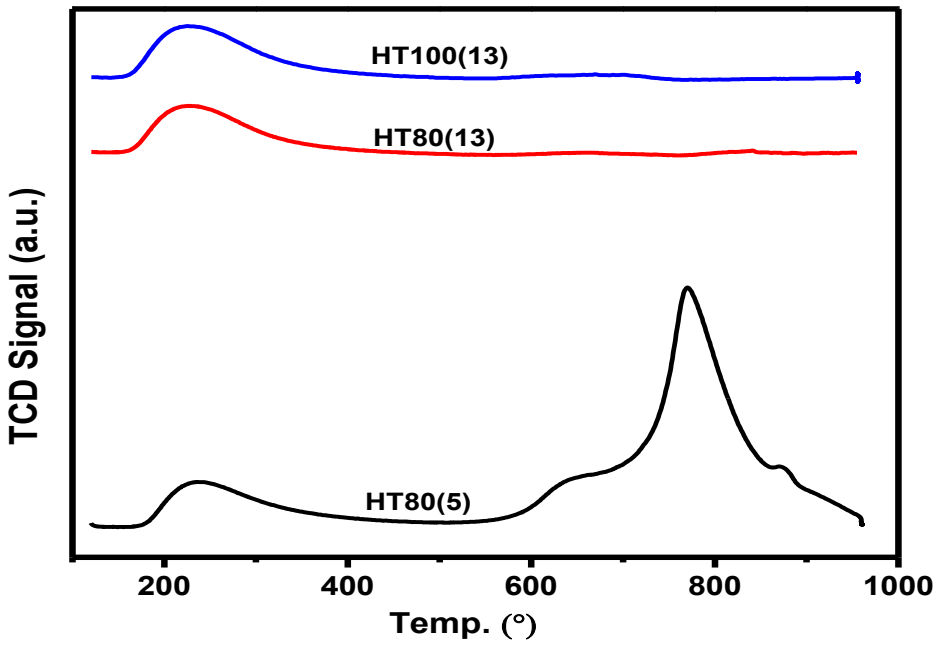

Figure 4-6 Temperature programmed desorption analysis by ammonia of hydrothermally synthesized HDS catalysts at 5 and 13 wt.% molybdenum.

4.3.4 Temperature Programmed Reduction

TPR analysis of oxide NiMo catalysts revealed the effect of HT-SynT on the reducibility potential and the strong metal support interaction (SMSI). As observed from **Figure 4-7**, the H_2 reduction of octahedral Mo species characteristic (from Mo^{6+} to Mo^{4+}) is observed between peak temperatures of 507 ^oC and 520 ^oC. The characteristic second reduction step of molybdenum oxide from Mo^{4+} to Mo^0 is observed between 647 ^oC and 687 ^oC [94]. It is observed that the reduction temperature of the catalyst prepared at 80 ^oC, within the same loading content (8 wt. %) is relatively lower compared to others. Moreover, the quantitative amount of H_2 consumed during TPR experiment is higher, which confirms that the active species are embedded within the structure of support and not outside, as opposed the observation for higher synthesis temperature (See **Table 4-3**). Furthermore, increase in loading percent of Mo from 8 wt. % to 13 wt. % resulted in the formation of MoO_3 particle at the external surface of Ti-SBA-15 support, and was evident by low consumption of H_2 at reduction temperatures. Active phase (NiMo) particles at low Mo loading concentration, such as HT80*(5)*, were found to be confined within Ti-SBA-15 matrix as observed by the decrease in the reduction temperature, but quantitative amount on the support is lower and easily accessible [95]. There is possibility of support-metal interaction (SMI) as reduction temperature was shifted to a relatively higher value, 525 ^oC and 725-740 ^oC for first and subsequent reduction of Mo species, respectively. (See **Figure 4-8**) [19, 96]. In essence, the lower reducible temperature for H_2 consumption can be ascribed to higher degree of active dispersion and the number of active sites that will be necessary for catalytic activity and selectivity.

Table 4-3 Temperature programmed reduction analysis by hydrogen.

Catalyst	TPR: H_2-consumption			
	Peak Temperature(s) (°C)	**Amount (mmol/g)**	**Peak Temperature(s) (°C)**	**Amount (mmol/g)**
HT60*(8)*	520	393.4	680	481.7
HT80*(8)*	510	516.6	649	533.2
HT100*(8)*	517	413.5	685	458.8
HT120*(8)*	507	412.6	687	380.3
HT80*(5)*	436	214.5	663	210.8
HT80*(13)*	525	19.91	740	117.2
HT100*(13)*	524	0.57	725	79.5

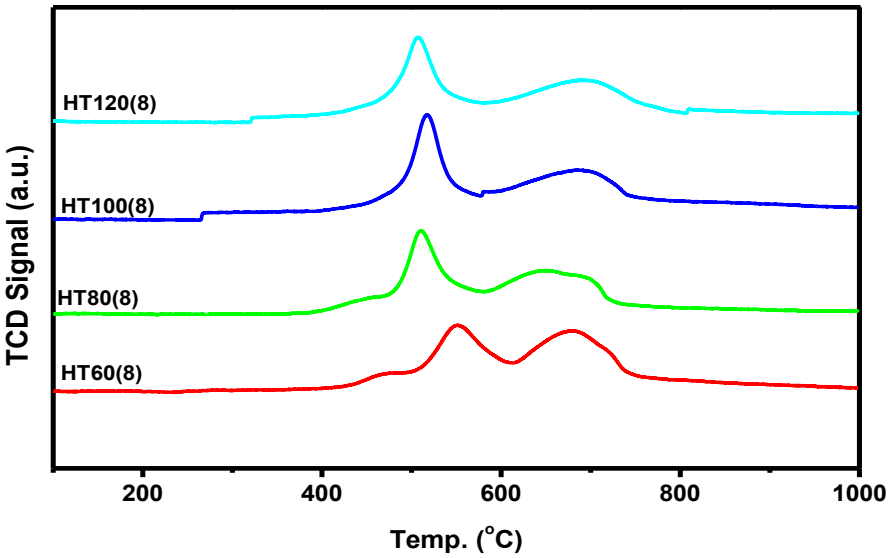

Figure 4-7 Temperature programmed reduction analysis by hydrogen of HDS catalysts with 8 wt.% Mo loading at different hydrothermal temperatures.

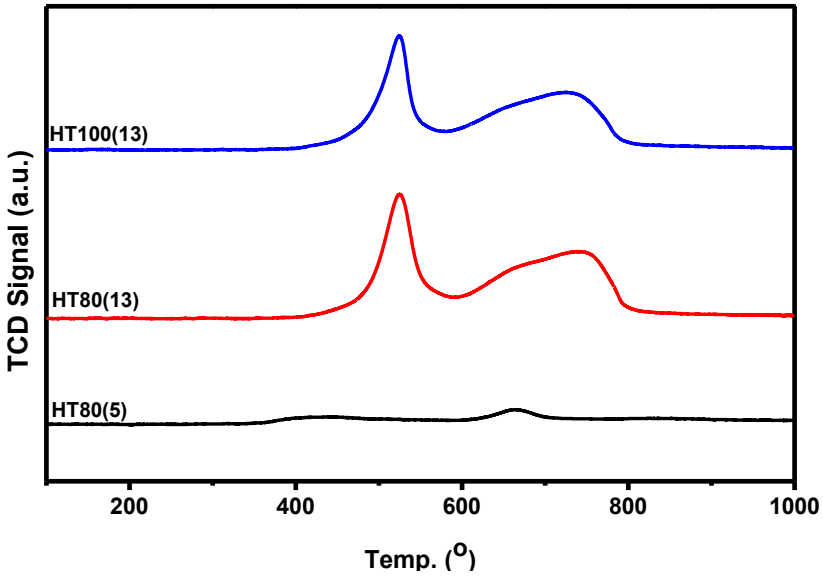

Figure 4-8 Temperature programmed reduction analysis by hydrogen of hydrothermally synthesized HDS catalysts at 5 and 13 wt.% molybdenum.

4.3.5 Morphological Examination

Scanning electron microscope (SEM) was used to conduct morphological examination of the catalysts. As shown in **Figure 4-9**, the SEM images confirm high crystallinity and low dispersion at higher HTsynT, and high dispersion and low crystallinity of active phase(s) at lower HTsynT. Increasing HTsynT resulted in the formation of cubical flat-sheet extra-particles on the surface of the support, which is due to MoO_3 and the effect is more pronounced at higher synthesis temperatures between 100 ^oC and 120 ^oC, when the loading of Mo was kept at 8 wt.%. This observation is attributed to high crystalline phases of MoO_3 as observed by XRD, and caused the loss of textural properties of the oxide HDS catalysts as explained by N2-physisorption analysis.

On the hand, Mo loading is another factor for the formation of crystalline phases on the support. The Mo loading at 5 wt. % for HT80*(5)*, reflects the morphology for as-synthesized pure SBA-15 or Ti-SBA-15, which indicates the incorporation of active metals within the support framework. As for the Mo loading of 13 wt. %, the MoO_3 particles become more visible and grown along the morphology of Ti-modified SBA-15 support. The morphology of catalyst HT100*(13)* as shown in (**Figure 4-10**) micrographs, show more of cubical flat-sheet MoO_3 particles than the corresponding HT100*(8)*, and this confirms the effect of MoO_3 loading percent on the dispersion and thus, consequently affect the catalytic performance of the final HDS catalysts.

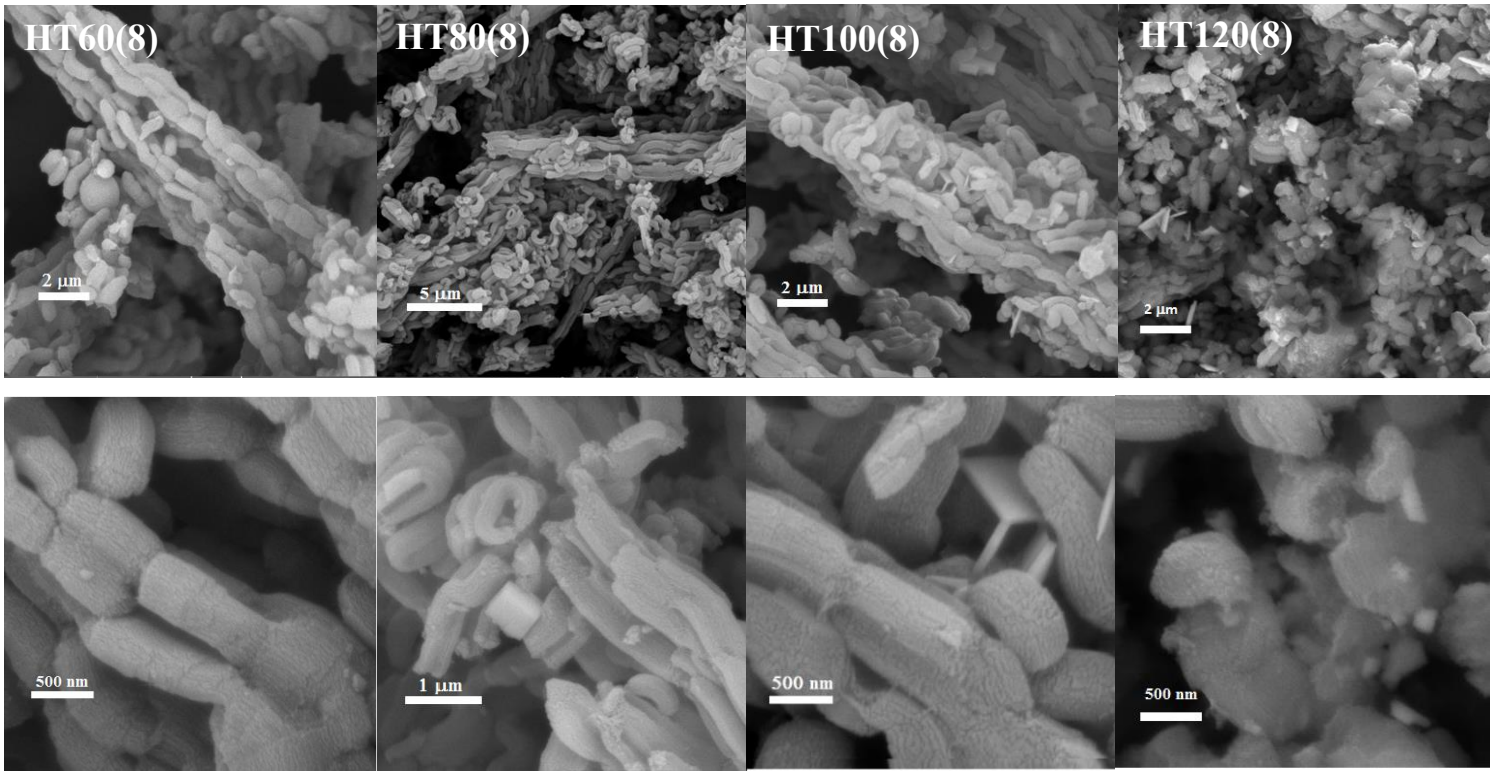

Figure 4-9 Scanning electron microscope of synthesized HDS catalysts at different temperatures and 8 wt.% molybdenum. (Low magnification (top) and corresponding high magnification (bottom).

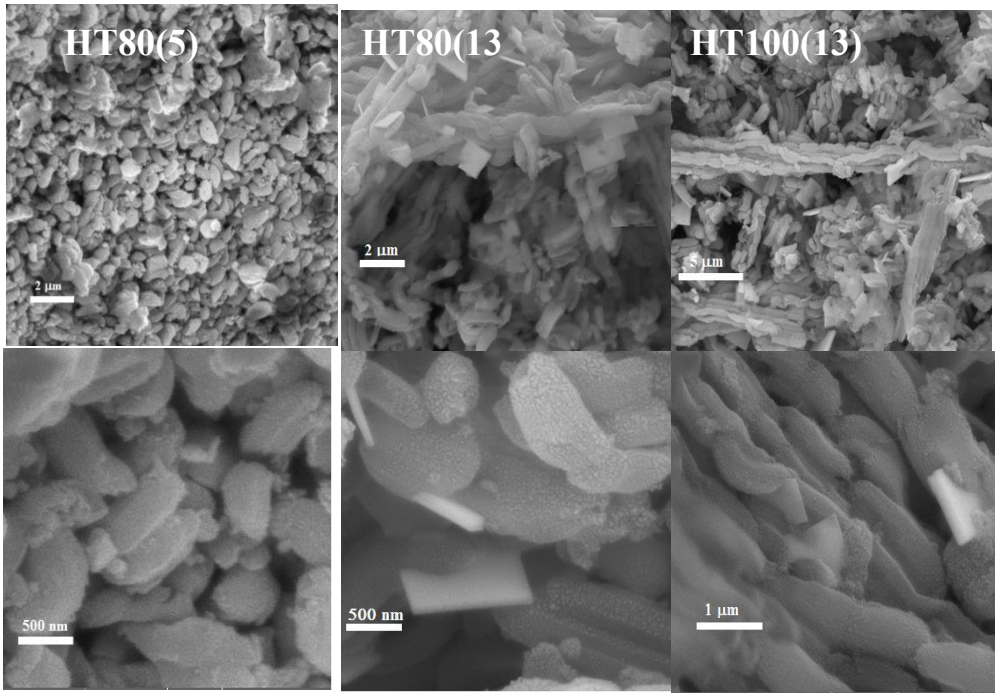

Figure 4-10 Scanning electron microscope of hydrothermally synthesized HDS catalysts at 5 and 13 wt.% molybdenum. (Low magnification (top) and corresponding high magnification (bottom).

4.3.6 Catalytic Performance

Performance of the catalysts was evaluated by conducting experiments in batch autoclave reactor for simultaneous HDS of DBT and 4-MDBT. The sulfur contents in the products over catalysts prepared by varying Mo loading and synthesized at different hydrothermal temperatures are presented in **Table 4-4**. The results show a significant variation in the performance of the synthesized catalysts, which indicates the influence of both the parameters namely HTsynT and Mo loading. The conversion of DBT was higher than 4-MDBT over all the catalysts as a result of steric hindrance due to the presence of methyl group in 4-MDBT. This result is in accordance with published reports. [68, 97]. Among the catalysts with Mo loading of 8 wt.%, the HT80*(8)* performed better than others for the HDS of DBT as well as of 4-MDBT. Increasing the Mo loading to 13 wt.% was beneficial when the HTsynT was 80^{o}C. However, an increase in Mo loading from 8 wt.% to 13 wt.% resulted in marked decrease in HDS when the HTsynT was increase to 100^{o}C. These results underscore the important role of HTsynT in dispersion of active metal and its impact on HDS activity. Thus, the advantage of increased Mo loading can be reaped only when the HTsynT is not too high.

Table 4-4 Catalyst performance test results: Product sulfur content (Process conditions: 350 ^{o}C , 5 MPa, Feed sulfur content = 1,000 ppm)

Catalyst	Product Sulfur Content for DBT (ppm)				Product Sulfur Content for 4-MDBT (ppm)			
	1h	2h	3h	4h	1h	2h	3h	4h
HT60*(8)*	432	136	40	13	511	193	56	18
HT80*(8)*	344	49	17	5	432	70	24	4
HT100*(8)*	336	108	41	8	429	176	66	18
HT120*(8)*	408	145	78	18	513	225	133	29
HT80*(5)*	521	157	46	27	554	161	36	6
HT80*(13)*	250	75	20	4	283	119	27	6
HT100*(13)*	475	156	67	27	580	232	114	43

The HDS rates were calculated assuming pseudo-first order kinetics, and the values of the reaction constant, $\boldsymbol{k}$ (min^{-1}), were determined using the initial conversion values – those obtained after the first hour of the reaction. The results presented in **Table 4-5** show that the value of the rate constants was in the range of 10 to 23 x 10^{-3} min^{-1} for the HDS of DBT and 9 to 21 x 10^{-3} min^{-1} for the HDS of 4-MDBT. These values compare well with the reported rate constant of 18.3 x 10^{-3} min^{-1} for the HDS of DBT at 350 °C over a $CoMo/Al_2O_3$ catalyst [68]. However, the ratio $\boldsymbol{k}_{DBT}/\boldsymbol{k}_{4MDBT}$ was 1.1 to 1.3 as compared to about 2.0 reported for $CoMo/Al_2O_3$ catalyst. This difference indicates higher rate of HDS of 4-MDBT over Ti-SBA-15-NiMo catalysts which could be attributed to the higher pore volume of mesoporous silica.

The HDS of DBT or 4-MDBT occurs via two parallel pathways as illustrated in **Figure 4-11**: (i) direct desulfurization (DDS) or hydrogenolysis by C-S bond cleavage in a single step; or (ii) hydrogenation (HYD) in 2-3 steps through the hydrogenation of one of the phenyl rings followed by C-S bond cleavage [98]. The HDS of DBT via the DDS pathway yields biphenyl (BP) and H_2S as final products. However, the HYD pathway results in the formation of intermediates, such as tetrahydro dibenzothiophene (THDBT) and hexahydro dibenzothiophene (HHDBT), followed by fast desulfurization to form cyclohexyl benzene (CHB). Because the DDS pathway consumes substantially less hydrogen, it is the preferred route.

BP and MBP were the hydrocarbon compounds in the products obtained from the HDS of DBT. In addition to 4-MBP and MCHB, 3-MBP and 4-THMDBT were identified among the products of HDS of 4-MDBT. Products distribution for obtained over NiMo-SBA-15-Ti catalysts at different HTsynT and Mo-loading from the HDS of DBT and 4-MDBT are presented in **Table 4-6 and Table 4-7**, respectively as Supplemental Information. The pseudo first-order rate constants of DDS and HYD routes were calculated from the product composition obtained after one hour and they are presented in **Table 4-5**.

Table 4-5 First-order HDS rate constants for HDS of DBT and 4MDBT at 350°C.

Catalyst	DBT				4-MDBT			
	k_{HDS} x 10^3 (min^{-1})	k_{DDS} x 10^3 (min^{-1})	k_{HYD} x 10^3 (min^{-1})	k_{DDS}/ k_{HYD}	k_{HDS} x 10^3 (min^{-1})	k_{DDS} x 10^3 (min^{-1})	k_{HYD} x 10^3 (min^{-1})	k_{DDS}/ k_{HYD}
HT60*(8)*	14.0	10.3	1.9	5.5	11.2	9.4	1.0	9. 6
HT80*(8)*	17.8	13.5	1.8	7.7	14.0	12.0	0.9	12.9
HT100*(8)*	18.2	12.5	2.5	5.1	14.1	11.7	1.2	10.1
HT120*(8)*	14.9	10.5	2.2	4.8	11.1	9.3	1.0	9.3
HT80*(5)*	10.9	8.4	1.5	5.7	9.8	8.4	0.9	9.5
HT80*(13)*	23.1	18.3	1.4	12.6	21.0	18.2	0.9	20.5
HT100*(13)*	12.4	9.0	1.9	4.7	9.1	7.5	1.0	7.5

Table 4-6 Products distribution for DBT over NiMo-SBA-15-Ti catalysts at different HTsynT and Mo-loading

Catalyst	Product Distribution (wt.%) for DBT			
	Reaction Time: 1h		Reaction Time: 3h	
	CHB	BP	CHB	BP
HT60*(8)*	18.8	81.2	12.7	87.3
HT80*(8)*	15.3	84.7	11.3	88.7
HT100*(8)*	20.7	79.3	17.0	83.0
HT120*(8)*	20.8	79.2	16.6	83.4
HT80*(5)*	17.6	82.4	13.8	86.2
HT80*(13)*	11.1	88.9	9.1	90.9
HT100*(13)*	20.7	79.4	16.4	83.6

Abbreviations:

CHB: Cylcohexyl benzene
BP: Biphenyl

Table 4-7 Products distribution for 4-MDBT over NiMo-SBA-15-Ti catalysts at different HTsynT and Mo-loading

Catalysts	Product Distribution (wt.%) for MDBT									
	Reaction Time: 1h					Reaction Time: 3h				
	MCHB	4MBP	3MBP	4TH-MDBT	3-MDBT	MCHB	4MBP	3MBP	4TH-MDBT	3-MDBT
HT60(8)	9.8	71.0	2.9	10.2	6.1	5.0	87.5	7.5	-	-
HT80(8)	8.7	79.7	2.7	5.2	3.7	4.4	88.9	6.6	-	-
HT100(8)	9. 9	71.3	3.4	9.9	5.5	6.8	83.6	6.6	1.7	1.3
HT120(8)	10.0	70.3	3.2	11.1	5.4	7.3	82.8	5.7	1.8	2.4
HT80(5)	10.3	77.0	2.3	6.3	4.2	5.5	88.0	6.3	-	-
HT80(13)	6.8	84.9	2.2	2.2	3.8	4.0	90.6	5.5	-	-
HT100(13)	11.2	69.6	-	12.7	6.5	7.5	82.6	5. 9	1.9	2.2

Abbreviations:

MCHB: Methyl cylcohexyl benzene
4-MBP: 4-Methyl biphenyl
3-MBP: 3-Methyl biphenyl
4THMDBT: 4-tetrahydromethyl dibenzothiophene
3-MDBT: 3-methyl dibenzothiophene

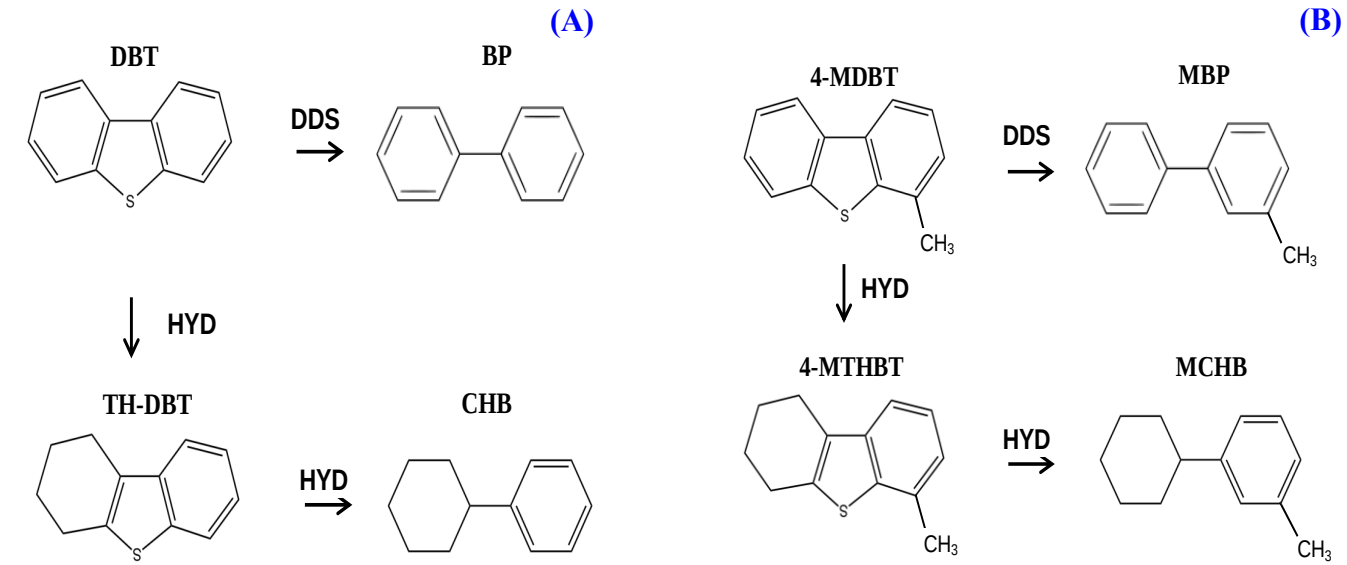

Figure 4-11 Reaction pathways for HDS of DBT (A) and 4-MDBT (B).

4.3.7 Effect of Hydrothermal Synthesis Temperature

Figure 4-12A presents the effect of hydrothermal synthesis temperature on HDS rate constants for catalysts having Mo content of 8 wt.%. With the increase in HTsynT from 60 ^{o}C to 80 ^{o}C, the $\boldsymbol{k}_{HDS}$ for DBT as well as 4-MDBT increased by about 25%. An increase in HTsynT to 100^{o}C resulted in marginal increase in HDS rate. Further increase in HTsynT to 120^{o}C resulted in about 25% decrease in HDS rate. These trends in HDS rates are in accordance with the drastic drop in surface area and acid site concentration when HTsynT was increased from 100^{o}C to 120^{o}C which also caused agglomeration of MoO_3 crystallites.

Comparison of the HDS rate constants for the DDS and HYD pathways (**Table 4-5**) shows that DDS is the dominant reaction route for both DBT and 4-MDBT. Among the catalysts containing 8 wt.% Mo, the $\boldsymbol{k}_{DDS}/\boldsymbol{k}_{HYD}$ ratio was highest for HT80*(8)* which reflects higher acid site concentration and dispersion of Mo resulting in improved C-S bond scission activity. Although, there was a slight improvement in overall $\boldsymbol{k}_{HDS}$ of HT100*(8)* compared to HT80*(8)*, there was a reduction in $\boldsymbol{k}_{DDS}$ accompanied by an increase in $\boldsymbol{k}_{HYD}$. Lower $\boldsymbol{k}_{DDS}$ could be due to drastic reduction in acid site concentration. With the increase in HTsynT to 120^{o}C, the drop in the rates of both the HDS routes is evident.

4.3.8 Effect of Mo-loading

Figure 4-12B presents the effect of Mo loading on HDS rate constants for catalysts synthesized at the hydrothermal temperature of 80^{o}C. With the increase in Mo loading from 5 wt.% to 8 wt.%, the $\boldsymbol{k}_{HDS}$ for DBT was increased by about 65% and $\boldsymbol{k}_{HDS}$ for 4-MDBT by about 45%. An increase in Mo loading to 13 wt.% resulted in further increase in HDS rate by 30-50%. Hence there was almost a linear increase in HDS rate with the increase in Mo loading. Such a consistent improvement on HDS rates reflects availability of more active sites with increased Mo loading. When the hydrothermal temperature is increased to 100^{o}C, the increase in Mo loading from 8 wt.% to 13 wt.% had a significantly negative effect resulting in loss of HDS rate by about 30%. Divergent trends in HDS rates at HTsynT of 80^{o}C and 100^{o}C underscores the significance of interplay of hydrothermal synthesis temperature and Mo loading. Apparently, the agglomeration of MoO_3 crystallites due to higher HTsynT of 100^{o}C accelerated at higher loading of Mo.

Comparison of the HDS rate constants for the DDS and HYD pathways (**Table 4-5**) shows that DDS is the dominant reaction route for both DBT and 4-MDBT. Among the catalysts synthesized at the hydrothermal temperature of 80^{o}C, there was a significant increase in $\boldsymbol{k}_{DDS}$ with increase in Mo loading from 5 wt.% to 13 wt.% while $\boldsymbol{k}_{HYD}$ remained almost constant. These results indicate that the increase in HDS rate with Mo loading was entirely due to availability of more metallic active sites. The $\boldsymbol{k}_{DDS}/\boldsymbol{k}_{HYD}$ ratio was highest for HT80*(13)* which also reflects higher dispersion of Mo resulting in improved C-S bond scission activity. However, higher Mo loading caused severe loss of $\boldsymbol{k}_{DDS}$ when the HTsynT was increase to 100^{o}C due to agglomeration of MoO_3.

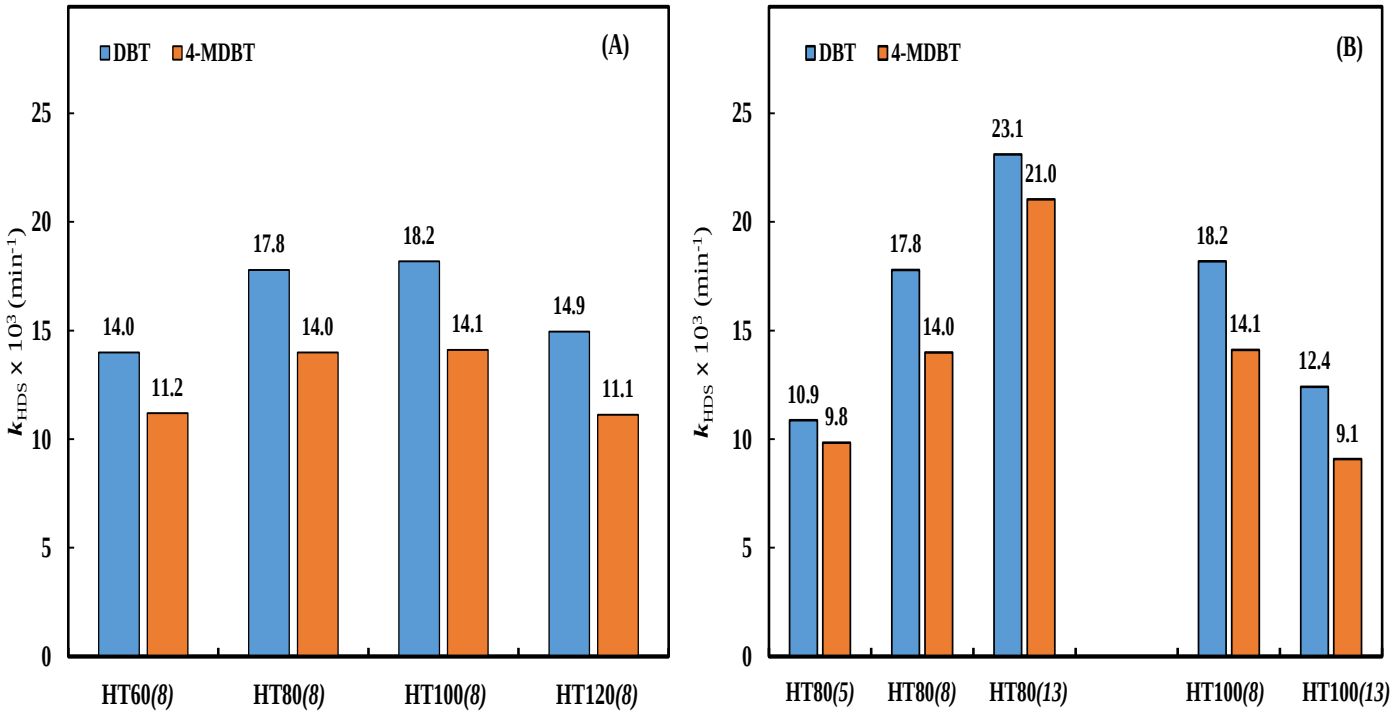

Figure 4-12 First-order HDS rate constants of DBT and 4-MDBT over catalysts prepared at different hydrothermal temperatures (A) and with different Mo loading (B).

4.4 Conclusions

The results of this study show that hydrothermal synthesis temperature of Ti-SBA-15-NiMo catalyst above 80 ^{o}C leads to decrease in catalytic performance due to agglomeration of MoO_3. The effect of Mo loading on catalytic performance was also influenced by the hydrothermal synthesis temperature. Hydrothermal temperature of 80^{o}C and 13 wt.% Mo loading of resulted in improved overall HDS activity as well as HDS by direct desulfurization route. Divergent trends in HDS rates at HTsynT of 80^{o}C and 100^{o}C for catalyst containing 13 wt.% Mo underscores the significance of interplay of hydrothermal synthesis temperature and Mo loading. The catalytic performance was consistent with the characterization data particularly in terms of textural properties, dispersion and morphology. Further studies are required to confirm the applicability of mesoporous silica support for HDS of heavier sulfur compounds.

ACKNOWLEDGEMENTS

The authors acknowledged the support provided by King Fahd University of Petroleum & Minerals (KFUPM) for funding this work through project No. DSR NUS15105.

Chapter 5

Simultaneous HDS of DBT and 4,6-DMDBT Over Single-Pot Ti-SBA-15-NiMo Catalysts: Influence of Si/Ti Ratio on the Structural Properties, Dispersion and Catalytic Activity

ABSTRACT

A series of Ti-SBA-15-NiMo catalysts with Si/Ti ratio of 1, 2.5, 5 and 10 were prepared by single-pot method. The catalysts dispersion and performance were characterized by N_2-adsorption, temperature programmed techniques (NH_3-TPD and H_2-TPR), X-ray diffraction (XRD) and fluorescence (XRF) as well as by Raman and Fourier transform infrared (FTIR) spectroscopy. The catalytic activity was determined by simultaneous hydrodesulfurization (HDS) of dibenzothiophene (DBT) and 4,6-dimethyl dibenzothiophene (4,6-DMDBT) in a batch autoclave reactor. Variation in Si/Ti ratio resulted in noticeable difference in catalysts' characteristics. XRD diffractograms show that titanium is well incorporated into the SBA-15 support at Si/Ti ratios of 10 and 5. However, at Si/Ti ratio below 5, the Ti phases predominate and the peaks corresponding to MoO_3 phases were not observed. As the Ti incorporation is increased, the moderate surface acidity decreases while the contribution from strong acidity becomes evident. TPR results indicate that higher amount of Ti increases the metal-support interaction. The HDS rates for DBT and 4,6-DMDBT over catalyst with Si/Ti of 10 increased by 33% and 49%, respectively. The enhancement in HDS can be attributed to lower metal-support interaction. However, further increase in Si/Ti ratio gave away the enhancement in HDS rates. Direct desulfurization was the preferred route for both DBT and 4,6-DMDBT. The HDS rate by DDS is enhanced by the addition of Ti while HDS rate by hydrogenation route remain almost constant. The divergent effects on the DDS and HYD pathways indicate that the active sites for hydrogenolysis and hydrogenation are not the same and are influenced differently by titania addition.

5.1 Introduction

Deep desulfurization of transportation fuels requires highly active and well-dispersed catalysts to comply with the stringent environment-driven regulations as well as to process feedstock obtained from deteriorating quality of crude oil [99, 100]. Achieving highly dispersed active phase depends on the physicochemical properties of support upon which the active phase is deposited, the nature of interaction between the support and active metals, method of deposition, composition of active species, pH of solution, stirring rate and temperature, aging temperature, drying process, calcination temperature etc. [101-103]. The dispersion, reducibility, sulfidation and morphology of the Ni(Co)Mo(W) supported hydrodesulfurization (HDS) catalysts are strongly influenced by the support [104]. Therefore, a series of supports such as Al_2O_3[105], SiO_2[106], carbon[107], TiO_2[70], ZrO_2[72], ZrO_2-TiO_2[108], ZrO_2-SiO_2[109], TiO_2–Al_2O_3[74], ZrO_2-Al_2O_3[75], and mesoporous molecular sieves [110, 111] (MCM-41 and SBA-15) have been reported.

Currently, the most common industrially used support for HDS catalysts is γ-alumina owing to its good mechanical and textural properties as well as abundance and low cost. However, the surface OH-group of γ-alumina results in strong interaction with Ni(Co)Mo(W)-oxide (referred to as strong metal support interaction, SMSI) to form type I active phase of low catalytic activity during sulfidation [112]. In addition, coke formation on alumina supported HDS catalysts is considerable [113]. Other types of supports such as ZrO_2, TiO_2 etc. have been explored. Their major drawback is low surface area and porosity, even though their intrinsic activity is high, but the specific activity is lower than that reported for alumina [114, 115].

Synthesis of various mesoporous molecular sieves have attracted great attention owing to their large surface area, good mechanical property, hexagonal array, uniform pore channel and hydrothermal stability etc. [116, 117] These materials have found different applications in catalysis (heterogeneous and photocatalysis) [118, 119], adsorption of environmental pollutants and large organic molecules [120, 121], chromatographic separation [122], and advance-templated material for metal-oxides [123, 124] and porous carbon [125, 126].

SBA-15, being an ordered 2D-p6mm hexagonal structure with high textural properties, thicker walls, and higher hydrothermal stability is more widely studied among mesoporous molecular sieves. It has a potential of becoming a viable support for hydroprocessing operations, especially

for catalytic reactions involving bulky molecules present in heavy petroleum fractions [77, 127]. However, dispersion of active phase remains an area of research focus. Different scientific approaches such as the use of additives, complexing agents, and modification with heteroatoms have been reported to achieve dispersion of active species on the SBA-15 [6, 9]. The later approach is receiving great attention due to ease of incorporation either by direct or post-synthesis method, and the ability to improve the dispersion greatly via increase in surface acidity character from weak to moderate [128].

Kumaran *et al.* [129], reported the variation of Si/Al (10-40) in Mo content in NiMo, CoMo supported SBA-15 as catalysts for thiophene HDS and cyclohexene hydrogenation. Their studies showed that the Mo dispersion and catalytic activities are greatly influenced by ratio of Al present in the support, and the catalysts supported on Al-SBA-15 showed better performance than SBA-15 supported catalysts. Gutiérrez *et al.* [115] synthesized NiMo supported on a series of Ti and Zr modified SBA-15 for HDS of DMDBT. These catalysts showed better dispersion of active species in both oxidic and sulfided form at 19 wt. % Ti and 22 wt. % Zr, as confirmed by XRD, TPR and HRTEM, and higher catalytic activity than SBA-15/NiMo catalyst. Tatiana *et al.* prepared a series of Al-containing SBA-15 with different Si/Al ratios (10-50) by chemical grafting and tested for HDS of 4,6-DMDBT, and the catalytic activity increases as Si/Al ratio increases (optimum at 20) due to strong interaction of active metals (NiMo) with Al serving as anchoring sites on the support [130]. More recently, the effect of direct synthesis on Al-SBA-15 supports with different Si/Al ratios (40-2.5) for HDS of DBT over NiMoS was reported [131]. Their study showed that the enhanced catalytic activity and selectivity is related to surface density and roughness of the support, and that the total acidity density of support increases with increasing Al-loading, and the optimum bronsted acid sites was found at Al-SBA-15(10).

In spite of different reported studies on the effect of Si/X ratios (X= Al, Ti or Zr) of heteroatoms, on the dispersion and activity of supported Ni(Co)Mo(W)-S HDS catalysts, which is usually followed by impregnation of active species, there is no report on one-pot synthesis of Ti-SBA-15-NiMo with varied Si/Ti ratios, and more importantly structural changes observed at higher Ti-loading. In this study, we studied the effects of Si/Ti ratio on the chemical and structural properties as well as the catalytic activities of Ti-SBA-15-NiMo catalysts for simultaneous HDS of dibenzothiophene (DBT) and 4,6-dimethyldibenzo-thiophene (4,6-DMDBT).

5.2 Experimental

5.2.1 Materials and Methods

The reagents required for catalyst preparation such as Tetraethylorthosilicate (TEOS) $(C_2H_5O)_4Si$, pluronic P123 PEO_{20}-PPO_{70}-PEO_{20} triblock copolymer, nickel nitrate hexahydrate (Sigma-Aldrich, 99%), and titanium isopropoxide (97%) were purchased from Sigma-Aldrich, while ammonium molybdate (V1) tetrahydrate (99%) was purchased from ACROS organics. DBT (Sigma-Aldrich, 98%), and 4,6-DMDBT (Sigma-Aldrich, 97%) were used as the model sulfur compounds present in gas oils. Dodecane (Merck Chemicals, >99%) was used as a solvent in catalyst evaluation tests without further purification. High-purity deionized water (DI-H_2O) (18 μS/cm) was produced in-house using Thermo-Scientific Barnstead NANOPURE after distillation with a Labstrong FiSTREEM^{TM} II 2S Glass Still distiller.

5.2.2 Synthesis of Titanium Modified SBA-15-NiMo with Different Si/Ti ratios

NiMo supported on Ti-SBA-15 catalyst by single-pot approach is prepared as described in our recent work [76]. The typical synthesis procedure involves dissolution of 4 g of (P123) triblock copolymer in 120 g of 2M HCl and 30g DI-H_2O and stirred vigorously for 1h before addition of TEOS (8.32 g) and required amount of titanium isopropoxide. The amount of Ti-precursor was varied in order to prepare a series of catalysts with Si/Ti ratio of 1, 2.5, 5, and 10. The mixture was stirred for 18 h before addition of molybdenum and nickel previously mixed with their respective precursors in DI-H_2O to adjust the pH, and the whole mixture was stirred for additional 6 h at room temperature (RT) before hydrothermal synthesis. The light-yellow mixture obtained after several hours of stirring was transferred into Teflon coupled in an autoclave stainless steel and subjected to hydrothermal (HT) synthesis at 80 ^oC for 20-24 h. The light-yellow solid was centrifuged once without further washing, to avoid leaching of active phase(s) into solvent, and dried in oven at 80 ^oC overnight, before final calcination at 300 ^oC.

The Ti containing catalysts are denoted as ***C***(*x*), where *x* represents the Si/Ti ratio and the catalyst without Ti is labeled as ***C***. The Mo and Ni loading in as-synthesized catalysts were kept constant at 8 and 3 wt. %, respectively.

5.2.3 Catalyst Characterization

The textural characteristics of Ti-SBA-15-NiMo catalysts were determined using Micromeritics unit (ASAP 2020). Prior to adsorption and desorption isotherms analysis, the calcined sample was degassed at 250^{o}C for 1.5h under vacuum to remove the physisorbed moisture and impurities.

Active species (Ni, Mo) and heteroatom (Ti) crystallinity was examined by Rigaku X-ray diffraction (XRD Miniflex using CuKα radiation (λ= 1.5406 Å) at 3 ^{o}C/min scan rate of 0.03 width. A Raman spectrometer (HORIBA, iHR320 with CCD detector) with a laser wavelength of 532 nm (300 mW, green laser) was used to characterize the MoO_3 and TiO_2 phases. FTIR spectroscopy was used to identify the functional groups present in the supports and catalysts. The absorption spectra of Ti-SBA-15-NiMo catalysts were recorded on a Thermo Scientific Nicolet 6700 FTIR spectrometer with a scanning range of 400-4000 cm^{-1}. The samples for FTIR analysis were prepared using KBr powder mixed with the catalyst in a ratio of 100:2 to form pellet-like translucent discs.

Temperature programmed desorption (TPD) using 10 wt.% NH_3 as a probe molecules to measure surface acidity and number of active sites was performed on a Micromeritics Chemisorb 2750 (pulse chemisorption system). About 100 mg of oxidic-NiMo- supported on Ti-SBA-15 was loaded in a quartz tube and pre-treated in a flow of helium at 600 ^{o}C for 30 min. The sample was cooled to 100 ^{o}C before passing 10% NH_3 in helium at 25 mL/min for about 30 mins, which was then followed by purging of helium at the same flow rate for 1 h to remove physically adsorbed NH_3. Desorption of NH_3 was achieved by heating the sample to 800°C at 10°C/min, and the data were recorded with a thermal conductivity detector (TCD) using TPx software for data analysis. The reducibility and dispersion of the catalysts were determined by temperature-programmed reduction (TPR) using hydrogen as the adsorbate molecules using Micromeritics (Autochem II-2920) chemisorption analyzer. About 30-40 mg of the catalyst previously calcined at 300°C was pre-treated for 1 h in high-purity helium at 400°C and then cooled to ambient temperature before temperature programmed reduction experiment by hydrogen. The reduction temperature characteristic by hydrogen consumption was measured by linearly increasing the furnace temperature at 10°C/min to 1000°C under a steady flow (50 ml/min) of 10% hydrogen in helium. The consumption of hydrogen at the reducible temperature(s) was recorded on a thermal

conductivity detector (TCD). Elemental composition in bulk catalysts were determined and calculated by SPECTRO XEPOS energy dispersive X-ray fluorescence (ED-XRF) spectrometer (AMETEK, Materials analysis division) equipped with AMECARE M2M.

The morphological structural variation of Ti-SBA-15-NiMo catalysts as a function of Si/Ti ratios was examined by scanning electron microscope (SEM), TESCAN LYRA 3, using secondary electron (SE) and backscattered electron (BSE) modes at an accelerating voltage of 30 kV. The unit was equipped with an energy-dispersive X-ray spectrometer (EDS, Oxford, Inc.) detector for elemental analysis.

5.2.4 Catalytic Performance Evaluation

Prior to catalytic evaluation testing, the pelletized catalyst samples (300-500 µm) were reduced for 150 mins at 400 ^{o}C to form metallic active species, and then sulfided with 2 wt.% CS_2 dissolved in cyclohexane at 350 ^{o}C (10^{o}C/min) for 6h. Binary solutes of DBT and 4,6-DMDBT (1000 ppm-S each) dissolved in hexadecane, employed as model diesel fuel, were tested and evaluated for HDS reaction in high-pressure batch reactor (Parr 4576B). The temperature, initial pressure of H_2, weight of sulfided catalyst, stirring speed of reactor, feedstock volume was maintained constant at 350^{o}C, 5 MPa, 250 mg, 300 rpm, 100 mL, respectively.

Catalyst evaluation was conducted for 2h after process conditions were achieved and stabilized. Sulfur and hydrocarbon contents in the product was determined by gas chromatograph sulfur chemiluminiscence detector (GC-SCD) and mass spectrometer (GC-MS), respectively.

5.3 Results and Discussion

5.3.1 Adsorption-Desorption Isotherm

Textural properties analysis of Ti-SBA-15-NiMo HDS catalysts at different Si/Ti ratios were determined by calculating BET surface area and BJH-adsorption pore volume and pore size. The catalyst without addition of Ti exhibit high surface area, and pore volume than others. However, the pore size of catalyst ***C*** is similar to other catalysts prepared with the addition of titanium between (6-6.9 nm) **(Table 5-1)**. An increase in Ti-content in the catalyst matrix resulted in the decrease in BET surface area and micropore surface area until *C(5),* and the surface area again increase between ***C****(2.5)* and ***C****(1),* due to formation of new catalytic material or phases attributed to TiO_2 as discussed in the next section. It should be mentioned that the BET and the micropore surface area of catalyst ***C****(1)* with highest loading of titanium resembles that of C without even with the formation new phases other the active species of the catalyst. All catalysts exhibit the type-IV isotherm of mesoporous material with the characteristics of plugged nanoparticles as observed from two desorption steps on the isotherm loop, as shown in **Figure 5-1(left)** and the pore-size distribution is presented in Figure 5-1**(right)**.

Table 5-1 Textural Properties of HDS Catalysts. (error = ± 2.0%)

Catalyst	BET Surface Area (m^2/g)	Micropore Area (m^2/g)	External Surface Area (m^2/g)	Total Pore Volume (cm^3/g)	Average Pore Size (nm)
C	570	68	502	0.89	6.1
C(*10*)	473	43	430	0.76	6.0
C(*5*)	423	37	386	0.79	6.6
C(*2.5*)	464	47	417	0.82	6.9
C(*1*)	562	67	495	0.85	6.4

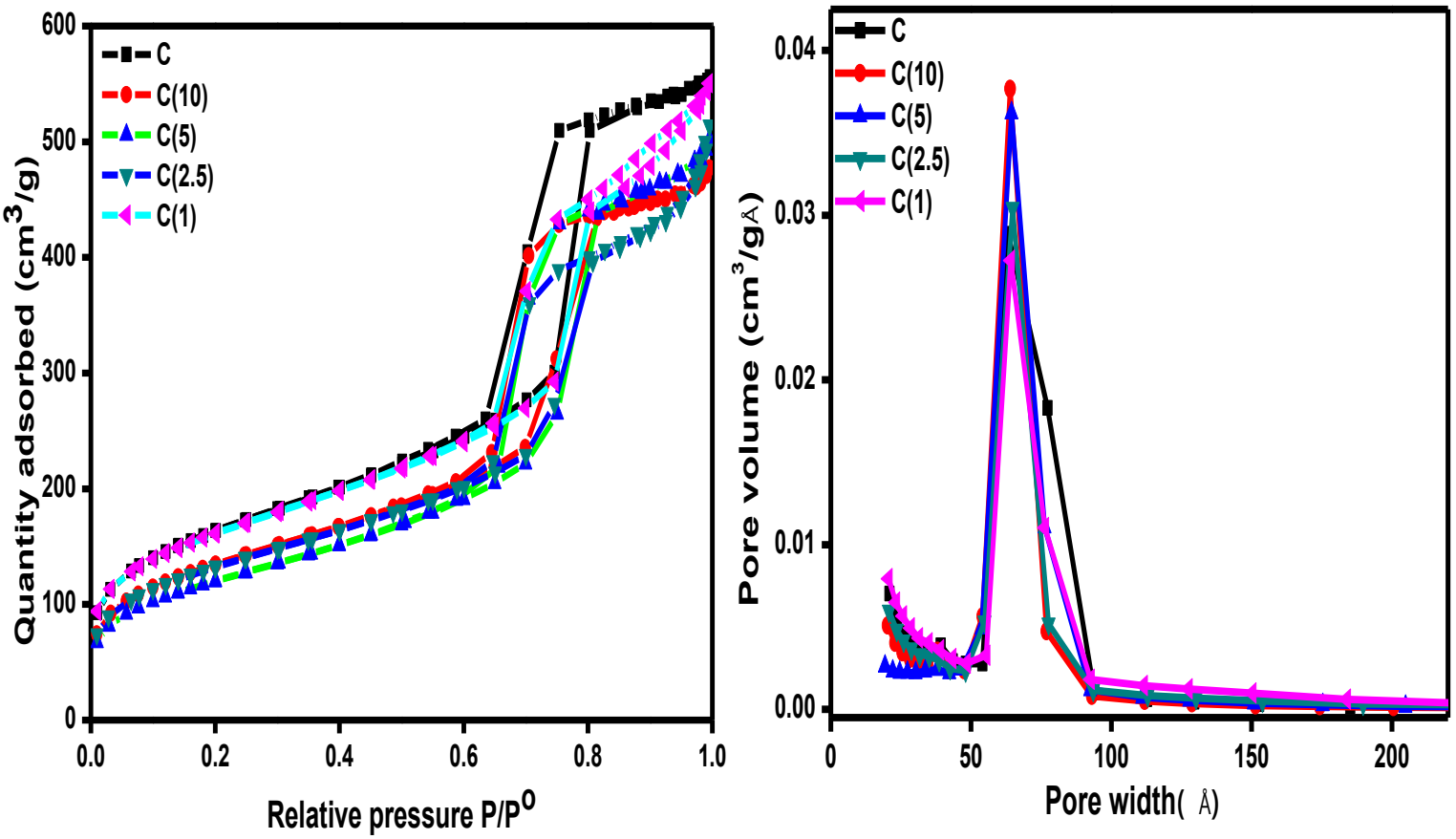

Figure 5-1 N2 adsorption –desorption isotherms by BET (left) and PSD by BJH-adsorption (right) for Ti-modified SBA-15 NiMo catalysts.

5.3.2 XRD Analysis of Catalysts

The diffractograms of the oxide catalysts with different Si/Ti ratio were presented in Figure 5-2. The incorporation of Ti into siliceous matrix is described as being perfect, due to tetravalent nature of the latter atoms and the flexibility to anchor into silicon framework without affecting its hexagonal structure [65]. However, beyond a certain compositional ratio, titania phases dominate and the X-ray diffraction peaks of the HDS Ti-SBA-15-NiMo catalyst resembles that of silica-templated TiO_2 pure anatase phases [132]. As observed from the **Figure 5-2,** the titanium is well incorporated into the SBA-15 supports at Si/Ti ratios of 10 and 5, and the diffraction peaks can be indexed to (JCPSD 05-0508) of orthorhombic MoO_3. At Si/Ti ratio below 5, the Ti phases predominate on the XRD diffractograms, and the peaks corresponding to MoO_3 phases were not observed. This indicates structural and physicochemical changes to the HDS catalyst, and might induce differences in catalytic behavior.

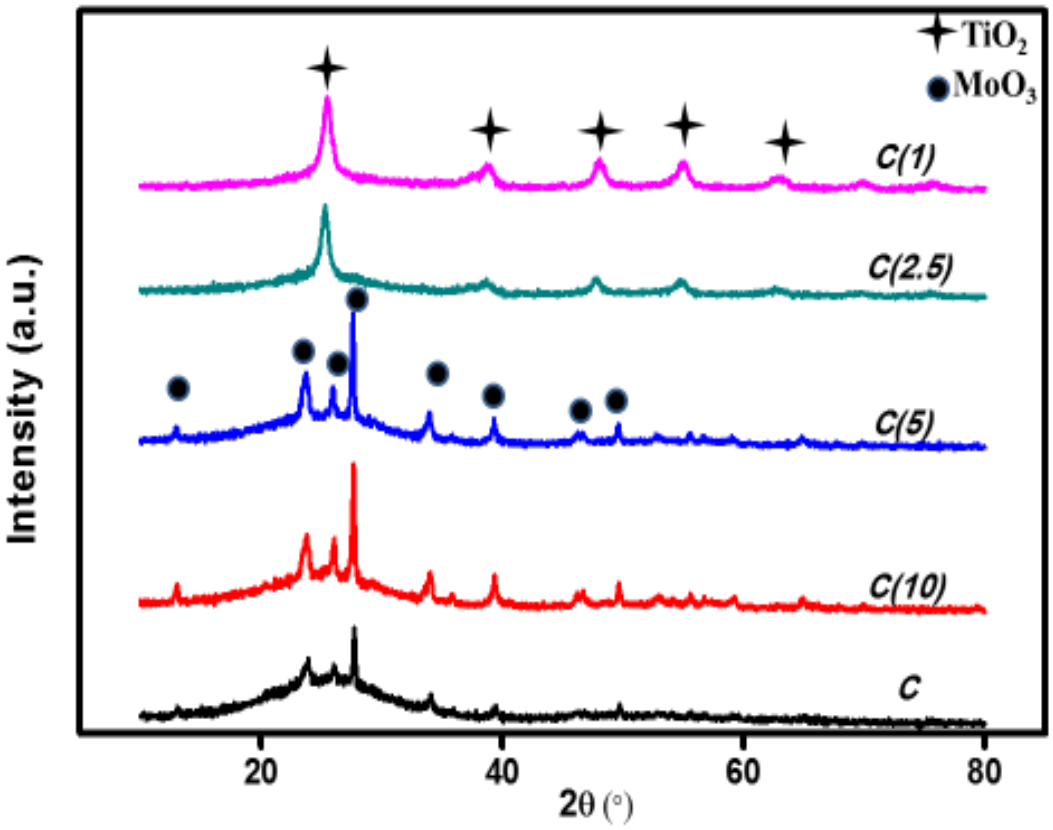

Figure 5-2 X-ray diffraction (XRD) analysis of Ti-modified SBA-15 NiMo catalysts at different Si/Ti ratios.

5.3.3 Temperature Programmed Desorption

The number of active sites with respect to structural changes in Ti-modified-SBA-15- NiMo HDS catalysts were examined by quantitative amount of ammonia desorbed by temperature programmed analysis. The nature of the surface acidity of as-synthesized catalysts as determined by amount of NH_3 desorbed is combination of moderate and strong acidity, and the former is dominated as shown in **Figure 5-3**. An interesting result, which can be correlated to the catalyst activity, is obtained. The catalyst ***C*** prepared with no incorporation of titanium shows highest amount of desorbed NH_3 at moderate acidity which may be interpreted as better dispersion. However, catalyst ***C*** also exhibits strong surface acidity at relatively higher temperature (712^{o}C) compared to catalyst ***C***(*10*). As the amount of titanium increases in the silica-titania composite catalysts, the characteristic strong surface acidity increases as reflected by the increase in the amount of NH_3 desorbed. Furthermore, as the titanium incorporation is increased, the amount of ammonia desorbed at moderate surface acidity decreases while the contribution from strong acidity becomes evident. This observation can be attributed to the decrease in the dispersion of active metals on the support with the increase in Si/Ti ratio. However, the case of catalyst ***C***(*1*) is quite unique as it exhibits lowest amount of moderate surface acidity but extremely high strong acidity (**Table 5-2**).

Table 5-2 Temperature Programmed Desorption Analysis by Ammonia. (error = ± 3.0%)

Catalyst	TPD: NH_3 desorbed				
	Peak Temperature (200-350 °C)	**Amount (µmol/g)**	**Peak Temperature (> 350 °C)**	**Amount (µmol/g)**	**Total (µmol/g)**
C	223	489	712	9	498
C(*10*)	223	400	682	4	404
C(*5*)	216	366	669	9	375
C(*2.5*)	218	375	671	26	401
C(*1*)	229	200	703, 875	134	334

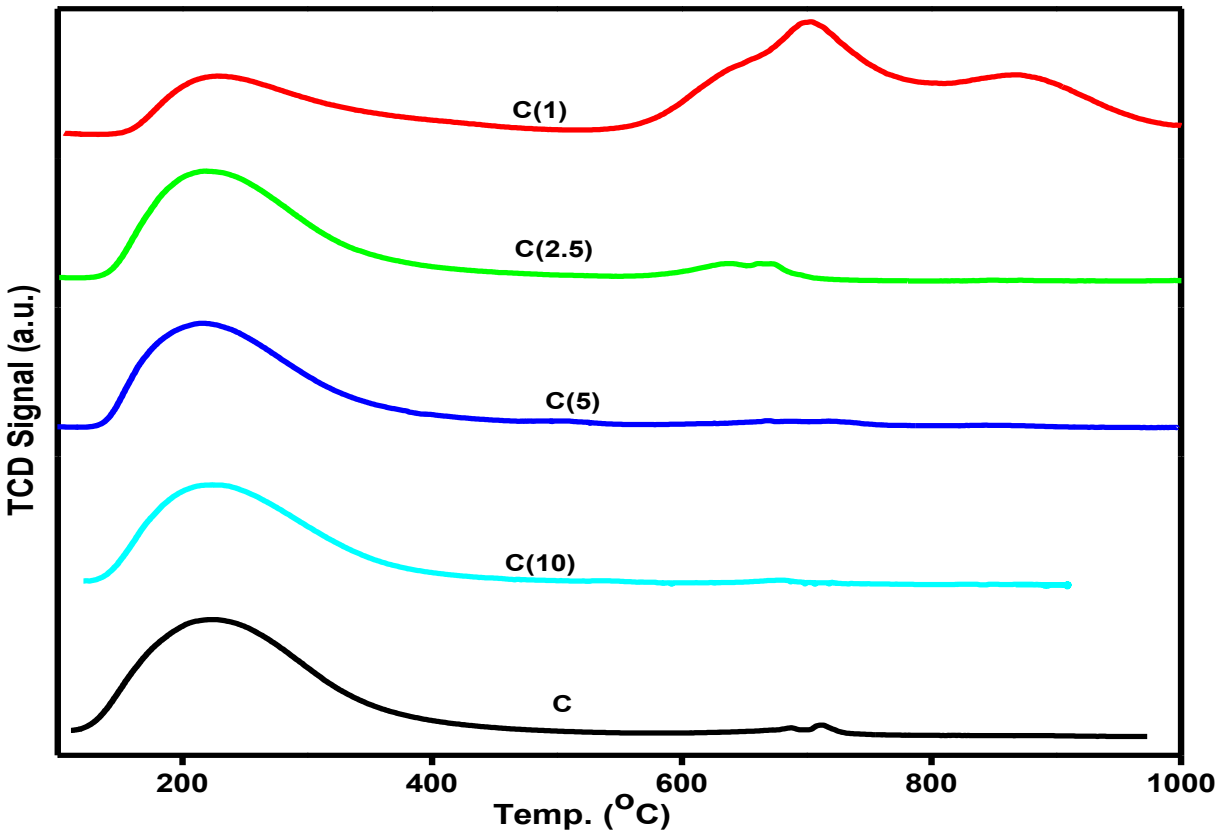

Figure 5-3 Ammonia temperature programmed desorption analysis of Ti-modified SBA-15 NiMo catalysts at different Si/Ti ratios.

5.3.4 Temperature Programmed Reduction

The reducibility and degree of sulfidation can be measured by the temperature programmed reduction analysis by using H_2 as a probe molecule. The degree of reducibility of active species in as-developed HDS catalysts has been altered by different Si/Ti ratios, and hence, the degree of sulfidation and dispersion of active species can be correlated. As shown in **Figure 5-4**, the first reduction peak associated with reduction of Mo^{6+} to Mo^{4+}, while the second reduction peak at extended temperature range is for reduction of Mo^{4+} to Mo^0 [4]**.** The first reduction peaks of hydrogen consumption for catalysts ***C***, ***C(10)***, ***C(5)***, and ***C(2.5)*** were between 502 and 506 ^oC, while that of catalyst ***C(1)*** exhibit lower reduction peak at 471 ^oC due to increase in the amount of Ti in the catalyst matrix. The second H_2 reduction temperature for catalysts ***C(2.5)*** and ***C(1)*** were significantly higher than the catalysts with higher Si/Ti ratios (***C(10)*** and ***C(5)***). These results indicate that higher amount of titanium in catalysts ***C(2.5)*** and ***C(1)*** increases the metal-support interaction resulting in shifting of the reduction temperature to higher value (**Table 5-3**). These results are in good agreement with NH_3-TPD results. The strong interaction of active phase for supported catalyst has been reported to cause decrease in the catalyst activity and selectivity [133]**.**

In addition, the degree of interaction of active phase with support as a function of dispersion can be correlated to the amount of hydrogen consumed by each catalyst at different reduction temperatures. The results presented in Table 5-3 indicate that the amount of hydrogen consumed at first peak (about 500^oC) increased with the addition of titanium for catalysts ***C(10), C(5)*** and ***C(2.5)***. However, further addition of titanium for ***C***(*1*) resulted in decreased in the amount of hydrogen consumed. This shows that molybdenum particles are possibly confined within the support structure, as amount of H_2 needed is higher. The typical H_2-TPR behavior of ***C***(*2.5*) and ***C***(*1*) at second reduction peak seems to be in line with the NH_3-TPD result which indicates very strong acidity. Therefore, an optimum loading of titanium for improved dispersion of active metals is established for catalysts ***C(10)*** and ***C(5)***.

Table 5-3 Temperature Programmed Reduction Analysis by Hydrogen. (error = ± 2.0%)

Catalyst	TPR: H_2-consumption			
	Peak Temperature (°C)	**Amount (mmol/g)**	**Peak Temperature (°C)**	**Amount (mmol/g)**
C	502	453	688	485
C(*10*)	502	546	685	512
C(*5*)	502	520	682	436
C(*2.5*)	503	459	777	372
C(*1*)	471	425	759	402

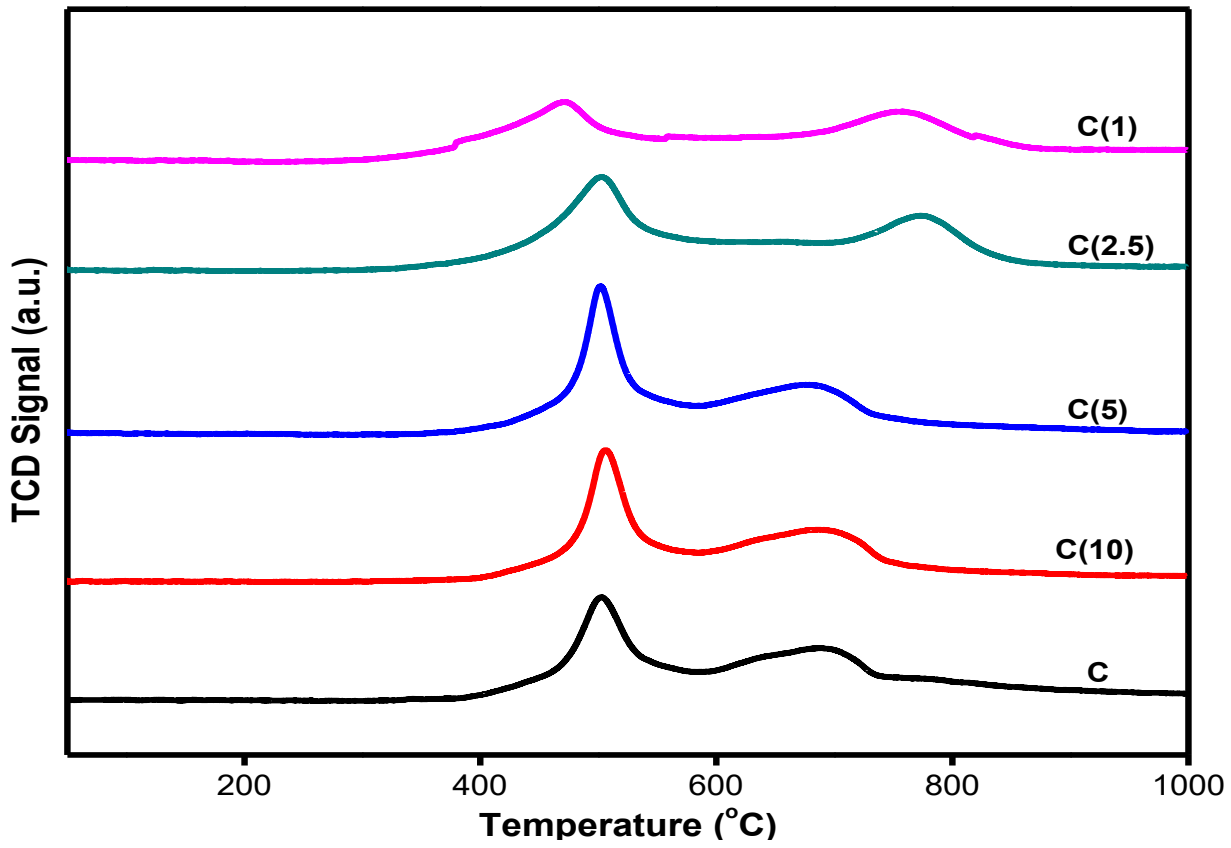

Figure 5-4 Hydrogen temperature programmed reduction analysis of Ti-modified SBA-15 NiMo HDS catalysts at different Si/Ti ratios.

5.3.5 XRF Spectroscopy

X-ray fluorescence spectroscopy analysis of bulk samples was used to avail the elemental composition of the catalysts in oxide-form. **Table 5-4** shows the actual composition of each element as compared to calculated amount. Mo-loading amount in catalyst ***C*** shows the lowest value and ***C(1)*** shows the highest, in comparison to catalysts in the series, however, all the catalysts possess good quantitative and statistical amount. In addition, the order of Si/Ti ratios observed follows good correlation with calculated amount, and the actual amount of nickel is less than calculated amount, owing to the reason reported in our previous work [76].

Table 5-4 Elemental compositions by XRF. (error = ± 3.0%)

Catalyst	Elements		
	Mo (%)	**Ni (%)**	**Si/Ti**
C	7.65 (8)	1.40 (3)	-
C*(10)*	7.86 (8)	1.62 (3)	10.1 (10)
C*(5)*	7.86 (8)	1.34 (3)	5.23 (5)
C*(2.5)*	7.90 (8)	1.23 (3)	2.9 (2.5)
C*(1)*	7.95 (8)	1.20 (3)	1.3 (1)

Note: The values in parenthesis is the calculated amount

5.3.6 Raman Spectroscopy

Raman spectroscopy is an excellent technique to study, not only mode of vibrations, but dispersion and oxidation state of active metals for catalytic applications. It is a complimentary technique to XRD, to study the crystallinity and dispersion of most of the active metals in different catalysis fields [54]**.** The oxide phases of molybdenum and titanium at different Si/Ti ratios in as developed HDS catalysts were investigated by Raman spectrometer at 532 nm green-lasers. The characteristic MoO_3 Raman bands at 994 cm^{-1}, due to a symmetric stretching mode of M=O groups and Mo-O-Mo vibrations (due to stretching mode) at 819 and 665 cm^{-1} are usually observed for crystalline MoO_3 particles. Furthermore, the wagging mode of vibrations corresponding to terminal Mo=O is at 290- 280 cm^{-1}, and the bands at 336 and 375 cm^{-1} could be assigned to the bending and deformation modes of vibrations of O=Mo=O and O-Mo-O, respectively [56, 59]**.** As shown in **Figure 5-5,** the effect of Si/Ti ratios was noticeable and similar to structural changes observed in the XRD characterization results. We observed no structural changes to the mode of vibrations of molybdena species at low Si/Ti ratios (5-10), and all assigned Raman peaks were visible as described above. In contrast, different trend was observed when the ratio of Si/Ti is between 1 and 2.5, the Raman mode of vibrations for MoO_3 is no longer visible, and a high fluorescence background was observed without reference peaks to titania as observed in XRD analysis.

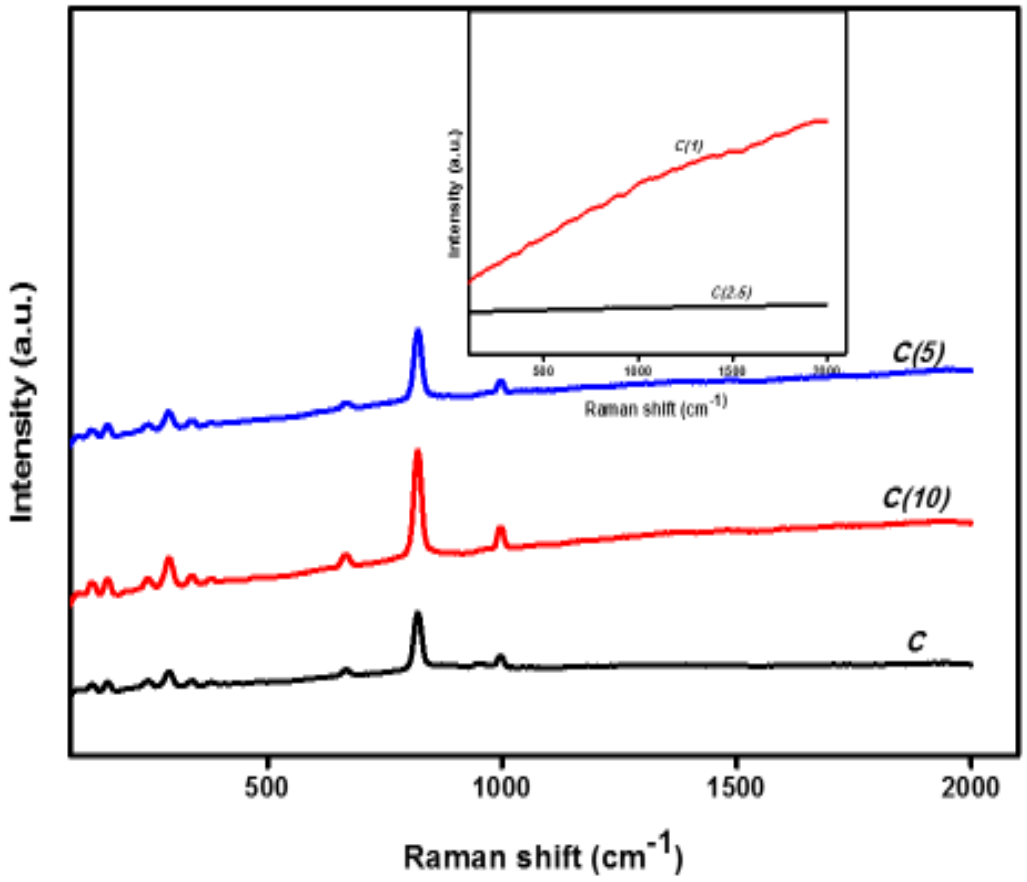

Figure 5-5 Raman Analysis of Ti-modified SBA-15 NiMo HDS catalysts at different Si/Ti ratios.

5.3.7 FTIR Analysis

The insight to the incorporation of Ti and NiMo into the mesoporous silica SBA-15 framework was obtained by means of FTIR. The identification and assignment of peaks for different Si/Ti ratios catalysts were conducted with their characteristics features, as shown in **Figure 5-7**. The observed broad band at 1100 cm^{-1} is assigned to Si-O-Si asymmetric mode of vibrations, while the symmetric stretching and bending associated with Si-O-Si appeared at 805 cm^{-1} and 466 cm^{-1}, respectively. The characteristic stretching band due to incorporation of Ti and active metal oxide species into SBA-15 matrix (Si-O-X, X= Ti, Ni, Mo) is observed at 960 cm^{-1}. The surface hydroxyl of silanol end group of (Si-OH) and metal hydroxides (M-OH) is observed at broad region between 3100-3700 cm^{-1}. This characteristic peak is used as an indication of structural change or effect of increase in the Ti-content on the HDS catalysts. This band becomes more shrink as the ratio or amount of Ti increases in the catalyst, which is due to more substitution of hydroxyl group by Ti-atoms [134]. In addition, the intensity of the band at 960 cm-1 due to Si-O-X interaction is more pronounced when Si/Ti is low, and this indicates increase in Ti-content in the catalyst's structure. The bands due to molybdenum species appear at 800-1200 cm^{-1}, and more specifically the tetrahedral appeared at 830-930 cm^{-1}, while octahedral mode of vibrations are found at 800-860 and 930-990 cm^{-1} [62].

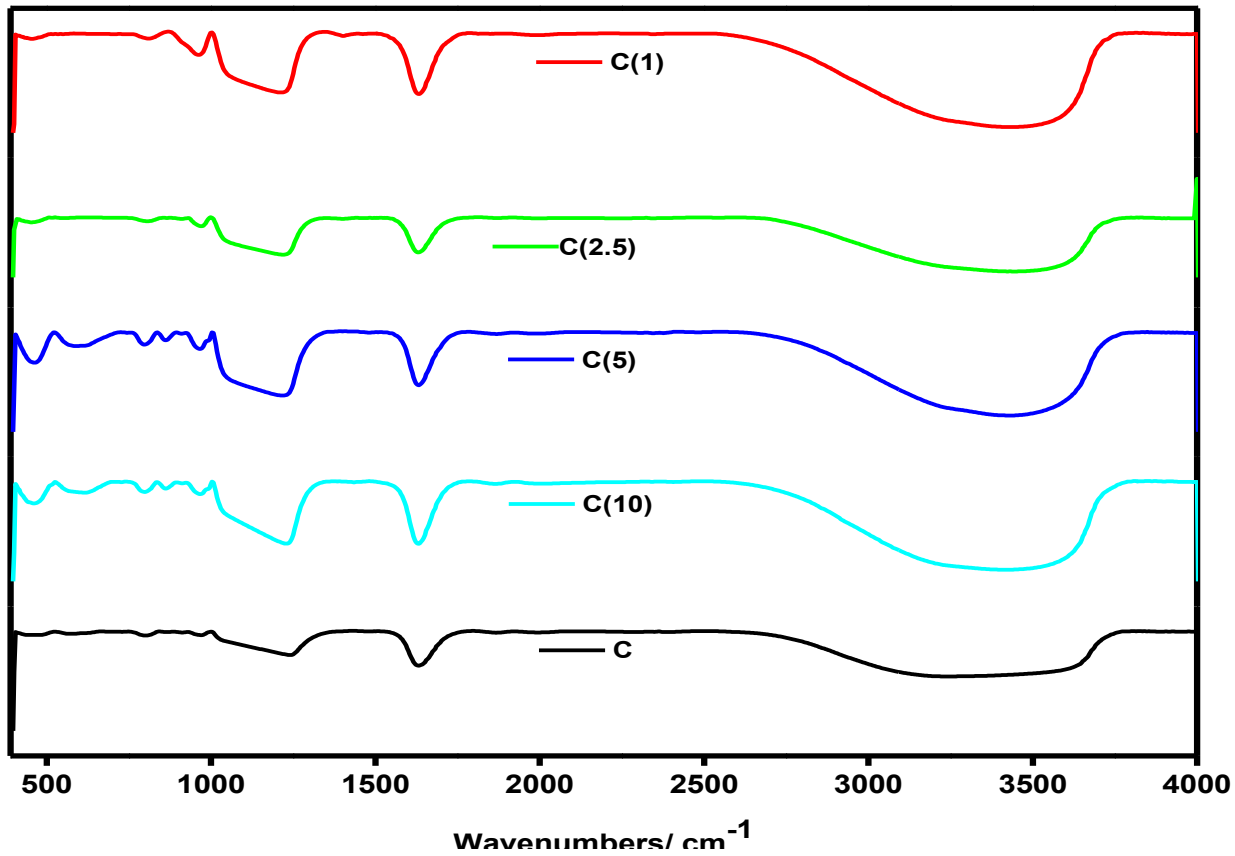

Figure 5-6 . FTIR analysis of Ti-modified SBA-15 NiMo HDS catalysts at different Si/Ti ratios

5.3.8 Scanning Electron Microscopy

Morphological examination and variation due to varying concentration of Si/Ti ratios in catalysts prepared is presented in **Figure 5-7.** The morphology of the catalyst ***C*** and ***C(1)*** has close resemblance with that of pure and unmodified SBA-15, with characteristic of long-channel hexagonal structure. With the increase in Ti-content there is morphological variation which might be due to intra-growth of TiO_2 and main SBA-15 phases, as the long-channel hexagonal morphology of SBA-15 is distorted or disturbed. This observation is in perfect agreement with XRD analysis (section 3.2), where titanium phases corresponding to anatase dominates at higher Ti-content, especially for ***C(2.5)*** and ***C(1).*** In addition, the catalyst ***C(1)*** shows presence of extra particles wounded around the support and looks more of encapsulated material than others at lower Ti-content.

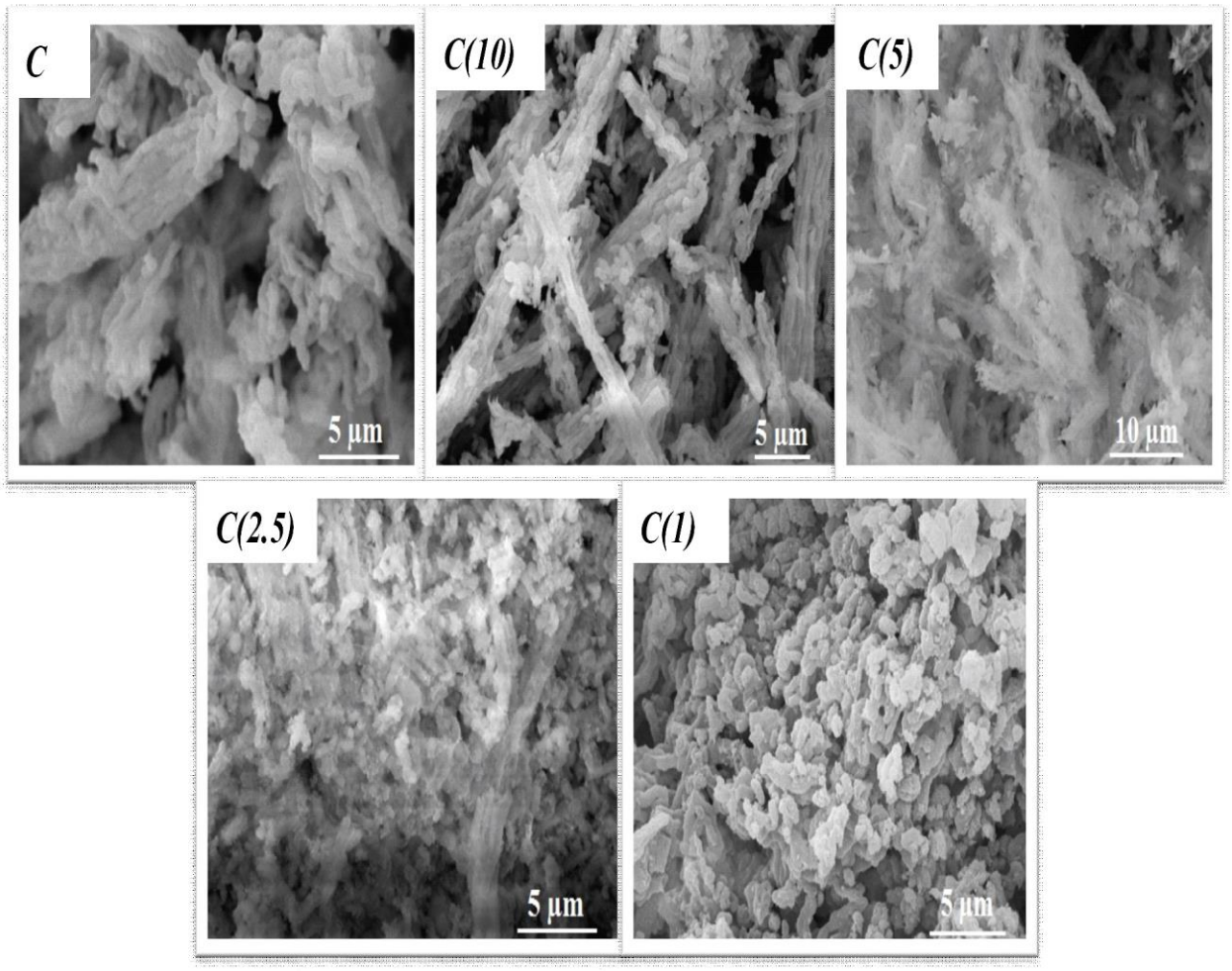

Figure 5-7 SEM analysis of Ti-modified SBA-15 NiMo HDS catalysts at different Si/Ti ratios. (showing morphology variation as Ti-content increases).

5.3.9 Simultaneous HDS of DBT and 4,6-DMDBT

Catalytic activities of the catalysts as a function of Si/Ti ratios for Ti-SBA-NiMo were evaluated in a batch autoclave reactor according to the procedure described in Section 2.4. The HDS of DBT ($\boldsymbol{x}_{DBT}$) over different catalysts is presented in **Table 5-5**. The HDS of DBT increases from 82% to about 90% (by addition of small quantities of titanium) over catalysts ***C(10)*** and ***C(5)*** compared to catalyst ***C***. However, further increase in the quantities of titanium was not beneficial for HDS of DBT. The improvement in activity was more pronounced in the case of HDS of 4,6-DMDBT (**Table 5-6)**. The HDS of 4,6-DMDBT increases from 62% to about 75% over catalysts ***C(10)*** and ***C(5)***. Further increase in the quantities of titanium resulted in almost the same 4,6-DMDBT conversion as with catalyst without titania. These trends are in line with the characterization data which showed better dispersion in catalysts ***C(10)*** and ***C(5)*** compared to catalysts ***C(2.5)*** and ***C(1)***.

The HDS rates were calculated assuming pseudo-first order kinetics and the values of reaction constant, $\boldsymbol{k}$ (min^{-1}), are presented in **Table 5-5 and Table 5-6**. The values for the HDS rate for DBT, $\boldsymbol{k}_{DBT}$, are in the range of 14-19 x 10^{-3} min^{-1} whereas the values for the HDS rate for 4,6-DMDBT, $\boldsymbol{k}_{DMDBT}$, are in the range of 8-12 x 10^{-3} min^{-1}. Lower rate of HDS of 4,6-DMDBT compared to that of DBT is in accordance with the trends reported for simultaneous HDS of DBT and 4,6-DMDBT over CoMoP/Al_2O_3 catalysts [51].

Table 5-5 HDS of DBT: Conversions and Reaction Rates. (Process conditions: 350ºC; 5 MPa; 2h). (error = ± 3.0%)

Catalyst	x_{DBT}	y_{BP}	y_{CHB}	$k_{DBT} \times 10^3$ (min^{-1})	$k_{DDS} \times 10^3$ (min^{-1})	$k_{HYD} \times 10^3$ (min^{-1})	k_{DDS}/k_{HYD}
C	0.82	0.66	0.16	14.2	8.9	1.5	6.0
C(*10*)	0.90	0.73	0.17	18.9	10.9	1.5	7.0
C(*5*)	0.88	0.71	0.17	17.9	10.5	1.5	7.0
C(*2.5*)	0.82	0.69	0.13	14.2	9.7	1.2	8.1
C(*1*)	0.81	0.69	0.12	14.1	9.8	1.1	8.9

Table 5-6 HDS of 4,6-DMDBT: Conversions and Reaction Rates.

(Process conditions: 350ºC; 5 MPa; 2h) (error = **± 3.0%)**

Catalyst	$x_{4,6\text{-DMDBT}}$	y_{DMBP}	y_{DMCHB}	$k_{DMDBT} \times 10^3$ (min^{-1})	$k_{DDS} \times 10^3$ (min^{-1})	$k_{HYD} \times 10^3$ (min^{-1})	k_{DDS}/k_{HYD}
C	0.62	0.51	0.11	8.0	6.0	1.0	6.0
C(*10*)	0.76	0.63	0.13	11.9	8.3	1.1	7.5
C(*5*)	0.73	0.61	0.12	10.9	7.9	1.1	7.2
C(*2.5*)	0.63	0.56	0.07	8.2	6.7	0.7	9.6
C(*1*)	0.62	0.58	0.04	8.1	7.3	0.3	24.3

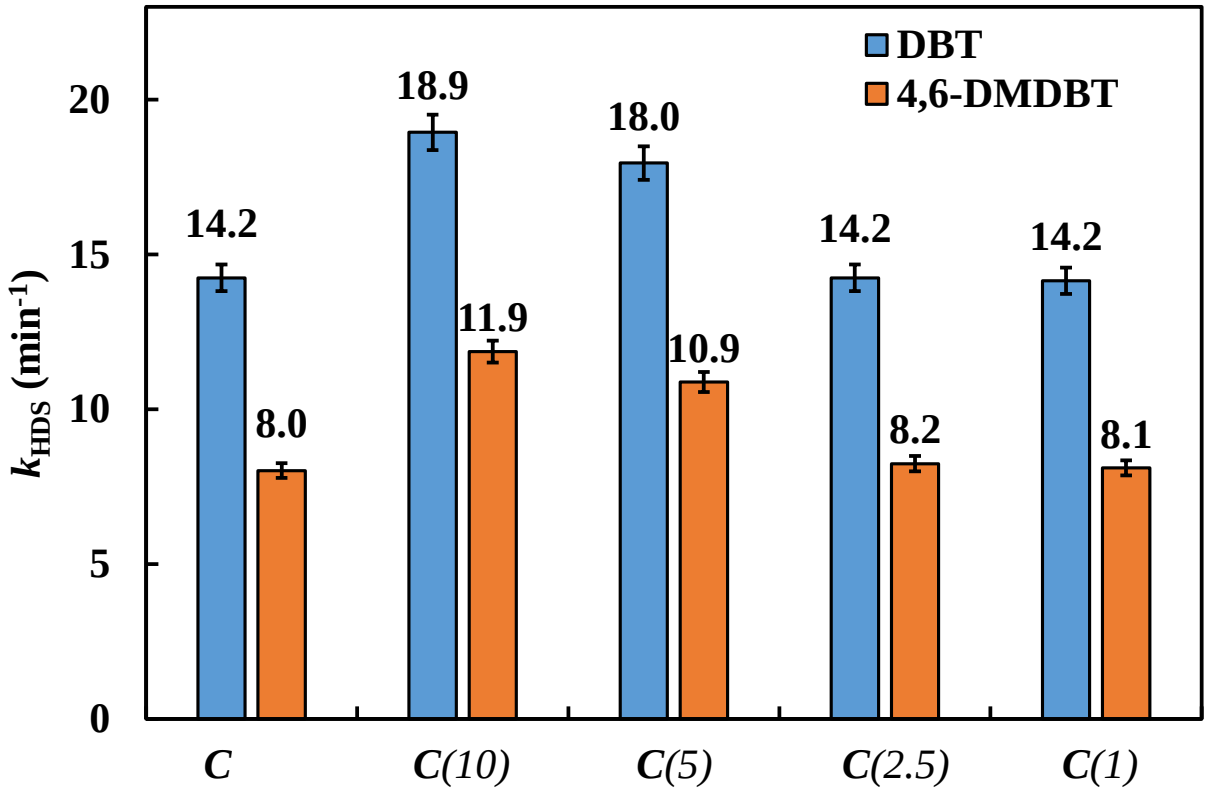

Figure 5-8 Pseudo-First-Order Rate Constants for HDS of DBT and 4,6-DMDBT at 350°C.

Compared to catalyst ***C***, the HDS rate for DBT, $\boldsymbol{k}_{DBT}$, increased by 33% for catalyst ***C***(*10*) and by 26% for catalyst ***C***(*5*). The enhancement in HDS rate was more prominent in the case of 4,6-DMDBT. Compared to catalyst ***C***, the HDS rate for 4,6-DMDBT, $\boldsymbol{k}_{DBT}$, increased by 49% for catalyst ***C***(*10*) and by 36% for catalyst ***C***(*5*). However, further increase in Si/Ti ratio in the catalysts gave away the enhancement in HDS rates due to Ti addition. Hence, the HDS rates for catalysts ***C***(*2.5*) and ***C***(*1*) were almost same as that of catalyst ***C*** for DBT as well as for 4,6-DMDBT. These results can be attributed to increased metal-support interaction in catalysts ***C***(*2.5*) and ***C***(*1*) as observed by NH_3-TPD and H_2-TPR data.

The HDS of DBT occurs via two parallel pathways as reported previously [76]: (i) direct desulfurization (DDS) or hydrogenolysis by C-S bond cleavage in a single step; or (ii) hydrogenation (HYD) in 2-3 steps through the hydrogenation of one of the phenyl rings followed by C-S bond cleavage. The HDS of DBT via the DDS pathway yields biphenyl (BP) and H_2S as final products. However, the HYD pathway results in the formation of intermediates, such as tetrahydro dibenzothiophene (THDBT) and hexahydro dibenzothiophene (HHDBT), followed by fast desulfurization to form cyclohexyl benzene (CHB). Similarly, the HDS of 4,6-DMDBT forms dimethyl biphenyl (DMBP) and dimethyl cyclohexyl benzene (DMCHB) by DDS and HYD routes of HDS, respectively. Because the DDS pathway consumes substantially less hydrogen, it is the preferred route.

The analysis of products obtained from HDS of DBT over different synthesized catalysts is presented in **Table 5-5**. BP is the predominant compound in all products, indicating that DDS is the generally preferred route. The values obtained for the rate of HDS of DBT by direct desulfurization route, $\boldsymbol{k}_{DDS}$, indicate that HDS by DDS is enhanced by the addition of Ti. The highest improvement is observed for the catalyst ***C***(*10*). However, further increase in titania content resulted in lower $\boldsymbol{k}_{DDS}$. On the other hand, the values obtained for the rate of HDS of DBT by hydrogenation route, $\boldsymbol{k}_{HYD}$, remain almost constant with slight decrease for catalysts ***C***(*2.5*) and ***C***(*1*). The divergent effects on the DDS and HYD pathways indicate that the active sites for hydrogenolysis and hydrogenation are not the same and are influenced differently by titania addition. However, the $\boldsymbol{k}_{DDS}/\boldsymbol{k}_{HYD}$ ratio continue to increase with the addition of Ti, which is desirable due to lower hydrogen consumption.

The analysis of products obtained from HDS of 4,6-DMDBT over different synthesized catalysts is presented in **Table 5-6**. Hydrogenation of DBT and DMDBT mainly occurs through π-bonding with the catalyst while the hydrogenolysis occurs through σ-adsorption via the sulfur atom of the molecule. The difficulty in converting the alkyl-substituted DBT compounds is known to be related to the steric hindrance of the alkyl groups positioned close to the sulfur atom which prevents the interaction of these molecules with the active sites of the catalyst through σ-adsorption. The partial saturation of one of the rings through π-bonding which is not sterically hindered in these compounds changes the spatial configuration of them, thus reducing the hindrance effect making them more flexible and accessible to the reaction sites of the catalyst [52,53]. Hence, HYD is the preferential route for the HDS of 4,6-DMDBT over $CoMo/Al_2O_3$ or $NiMo/Al_2O_3$ catalysts [51,53]. However, DMBP is the predominant compound in all products, indicating that DDS is the generally preferred route over Ti-SBA-NiMo catalysts. The hydrogenolysis sites which are responsible to C-S bond cleavage seems to be more active in Ti-SBA-NiMo catalysts than Al_2O_3-supported ones due to relatively weaker metal-support interaction. Thus, the values obtained for the rate of HDS of 4,6-DMDBT by direct desulfurization route, $\boldsymbol{k}_{\mathrm{DDS}}$, indicate that HDS by DDS is enhanced by the addition of Ti. As in the case of DBT, the highest improvement is observed for the catalyst ***C***(*10*). On the other hand, the values obtained for the rate of HDS of DBT by hydrogenation route, $\boldsymbol{k}_{\mathrm{HYD}}$, remain almost constant with a decrease for catalyst ***C***(*2.5*) and drastic decrease for catalyst ***C***(*1*).

The exceptional case of very low hydrogenation activity for catalyst ***C***(*1*) can be attributed to its unique characteristics which are very high strong acidity (**Table 5-2**) and very high hydrogen consumption at lower peak temperature (**Table 5-3**). While the rate of overall HDS of 4,6-DMDBT ($\boldsymbol{k}_{4,6\text{-}DMDBT}$) over catalyst ***C***(*1*) is comparable to that of catalyst ***C***, it should be noted that the $\boldsymbol{k}_{DDS}/\boldsymbol{k}_{HYD}$ ratio of 24.3 is unusually high. This result, especially for HDS of 4,6-DMDBT which is considered as the most refractory sulfur compound) is significant benefit of the composite silica-titania support.

5.4 Conclusions

A series of Ti-SBA-15-NiMo catalysts with Si/Ti ratio of 1, 2.5, 5 and 10 were prepared by single-pot method. The catalysts were characterized by N_2-adsorption, temperature programmed techniques (NH_3-TPD and H_2-TPR), X-ray diffraction (XRD) as well as by Raman and Fourier transform infrared (FTIR) spectroscopy. The catalytic activity was determined by simultaneous hydrodesulfurization (HDS) of dibenzothiophene (DBT) and 4,6-dimethyl dibenzothiophene (4,6-DMDBT) in a batch autoclave reactor. Variation in Si/Ti ratio resulted in noticeable difference in catalysts' characteristics. XRD diffractograms show that titanium is well incorporated into the SBA-15 support at Si/Ti ratios of 10 and 5. However, at Si/Ti ratio below 5, the Ti phases predominate and the peaks corresponding to MoO_3 phases were not observed. As the Ti incorporation is increased, the moderate surface acidity decreases while the contribution from strong acidity becomes evident. TPR results indicate that higher amount of Ti increases the metal-support interaction.

The HDS rates for DBT and 4,6-DMDBT over catalyst with Si/Ti of 10 increased by 33% and 49%, respectively. The enhancement in HDS can be attributed to lower metal-support interaction. However, further increase in Si/Ti ratio gave away the enhancement in HDS rates. Direct desulfurization was the preferred route for both DBT and 4,6-DMDBT. The HDS rate by DDS is enhanced by the addition of Ti while HDS rate by hydrogenation route remain almost constant. The divergent effects on the DDS and HYD pathways indicate that the active sites for hydrogenolysis and hydrogenation are not the same and are influenced differently by titania addition.

The exceptional case of very low hydrogenation activity for catalyst ***C***(*1*) can be attributed to its unique characteristics which are very high strong acidity (**Table 5-2**) and very high hydrogen consumption at lower peak temperature (**Table 5-3**). While the rate of overall HDS of 4,6-DMDBT ($\boldsymbol{k}_{4,6\text{-}DMDBT}$) over catalyst ***C***(*1*) is comparable to that of catalyst ***C***, it should be noted that the $\boldsymbol{k}_{DDS}/\boldsymbol{k}_{HYD}$ ratio of 24.3 is unusually high. This result, especially for HDS of 4,6-DMDBT (which is considered as the most refractory sulfur compound) is significant benefit of the composite silica-titania support.

Chapter 6

Dependence of HDS activity on Nickel promoter and its deposition strategy: New catalyst synthesis approach for highly efficient Ultra-HDS of fuel

ABSTRACT

This study reports a series of strategies to synthesize highly dispersed NiMoS on mesoporous silica support, and the influence of nickel deposition strategy on the HDS activity and selectivity. Four catalyst preparation strategies were adopted: (i) conventional co-impregnation (***CIP***) – simultaneous impregnation of Mo and Ni on the support followed by calcination; (ii) sequential impregnation (***SIP***) – impregnation of Mo followed by calcination and impregnation of Ni without further calcination; (iii) single-pot approach (***SP***) – introduction of Mo and Ni onto support at the same time followed by calcination; and (iv) modified-single-pot approach (***MSP***) – loading of Mo on the support followed by calcination, then impregnation of Ni without further calcination. The catalysts were characterized by N_2-physisorption, chemisorption (TPD, TPR), XRD, XRF, Raman and FTIR (pyridine), SEM and their performance for the simultaneous HDS of DBT and 4,6-DMDBT was determined. The drawback of low Ni content in catalyst prepared by single-pot approach was rectified by adopting the two-step modified single-pot strategy. The catalyst prepared by modified single-pot approach (***MSP***) grossly outperformed the other catalysts prepared without the addition of complexing agent. A significantly divergent influence of using complexing agent was obtained which underscores the importance of nickel loading method on catalytic behavior. The addition of citric acid showed little effect on the performance of ***CIP*** or ***SP*** catalyst whereas the catalyst prepared by sequential impregnation (***SIP***) method benefited most. The addition of complexing agent further improved the performance of ***MSP*** – especially for the HDS of 4,6-DMDBT. Therefore, catalyst ***MSP-CA*** was the best-performing HDS catalysts among all the catalysts investigated in this study with a great potential for deep desulfurization of diesel feedstock with minimum consumption of hydrogen.

6.1 Introduction

The search for highly dispersed and active HDS catalysts for producing ultra-low sulfur fuels continues to stimulate the researchers in order to meet the increasingly stringent environmental regulations and to save catalytic converters from poisoning [3, 16, 135]. Deep hydrodesulfurization (HDS) requires highly active and stable catalysts with excellent dispersion of active metals. The recent efforts to explore alternate hydrodesulfurization (HDS) support from γ-Al_2O_3 to mesoporous silica has witness tremendous achievements, with the later showing better performance in terms of activity and stability compared to the former [136, 137]. The improved performance has been attributed to higher surface area and hydrothermal stability of mesoporous silica – especially for SBA-15 – compared to γ-Al_2O_3 [4]. The advantages of mesoporous SBA-15 over γ-Al_2O_3 as a support for modified and unmodified HDS catalysts have been reported [53, 136, 138, 139].

The extent of metal-support interaction is important for activity and stability of supported catalysts. For example, the formation of tetrahedral molybdenum coordination which is usually resulted from strong metal-support interaction leads to low catalytic activities and fast deactivation. This behavior is a well-known characteristic of γ-Al_2O_3 supported Ni(Co)Mo(W) HDS catalysts due to excess Bronsted acidity and fewer coordinatively unsaturated sites (CUS) [19]. On the other hand, the mesoporous molecular sieves such as MCM-41, SBA-15, FDU-12, SBA-16, KIT-6 present better alternative, in spite of their weak interaction with the active phase that may affect the dispersion for catalytic activities [138].

The recent research efforts focusing on improving the interaction between the SBA-15 and the active species has achieved remarkable improvement by incorporation of the heteroatoms, complexing agents, additives etc. to improve the dispersion of the active species [6, 9, 140]. However, there are areas that require improvement; vis-à-vis, method of incorporating the heteroatoms, and active phase on the support.

Conventional method of incorporating active species Co(Ni)Mo(W) by impregnation approach is exhaustive and a better approach is necessary. Firstly, the impregnation method is multi-step and cumbersome that allow repetitive procedure for a catalyst. For example, calcination and drying steps must be done more than once (for support and after deposition of active species), which can

lead to loss of some of the characteristics and catalyst quality [12]. In addition, sequential impregnation is prone to re-dissolution and redistribution of initial impregnating species during consecutive steps.

A new synthesis strategy based on single-pot (SP) synthesis of both support and active species (NiMo) combined with the use of heteroatom (Ti) was recently reported by our group. We found that the catalysts prepared by applying SP method showed excellent HDS activity compared to impregnation method [141]. However, a drawback of this approach is that it could not incorporate Ni completely in the catalyst under strong acidic synthesis condition chosen, and significant amount was left in the solution. To overcome this drawback, a modified single-pot (MSP) strategy has been adopted. This modified approach involves incorporation of Mo (the main active metal) at the support preparation stage, followed by impregnation of Ni after calcination of Ti-SBA-Mo at 300 ^{o}C.

The catalyst activity was determined with a model fuel containing binary solutes of dibenzothiophene (DBT) and dimethyldibenzothiophene (DMDBT) in dodecane. The HDS performance of catalyst prepared by MSP method was compared with those prepared by SP approach as well as CIP and SIP that mimics the modified single-pot strategy. In addition, this research investigates the scientific argument in the literature that the catalyst with chelating agent and promoter should be calcined or not prior to sulfidation, in order to achieve highly dispersed HDS catalyst [6, 36, 142]. The recent report by Pawelec et al. [143], deals only with the impact of preparation method (simultaneous and sequential impregnation methods) and support modification on HDS activity of hexagonal mesoporous silica (HMS) CoMo catalysts with phosphorus additive. Detail studies were conducted in this work and comparison were made for NiMo catalysts supported on modified mesoporous silica (Ti-SBA-15). Characteristics of oxide and sulfided catalysts were explored by N_2-physisorption, chemisorption analysis by temperature programmed desorption and reduction (TPD, and TPR), X-ray diffraction (XRD), X-ray fluorescence (XRF), Raman spectroscopy, Fourier transform infra-red (FTIR) and FTIR-pyridine, scanning electron microscope (SEM).

6.2 Experimental

6.2.1. Synthesis of Ti-SBA-15-NiMo or Ti-SBA-15-Mo-Ni Catalysts

HDS catalysts by SP or MSP procedures were prepared by following the preparation route for SBA-15 by sol-gel method with addition of other components as described earlier [141]. Briefly, this involves addition of about 4.16 g of TEOS to a reaction mixture containing a well-dispersed surfactant (2 g P123) in 60g of 2M HCl and de-ionized water (DI-H_2O). Titanium precursor in 10:1 (Si:Ti) mole ratio was added before hydrolysis of TEOS and allowed to stir continuously for 20 h. The SP approach involve preparing a solution of Mo (13 wt.%) and Ni (3 wt.%) precursors at room temperature and stirred for 1 h. This solution is added to the synthesis pot and stirred vigorously for another 3 h at the room temperature. In the MSP approach, the solution of only Mo (13 wt.%) precursor is added. The sample was transferred into Teflon autoclave for hydrothermal (HT) synthesis at 100 ^oC for another 24 h. The solid sample was then centrifuged and washed before drying at 100 ^oC for 12 h, and subjected to final calcination at 300 ^oC for 6 h in muffle furnace. Nickel nitrate hexahydrate is added with or without (CA) was dissolved in DI-H_2O and stirred with calcined sample containing (SBA-15-Mo) for 3 h, before drying at 120 ^oC without further calcination. The catalysts thus obtained were denoted as Ti-SBA-15-NiMo and Ti-SBA-15-NiMo(CA) for single-pot strategy (labeled as catalysts *SP* and *SP-CA*, respectively), and Ti-SBA-15-Mo-Ni and Ti-SBA-15-Mo(CA)-Ni for modified-single-pot strategy (labeled as catalysts *MSP* and *MSP-CA*, respectively), as listed in **Table 6-1**.

6.2.2 Preparation of Ti-SBA-15/NiMo or Ti-SBA-15/Mo-Ni HDS catalysts

Ti-SBA-15 was prepared by the method described above without addition of active species precursors. Typically, a Ti and mesoporous SBA-15 are produced in one-step, by adding equivalent amount of Ti in the ratio of 1/10 to silica into a mixture containing 4.16g of TEOS, 60g (2M)-HCl, 15g DI-H_2O and 2g P(123) surfactant at 40 ^oC for 20 h. The solid obtained was subject to hydrothermal synthesis for 24 h under static condition. The solid support was the centrifuged and dried at 100 ^oC for 12 h before final calcination at 300 ^oC for 6h. The sample obtained was denoted Ti-SBA-15, and of active species was deposited via co- and sequential impregnation with or without complexing agent (citric acid) accordingly, then dried and calcined as described above. The catalysts were denoted as Ti-SBA-15/NiMo and Ti-SBA-15/NiMo(CA) for co-impregnation

(labeled as catalysts ***CIP*** and ***CIP-CA***), and Ti-SBA-15/Mo-Ni and Ti-SBA-15/Mo(CA)-Ni, for sequential impregnation (labeled as catalysts ***SIP*** and ***SIP-CA***), as listed in **Table 6-1**.

Table 6-1 Description of Supports and Catalysts.

Catalyst	Description	Catalyst Preparation Method	Complexing Agent
CIP	Ti-SBA-15/NiMo	Co-impregnation	No
SP	Ti-SBA-15-NiMo	Single-pot synthesis	No
SIP	Ti-SBA-15/Mo-Ni	Sequential impregnation	No
MSP	Ti-SBA-15-Mo-Ni	Modified single-pot synthesis followed by impregnation of Ni	No
CIP-CA	Ti-SBA-15/NiMo(CA)	Co-impregnation	Yes
SP-CA	Ti-SBA-15-NiMo(CA)	Single-pot synthesis	Yes
SIP-CA	Ti-SBA-15/Mo(CA)-Ni	Sequential impregnation	Yes
MSP-CA	Ti-SBA-15-Mo(CA)-Ni	Modified single-pot synthesis followed by impregnation of Ni	Yes

6.2.3 Characterization

N_2-physisorption measurement of catalysts was analyzed by Micromeritics ASAP 2020 at -196 ^oC. Samples were degassed to remove impurities and moisture at 250 ^oC for 180 min prior to adsorption-desorption of N_2 molecules. The surface area was calculated by Brunauer, Emmet, and Teller (BET) method, while pore size and pore volume was calculated by adsorption part of Barret, Joyner, and Halenda (BJH) method at $P/P^o = 0.9$. Crystallinity and degree of dispersion of the developed catalysts were determined by wide-angle x-ray diffraction (XRD) from Rigaku (miniflex II-desktop X-ray diffractometer) using Cu anode (9 kV) at $K\alpha = 1.5405$. The analysis was performed at 2Θ (20° - 80°) at scan rate of 3°/min. A laser-Raman spectrometer (iHR320) of 532 nm wavelength from HORIBA (France) coupled with charged coupled device detector (CCD) was employed to further characterized the crystallinity phases of oxide-NiMo supported HDS catalysts. Infra-red analysis of supported catalysts on Ti-SBA-15 was used to study the functional group of NiMo-oxide on the support together. The samples were prepared in form of a translucent pellet disc by mixing with KBr powder in 100: 1 KBR-sample ratio, and analysis was performed on Thermo-Scientific Nicolet 6700 FT-IR spectrometer with a scanning range of 400-4000 cm^{-1}. An in-situ pyridine FTIR of self-supported wafer was conducted in *Specac* cell adapted to Thermo-Scientific Nicolet 6700 spectrometer, the type of acidity was determined qualitatively and quantitively. The samples were pretreated under vacuum (1.33×10^{-3} Pa) at 300 ^oC for 60 min, followed by adsorption of pyridine vapor at 150 ^oC for 30 min. prior to acidity measurement physisorbed pyridine was evacuated for 15 min and the spectra was recorded after degassing at 200 ^oC to measure total acidity due to Lewis and Bronsted acid sites. Temperature-programmed desorption (TPD) of ammonia (NH_3) as a measure of the nature of surface acidity is determined by Micromeritics Chemisorb 2750 (pulse chemisorption system) using 10 wt. % NH_3 as a probe molecule. About 100 mg of oxide-NiMo catalyst loaded in quartz sample-holder for analysis was pretreated in a flow of helium (He) gas at 500 ^oC for 1 h. The sample was cooled down to 100 ^oC for adsorption of NH_3 for 30 min, followed by purging with He to remove physically adsorbed NH_3, at the same temperature for 1 h. Desorption of chemisorbed probe molecule was conducted by heating the furnace to 800 ^oC at the rate of 10 ^oC/min. The data was recorded on thermal conductivity detector (TCD) with TPx-software for data analysis. TPR analysis of supported oxide catalysts as a measure of reduction temperature potential were analyzed by Micromeritics (Autochem II-2920) chemisorption analyzer using hydrogen (H_2). About 50 mg of catalyst was

treated in helium (He) gas at 400 ^{o}C for 60 min and cooled than to 35 ^{o}C before heating at 10 oC/min to 1000 ^{o}C for catalysts' reduction under 10% hydrogen make up with He (10% H_2/He). The spectrum was recorded on a thermal conductivity detector (TCD) as a function of catalysts' reduction temperature due to H_2 consumption. The elemental analysis of bulk catalysts was determined by energy dispersive x-ray fluorescence (SPECTRO XEPOS) spectrometer from AMETEK, materials analysis division, equipped with AMECARE M2M.

Morphology of NiMo-oxide supported on Ti-SBA-15 was examined for possible morphological differences due to deposition of active phase by TESCAN LYRA 3, equipped with an energy-dispersive X-ray spectrometer (EDS, Oxford, Inc.) detector for elemental analysis.

6.2.4 Catalyst Sulfidation

The active species for HDS reaction is the sulfided Ni(Co)Mo(W) phase for supported and unsupported catalysts. Sulfidation of pelletized NiMo supported Ti-SBA-15 catalyst (300-500 µm) was conducted in a tubular furnace at 350 ^{o}C, by flowing of 2wt.% CS_2 solution in cyclohexane at 1 mL/min by the aid of HPLC pump for 4 h. Prior to this step, the oxide phase of NiMo was reduced in 10% H_2/He at 400 ^{o}C for 3 h at constant flow of 100 mL/min.

6.2.5 Catalytic Testing

HDS catalytic evaluation of sulfided NiMo was conducted in dodecane as model fuel containing dibenzothiophene (DBT) and dimethyldibenzothiophene (DMDBT) of 1000 ppm-S each using Parr batch reactor (Parr 4576) at 350 ^{o}C and 5 MPa. About 250 mg of catalyst was added in 100 mL of model fuel solution containing pre-dissolved organosulfur compounds mentioned above. HDS reaction was run for 4 h with hourly sample collection, and the product was analyzed for sulfur contents and hydrocarbon identification by gas chromatography sulfur chemiluminescence detector (GC-SCD) and gas chromatography mass spectrometry (GC-MS), respectively.

6.3 Results and Discussion

6.3.1 Physisorption analysis

The BET isotherms and textural properties data of the prepared catalysts are presented in **Figure 6-1** and **Table 6-2**, respectively. SBA-15 or heteroatoms modified-SBA-15 possesses high surface area (approx. 1000 m^2/g) [35], however, the introduction of active species reduces the surface and pore volume due to surface coverage and pores void resulted from their large atomic size. The ***SP*** and ***MSP*** catalysts preserved their surface areas and pore volumes better than the ***CIP*** and ***SIP*** catalysts. This is because the impregnation approach, especially at high Mo-loading, generally cover more surface and thus block some of the micropores. Addition of complexing agent to the catalyst matrix increased the surface area, but generally led to a decrease in average pore diameter. Notably, catalysts prepared with complexing agent have 6-15 % higher surface area than those without complexing agent. Catalysts ***MSP-CA*** and ***MSP*** have highest surface areas and lowest average pore diameters.

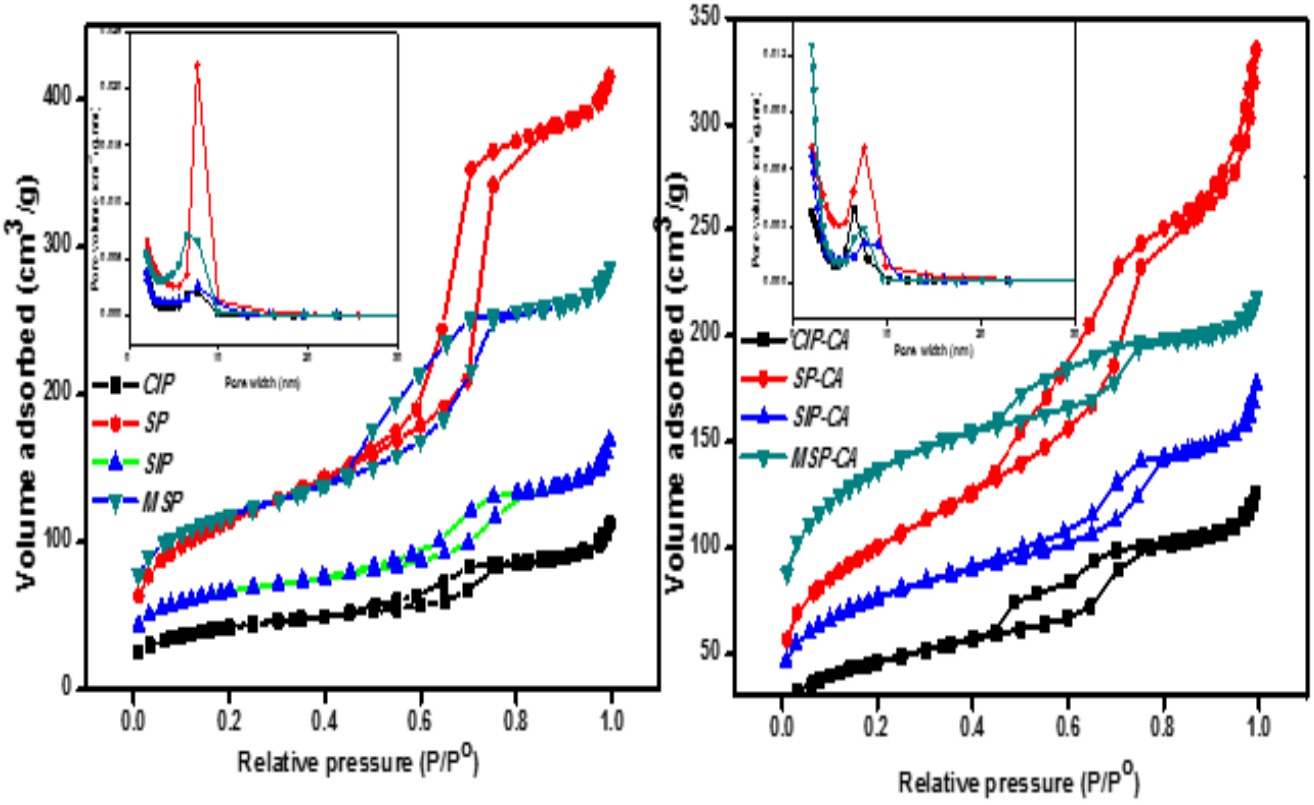

Figure 6-1 N_2 physisorption analysis of catalysts prepared without (left) and with (right) citric acid. Inset represent pore-size-distribution (PSD).

Table 6-2 Textural properties and quantitative acidity by FTIR pyridine of HDS catalysts.

Catalyst	BET Surface Area (m^2/g)	Total Pore Volume (cm^3/g)	Average Pore Diameter (nm)	Acid Sites				
				B (µmol/g)	L (µmol/g)	B+L (µmol/g)	B/L	Density (µmol/m^2)
CIP	152	0.16	6.1	75	160	235	0.47	1.55
SP	335	0.66	6.4	36	108	144	0.33	0.43
SIP	224	0.22	6.8	129	199	328	0.65	1.46
MSP	400	0.40	5.5	32	142	174	0.23	0.43
CIP-CA	162	0.19	5.5	61	146	207	0.42	1.28
SP-CA	352	0.51	6.3	51	181	232	0.28	0.66
SIP-CA	262	0.24	5.4	136	129	265	1.06	1.01
MSP-CA	460	0.23	4.1	39	193	232	0.20	0.50

6.3.2. Crystallinity analysis by X-ray Diffraction

The degree of dispersion of active species in oxide form catalysts can be correlated to the crystallinity of NiMo phase(s) obtained by wide-angle XRD analysis. The characteristic phases of ordered p6mm hexagonal symmetry SBA-15 siliceous material at low-angle XRD are 100,110 and 200 [50]. Moreover, the SBA-15 shows no crystalline peak on wide angle XRD, but there is a broad peak around $2\Theta = 26^{o}$.

As shown in **Figure 6-2**, the wide-angle diffractograms show the crystalline phases of molybdenum oxides corresponding to orthorhombic MoO_3 (JCPDS card #: 05-0508) with the space group Pbnm of octahedral form. It should be noted that the catalysts prepared by single-pot approach and co-impregnation method without citric acid (catalysts ***SP*** and ***CIP***) exhibited highly dispersed phase compared to the catalysts prepared by the modified single-pot approach and sequential impregnation method (catalysts ***MSP*** and ***SIP***) in oxide form, due to promoter effect of Ni. Similar trends were observed for the catalysts prepared by the addition of citric acid with both methods of adding Ni and Mo active species at the same time (catalysts ***CIP-CA*** and ***SP-CA***) showing more reflection of the support with little crystalline phase associated with Mo and/or NiMo crystallites. Interestingly, the modified-single-pot strategy shows more crystalline phase either with or without the addition of complexing agent than other catalysts. This preparation approach is similar to bulk catalyst preparation method that ensures high concentration and good distribution of active metal on the support. Moreover, the formation of stable and inactive crystalline phases due to $NiMoO_4$ is prevented due to careful selection of calcination temperature of 300 ^{o}C [12].

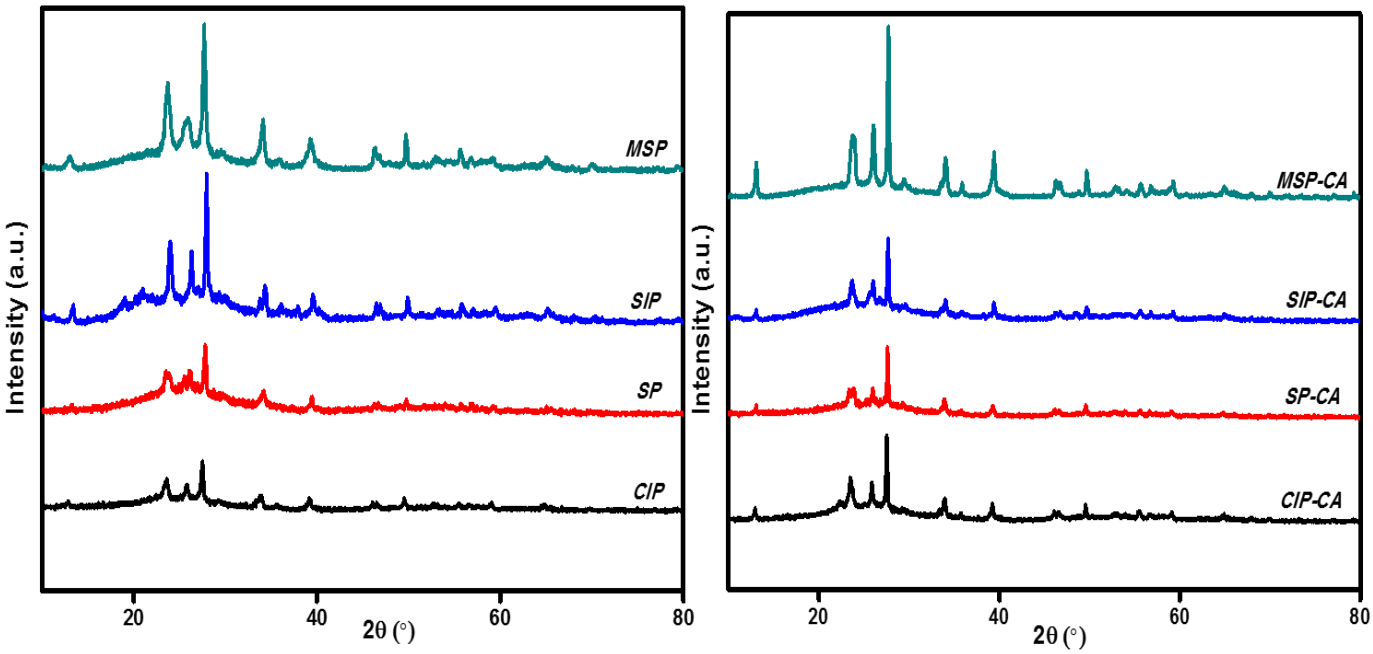

Figure 6-2 X-ray diffraction analysis of catalysts prepared without (left) and with (right) citric acid by different methods.

6.3.3 Raman analysis

Raman spectroscopy is a non-destructive characterization technique to identify oxide phases and measure the crystallinity of these phases with respect to dispersion. **Figure 6-3** presents the Raman spectroscopic analysis of Ti-modified-SBA-15 NiMo-oxide catalysts prepared by different approaches. Crystalline MoO_3 can exist in either tetrahedral or octahedral form [55]. In a typical molybdena material, peak occurring at about 994 cm^{-1} indicates symmetric stretching of the Mo=O terminal oxygen while peaks at 819 and 665 cm^{-1} represent Mo-O-Mo bridging [144]. In addition, vibration bands of O-Mo-O and O=Mo=O, and Mo=O are identified at 290-280 cm^{-1} [59]. The dominant molybdena species may exist in the form of tetrahedral (Si-O-)2Mo(=O)2di-oxo species, due to the interaction on SBA-15, by the bands occurring at 970 and 355 cm^{-1} [145]. However, calcination of NiMo catalyst is carried out at lower temperature displayed an excellent dispersion which is confirmed by the presence of amorphous peak at 950 cm^{-1} [61]. The peaks positions in all catalysts were similar, which may reflect the presence of similar surface oxide species. However, the observed intensities in each catalyst differs and can be correlated to different degree of dispersion and interaction with the support.

Catalyst ***MSP*** showed low intensity of peaks compared to other catalysts prepared without CA. In contrast, catalyst ***MSP-CA***, exhibited peaks with higher intensities than others, when comparing Raman mode of vibrations within the set of catalysts that employed addition of CA. Furthermore, the catalysts prepared by impregnation methods (catalysts ***CIP-CA*** and ***SIP-CA***) show better dispersion than those prepared by the single-pot and modified-one-pot methods with the complexing agent.

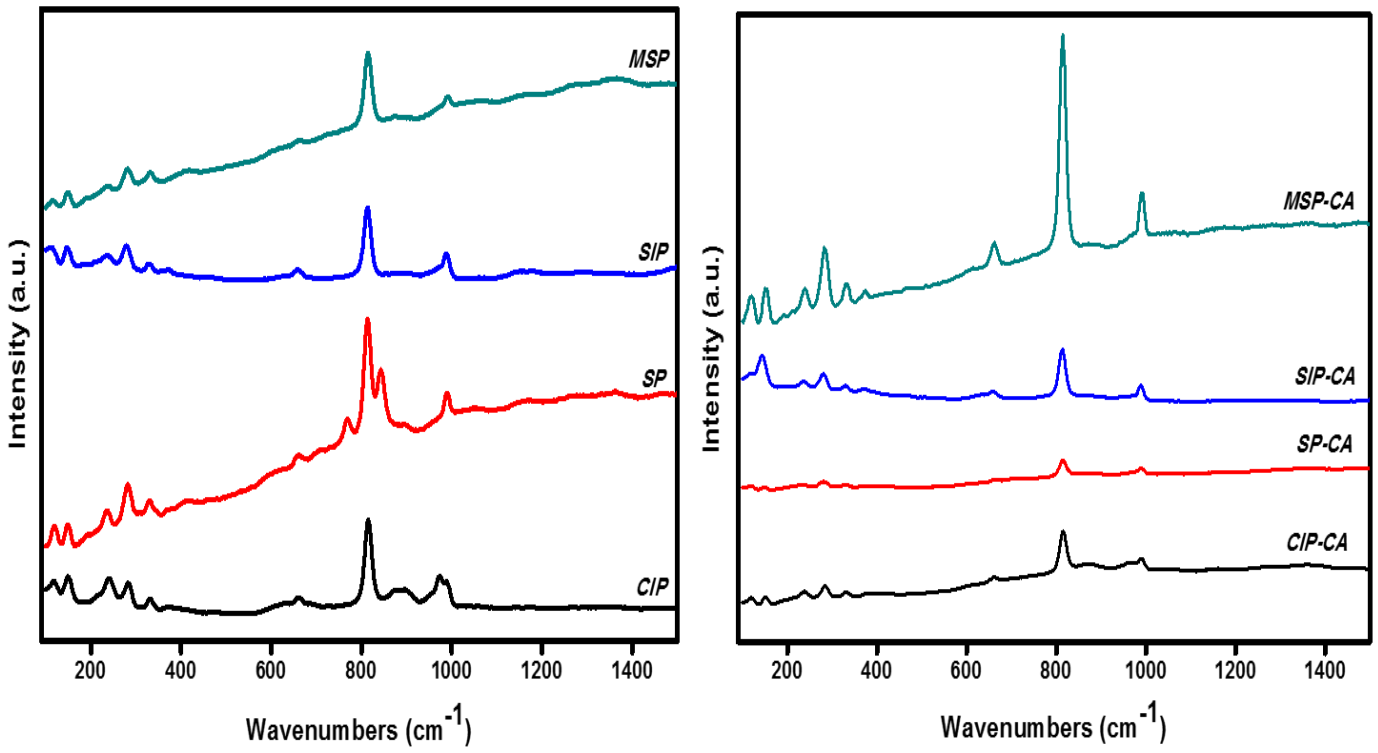

Figure 6-3 Raman analysis of catalysts prepared without (left) and with (right) citric acid by different methods.

6.3.4 FTIR analysis of oxide catalysts

FTIR spectroscopy was employed to gain insight into the functional groups of NiMo-supported on Ti-modified-SBA-15 catalysts. From the spectra displayed in **Figure 4**, a strong intensity band at approximately 1218 cm^{-1} is a characteristic of Si-O-Si asymmetric stretching modes in SBA-15, and a broad absorption band at 1628 cm^{-1} is a characteristic peak of hydroxyl group stretching frequency of absorbed water molecule [63]. In addition, the Si_3O-Ti-OH and silanol end group (Si-OH) which are significant to Brønsted acid sites, can be observed at 3500 cm^{-1} absorption band. The presence of Ti into mesoporous SBA-15 resulted in the presence of bands at 800 and 950 cm^{-1}. This is consequential to the symmetric stretching mode Ti-O and Ti-O-Si bending modes, respectively [6]. Considering the NiMo-supported SBA-15 bands, the Mo-O-Mo stretching mode is exhibited at around 620 and 850 cm^{-1}, with the presence of band at 797 cm^{-1} significant to the existence of polymolybdate (Mo_{36}) [64].

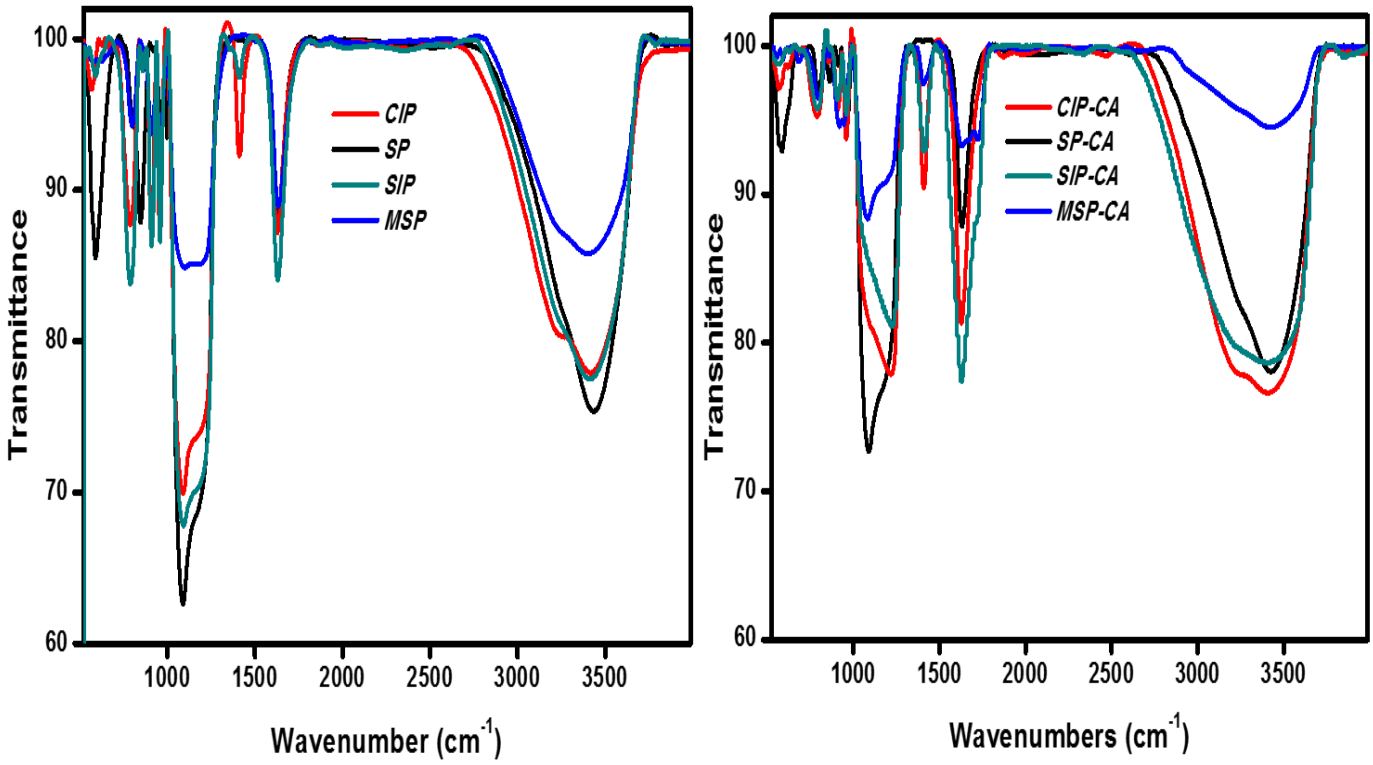

Figure 6-4 FTIR analysis of catalysts prepared without (left) and with (right) citric acid by different methods.

6.3.5 Fourier transformation infra-red analysis by pyridine adsorption

The type acidity type of all catalysts in oxide-form is examined by FTIR spectroscopy using pyridine as a probe molecule. The characteristics frequencies of pyridine in IR region can be classified as strong Lewis acid sites at 1450 cm^{-1} and 1610 cm^{-1}, weak Lewis acid sites 1575 cm^{-1} and the bronsted at 1542 cm^{-1} and 1640 cm^{-1}. Moreover, there exists a characteristic band for combination of Lewis and bronsted acid sites at 1492 cm^{-1} [146] Lewis acid sites are generally due to coordinatively unsaturated cations exposed at the surface of ionic metal-oxide, while the Bronsted sites are largely due to surface OH arising from adsorbed water on the surface of the metal oxides [146]. Assignment of peaks and quantitative amount of pyridine on each catalyst are presented in **Figure 6-5** and **Table 6-2**, respectively.

Except for catalyst ***SIP-CA*** (which is prepared by sequential impregnation with the addition of CA), all catalysts exhibit more Lewis acidic sites than Bronsted sites. A comparison of the total acidity contributions from Lewis and Bronsted acidic sites between methods of preparation, indicates that the impregnation (co-and sequential) approaches exhibited significantly more acid sites and acid-site density than single-pot and modified-single-pot approaches. Similarly, the amount of Bronsted acidity is higher in catalysts prepared by impregnation methods, and this may be attributed to more interaction of pyridine with metal centers largely on the surface of the catalysts by these methods. Overall, the Bronsted acid sites and the ratio of B/L in catalysts prepared by impregnation in two steps (sequential impregnation) is significantly higher than other catalysts, with or without CA addition.

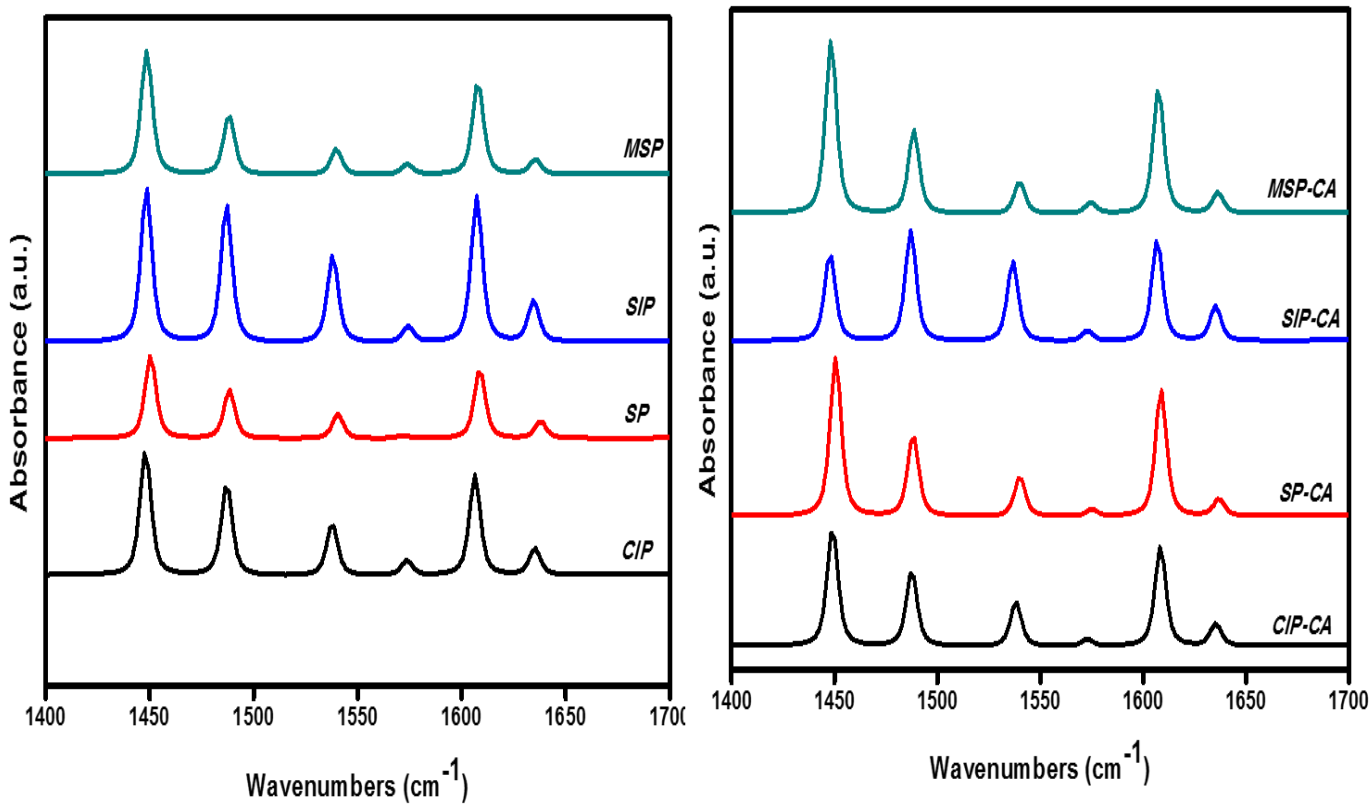

Figure 6-5 Pyridine-FTIR analysis of catalysts prepared without (left) and with (right) citric acid by different methods.

6.3.6 Temperature Programmed desorption analysis by ammonia

The nature of surface acidity in all catalysts prepared is determined by TPD-analysis using NH_3 (a strong base) as a probe molecule. The **Figure 6-6 (left)** presents the acidity of catalysts prepared without complexing agent, and the nature of acidity of catalysts prepared in this category is moderate (200-350 ^oC). Catalysts ***SP*** and ***MSP***, prepared by single-pot and modified-single-pot methods, respectively, possess more number of active sites than the catalysts prepared by impregnation approaches by quantitative amount of NH_3 desorbed, which can be correlated to the number of active sites (See **Table 6-3**) [147]. Likewise, the surface acidity analysis of catalysts with complexing agent (**Figure 6-6 (right)**) is moderate. The catalysts prepared by impregnation of active species exhibit some strong acidity between 590-655 ^oC and it is more pronounced for catalysts prepared by sequential impregnation approach. However, the quantity of NH_3 desorbed at this region is insignificant compared to moderate acidity, and may not significantly affect the catalytic activity. In general, the single-pot approaches are more efficient in providing more number of active species than impregnation approaches, due to preservation of specific surface area which facilitates better dispersion of the active species.

Table 6-3 TPD and TPR Results of Catalysts (in the Oxide Form)

Catalyst	TPD: NH_3 desorbed		TPR: H_2-consumption			
			$Mo^{6+} \rightarrow Mo^{4+}$		$Mo^{4+} \rightarrow Mo^{0}$	
	Peak Temperature(s) (°C)	Amount (μmol/g)	Peak Temperature(s) (°C)	Amount (mmol/g)	Peak Temperature(s) (°C)	Amount (mmol/g)
CIP	206	158	493	960	724	1285
SP	200	198	518	589	720	844
SIP	213, 656	194	407, 486	924	704	1104
MSP	213, 609	195	473	879	720	826
CIP-CA	200	138	488	873	696	583
SP-CA	202	235	510	533	659	583
SIP-CA	218, 686	161	414, 485	868	728	1104
MSP-CA	208, 593	209	469	874	733	874

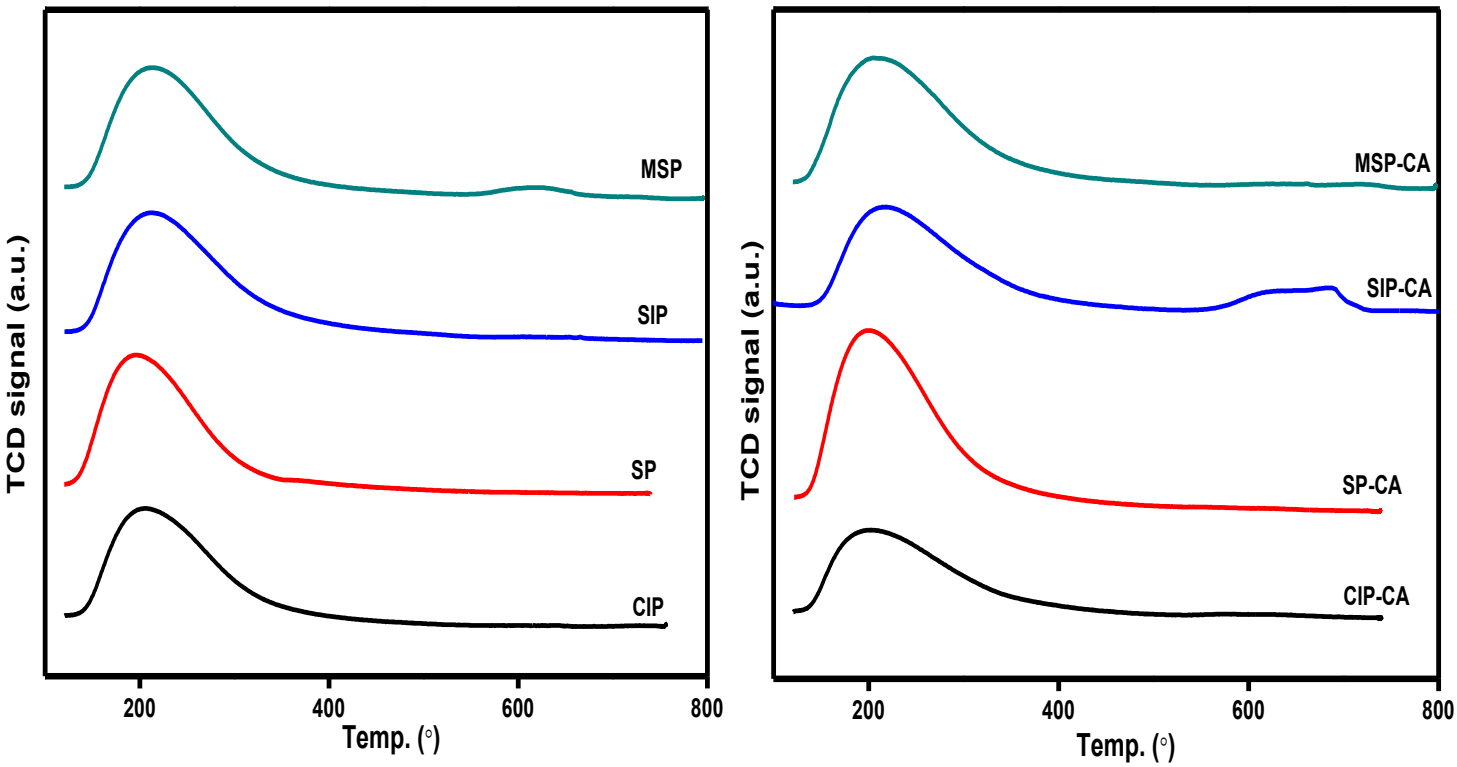

Figure 6-6 TPD analysis of catalysts prepared without (left) and with (right) citric acid by different methods.

6.3.7 Temperature programmed reduction analysis by hydrogen

The reduction of molybdenum species supported on heteroatoms modified-SBA-15 proceeds mainly via two steps, (i) reduction of Mo^{6+} to Mo^{4+} at relatively lower temperature, (ii) reduction of Mo^{4+} to Mo^{0} at higher or raised temperature. The characteristic reduction of metals on support defines the extent of its interaction with support and the availability for reaction. As shown in **Figure 6-7**, the first H_2 reduction temperature for catalysts prepared without inclusion of citric acid in the matrix are higher than the corresponding counterparts with complexing agent. Furthermore, the same trend of H_2 reduction is observed for reduction of Mo^{4+}-Mo^{0} between the two-set of catalysts prepared, that is catalysts prepared with complexing agent are reduced at lower temperature compared to catalysts without CA (See **Table 6-3**). This observation is in accordance with reported literature on the use of complexing agent to reduce support metal interaction [6]. In addition, it is worth mentioning that the catalyst prepared by direct incorporation of active species in single-step showed higher temperature for reduction of both oxide species of Mo than others, since the quantitative amount of Ni present in the final catalyst is low compared to calculated amount, and the reason was reported in our previous work [141]. Also, catalysts ***MSP*** and ***MSP-CA*** exhibit lower H_2 reduction temperatures for Mo^{6+} - Mo^{4+} and Mo^{4+} - Mo^{0} than others, which might signify ease of reduction and accessibility of active species.

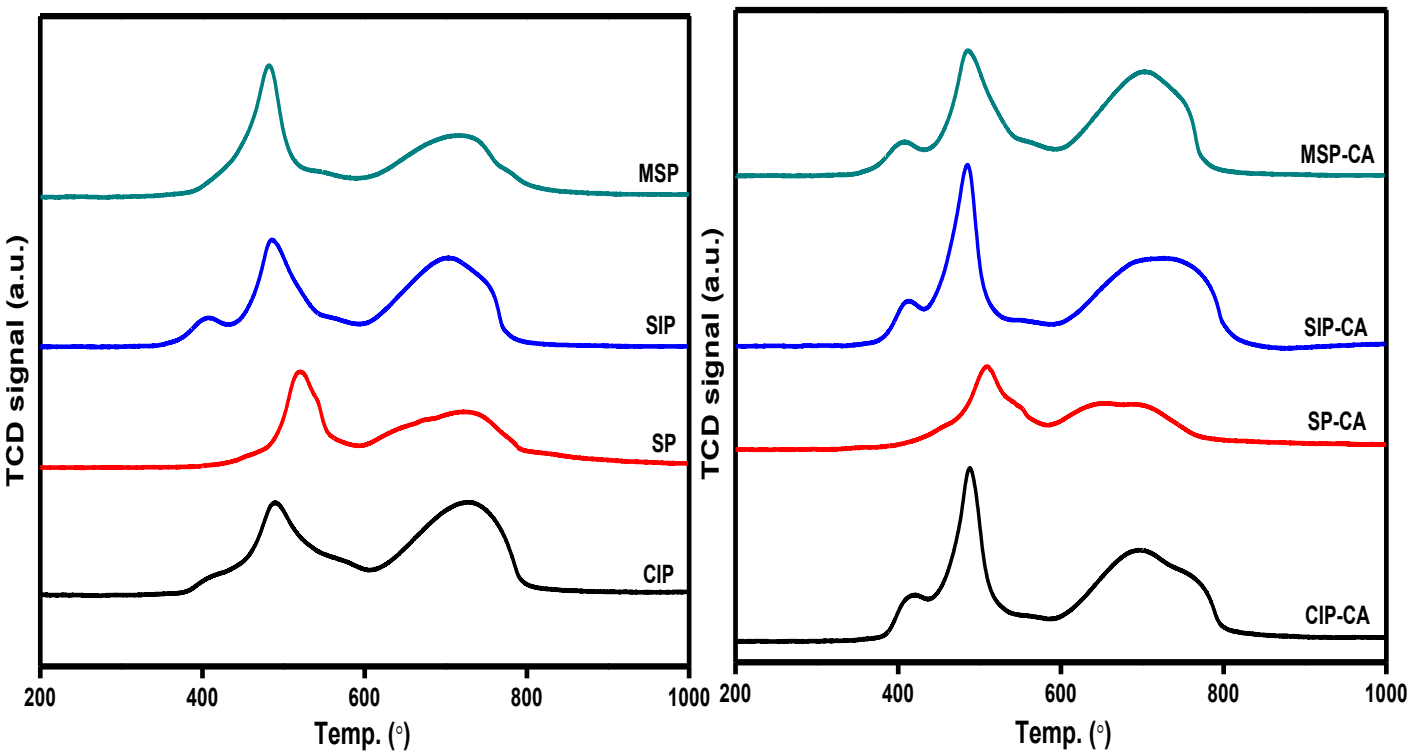

Figure 6-7 TPR analysis of catalysts prepared without (left) and with (right) citric acid by different methods.

6.3.8 Elemental analysis by X-ray Fluorescence

Quantitative amount of catalysts' composition was determined by X-ray fluorescence analysis for bulk catalysts in oxidic form, and shown in Table 6-4. The active species (Ni and Mo) and Ti are well dispersed on the Ti-SBA-15 support by different deposition strategies used, with the exception of Ni in single-pot approach that contained lesser amounts (<40 %) of the calculated percent in the final catalysts either with or without citric acid (catalysts ***SP*** and ***SP-CA***). This drawback for the single-pot approach is due to the presence of soluble nickel in the solution which could be not completely attached to the support framework under highly acidic synthesis condition [66]. Molybdenum being the active specie is well distributed and anchored on the support in all catalysts within acceptable standard deviation from calculated amount (13 wt. %). Furthermore, the ratio of calculated Si/Ti in agreement with the observed values from XRF.

Table 6-4 Bulk elemental by XRF

Catalyst	Elements		
	Mo (wt. %)	**Ni (wt. %)**	**Si/Ti Molar Ratio**
CIP	12.84 (13)	3.00 (3)	10.11 (10)
SP	13.16 (13)	1.36 (3)	10.15 (10)
SIP	13.01 (13)	3.06 (3)	9.97 (10)
MSP	13.04 (13)	3.04 (3)	9.99 (10)
CIP-CA	12.89 (13)	2.97 (3)	10.04 (10)
SP-CA	12.58 (13)	1.16 (3)	10.20 (10)
SIP-CA	12.69 (13)	2.95 (3)	10.26 (10)
MSP-CA	12.42 (13)	3.01 (3)	10.14 (10)

Note: The values in parenthesis is the calculated amount

6.3.9 SEM analysis

The morphology observation of NiMo supported on Ti-modified SBA-15 catalysts with respect to method of preparation and addition of complexing agent is presented in the micrographs shown in **Figure 6-8**. The regular morphology of SBA-15 can be in form of rods, spheres, fibers etc., depending on the synthesis procedures and parameters [148]. The ***CIP*** shows rod-like morphology of few microns length, and the addition of complexing agent (***CIP-CA***) shows no difference in the morphology. The catalyst prepared by single-pot (***SP***) shows rod-like morphology fused or chained, with the presence of cubical flat sheet morphology corresponding to MoO_3 (confirmed by EDX) grown outside the support. The addition of complexing agent during synthesis for ***SP-CA*** reduced the extraneous growth of MoO_3 particles as shown in the micrographs. The morphology observation of ***SIP*** and ***SP-CA*** catalysts are similar to ***SP*** catalyst, however, the presence of MoO_3 particles is minimal in both cases (wheat-like rods). The modified single-pot catalysts with or without (***MSP-CA*** or ***MSP***) complexing agent exhibit slight variation in morphology with irregular rods characterized by agglomerated particles without the presence of MoO_3 growth outside the support's morphology compared to other catalysts. The SEM analysis supports the XRD and Raman with ***CIP*** providing better dispersion at oxide phase than others.

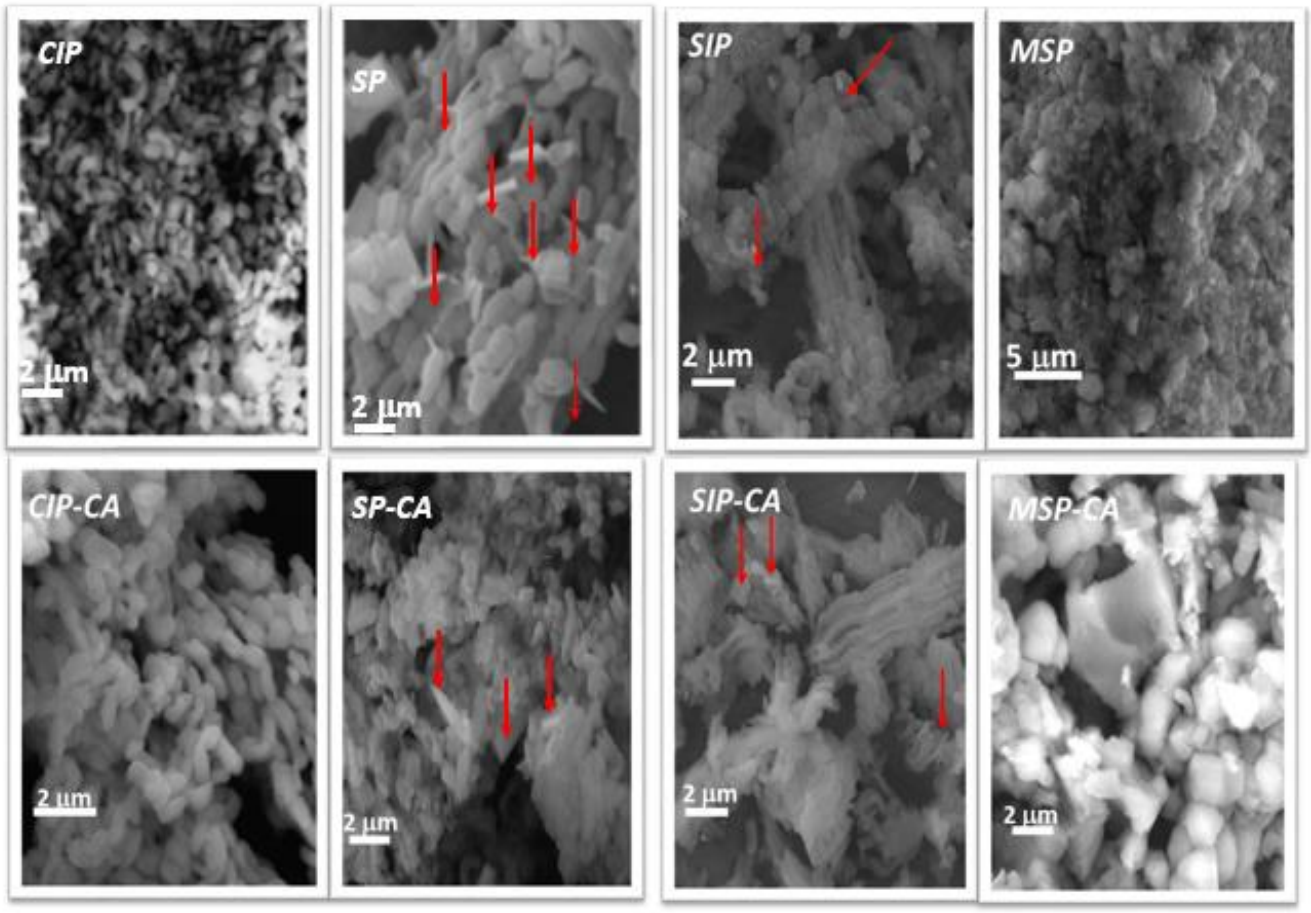

Figure 6-8 SEM analysis of catalysts prepared without (top) and with (bottom) citric acid by different methods.

6.3.10 HDS Catalytic Evaluation

Catalytic activities of different catalysts prepared were evaluated in a simulated binary mixture of organosulfur compounds containing 1000 ppm-S each for DBT and DMDBT. **Figure 6-9** and **Table 6-5** show desulfurization potential of catalysts at 2 h and over period of 4 h reaction time, respectively. Performance can be categorized and explained by method of preparations and the use of additives. Activity within method of preparation series without the use of citric acid show excellent performance, and the catalyst prepared by modified-one-pot has the highest sulfur conversion throughout. The catalytic activity of this series at 2 h of desulfurization operation can be ranked in the order of; ***MSP*** > ***SP*** > ***SIP*** > ***CIP***. Interestingly, the HDS conversion of ***MSP*** is more significant for DBT and DMDBT at 98 % and 95 %, respectively compared to others within the series. The above observation shows that the activity of catalyst prepared by ***MSP*** and ***SP*** are more active than their corresponding impregnation approaches (co-and-suc) when complexing agent is not employed.

On the other hand, activity of catalysts with the addition of citric acid follows slightly different trend. The ***MSP-CA***, which is as analogue of ***MSP*** prepared by modified-one-pot shows outstanding performance again with the addition of citric acid than other catalysts within the series. However, the catalyst prepared by direct incorporation of NiMo (***SP-CA***) has the lowest sulfur conversion at 2 h of desulfurization operation for both DBT and DMDBT. This observation might be connected to the lowest amount of nickel-promoter present on this catalyst with respect to others, as observed by XRF analysis. This is caused by the addition of citric acid to highly acidic solution during preparation stage, and resulted in further increase in the acidity of the resultant mixture, which brings more nickel into solution rather than being on the catalyst framework [66]. Moreover, the ***SIP-CA*** catalyst performs better than ***CIP-CA*** for conversion of both organosulfur compounds (DBT and DMDBT). The activity of these catalysts can be ranked in the order of; ***MSP-CA*** > ***SIP-CA*** > ***CIP-CA*** > ***SP-CA***.

Whilst comparing between the catalyst series with or without the use of additive (CA), the two-set of catalysts prepared by impregnation approach (co- and suc-) are favored by the addition of complexing agent to achieve more and better catalytic performance for DBT and DMDBT conversion. This observation is in line with the literature reports that addition of complexing agent enhances the dispersion of active phase dispersion [36, 47]. Therefore, catalysts prepared with

complexing agent by co-impregnation method of NiMo or sequential impregnation of Mo followed by Ni without final calcination showed improved performance of HDS activity in batch reactor as compared to their counterparts without complexing agents. However, both one-pot and modified-one-pot approaches are not favored by the addition of citric acid, and as a matter of fact, the catalysts' activity are slightly decreased. This shows that the use of complexing agent to aid dispersion is not necessary. Generally, the modified-one-pot catalysts show better catalytic performance in all ramifications (either with or without citric acid) than others. This observation can be attributed with high surface area which anchors more active species and more active sites density, as supported by physisorption, TPD and FTIR pyridine analysis.

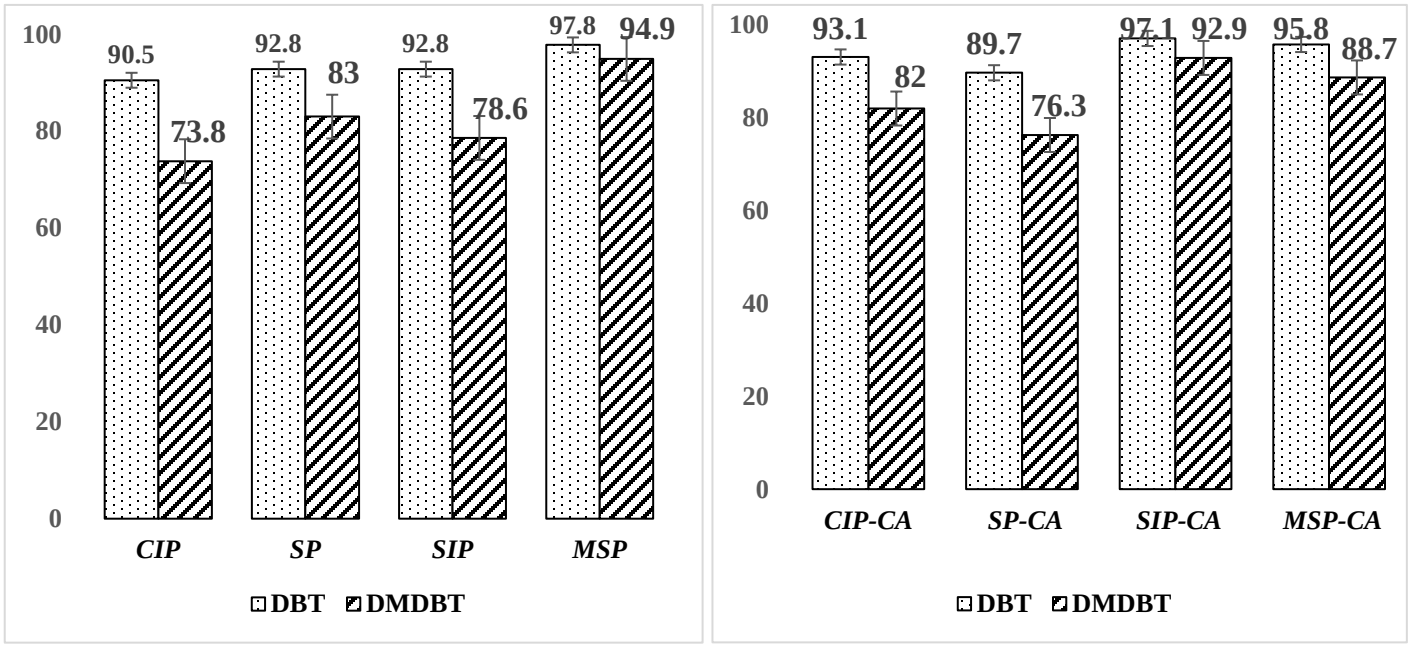

Figure 6-9 Percentage HDS conversion of DBT (1000 ppmw-S) and DMDBT (1000 ppmw-S) @ 2h reaction interval for all catalysts.

Table 6-5 Catalyst Performance Test Results: Product Sulfur Content. (Process Conditions: 350°C; 5 MPa; Reaction Time: 4 h; Feed Sulfur Content = 1,000 ppm)

Catalyst	Sulfur Content (ppmw) (DBT)				Sulfur Content (ppmw) (DMDBT)			
	1 h	**2 h**	**3 h**	**4 h**	**1 h**	**2 h**	**3 h**	**4 h**
CIP	221	95	30	20	452	262	88	32
SP	261	72	27	20	396	170	75	28
SIP	337	72	34	-	544	214	106	30
MSP	119	22	6	-	427	51	20	5
CIP-CA	277	69	26	-	469	180	55	17
SP-CA	314	103	28	20	500	237	68	28
SIP-CA	124	42	21	-	282	113	25	8
MSP-CA	86	29	10	-	189	71	22	5

6.3.11 Reaction Kinetics

The HDS rates were calculated assuming pseudo-first order kinetics for the overall HDS as well for the DDS and HYD pathways and the values of the reaction constants, ***k*** (min^{-1}), are presented in **Table 6-6**. The HDS rate constants varies between 19-35 x 10^{-3} min^{-1} for DBT and 11-25 x 10^{-3} min^{-1} for 4,6-DMDBT. The value for the HDS of DBT compares well with the reported rate constant of 25.1 x 10^{-3} min^{-1} at 350°C over a CoMo/γ-Al_2O_3 catalyst [68]. However, the values obtained in the present study for the HDS of 4,6-DMDBT are several fold higher than 4 x 10^{-3} min^{-1} reported under similar conditions over a CoMo/γ-Al_2O_3 catalyst [68]. This manifold difference in rate constants indicates the significant superiority of NiMo supported Ti-SBA-15 catalysts over conventional γ-Al_2O_3-based catalysts – especially for the HDS of 4,6-DMDBT. The $\boldsymbol{k}_{DBT}/\boldsymbol{k}_{DMDBT}$ ratio was in the range of 1.4-1.8 which is comparable to reported value of about 1.7 for NiMo/TiSBA-15 [149].

Despite possessing significantly higher surface area, the overall rate HDS of DBT ($\boldsymbol{k}_{DBT}$) over catalyst ***SP*** was comparable to that of catalyst ***CIP***. The reason for this behavior seems to be lower Ni content in ***SP*** – as shown by the XRF results – which resulted in lower desulfurization by hydrogenation route ($\boldsymbol{k}_{CHB}$) over ***SP (see figure 6-10)***. On the other hand, catalyst ***SP*** exhibited higher $\boldsymbol{k}_{BP}$ may be due to its higher acidity than ***CIP*** as observed by NH_3 TPD. A considerably higher HDS rate of 4,6-DMDBT by direct desulfurization route ($\boldsymbol{k}_{DMBP}$) over catalyst ***SP*** compared to ***CIP*** was also noted. However, rate of HDS by hydrogenation route ($\boldsymbol{k}_{DMCHB}$) over these catalysts was same. The overall effect was about 27% higher $\boldsymbol{k}_{DMDBT}$ over catalyst ***SP*** compared to ***CIP***.

Results show that the catalyst prepared by modified single-pot approach (***MSP***) grossly outperformed the catalyst prepared by successive impregnation (***SIP***) in terms of HDS rate of DBT and 4,6-DMDBT by both the routes. The effect was more pronounced on the HDS by DDS route over catalyst ***MSP*** in which $\boldsymbol{k}_{BP}$ was about 40% higher and $\boldsymbol{k}_{DMBP}$ was about 50% higher compared to the rates observed over catalyst ***SIP***. This significant enhancement in HDS by DDS route can be attributed to about 80% higher surface area resulting in highly dispersed active sites in catalyst ***MSP*** compared to catalyst ***SIP***. The modest enhancement in HDS by HYD route is not notable perhaps due to almost same nickel content in catalysts ***MSP*** and ***SIP***.

The main difference in the characteristics of catalysts ***SP*** and ***MSP*** is the nickel content as confirmed by the XRF results. Additionally, the catalyst ***MSP*** possesses higher surface area and

better reducibility as indicated by TPR results. Hence, it is not surprising that catalyst ***MSP*** performed better than catalyst ***SP*** in terms of HDS by HYD route for DBT as well as 4,6-DMDBT. The two-fold enhancement in $\boldsymbol{k}_{CHB}$ and $\boldsymbol{k}_{DMCHB}$ over catalyst ***MSP*** compared to catalyst ***SP*** reflects the availability of higher hydrogenation sites due to preservation of more than double the amount of nickel on catalyst surface. Although, there was no significant effect on the HDS by DDS route, the overall HDS was improved by about 50% for DBT and about 30% for 4,6-DMDBT due to the modification in single-pot approach.

A comparison of the HDS activity of catalysts prepared with or without the use of complexing agent shows that the effects vary significantly with the preparation method. The catalysts prepared by co-impregnation approach (***CIP*** and ***CIP-SA***) showed little effect on $\boldsymbol{k}_{DBT}$ and $\boldsymbol{k}_{DMDBT}$ but exhibited significant improvement in $\boldsymbol{k}_{CHB}$ and $\boldsymbol{k}_{DMCHB}$ due to the addition of complexing agent. This result is in line with the literature reports that addition of complexing agent enhances the dispersion of active phase dispersion [3636, 47]. The improved dispersion of active metals seems to have enhanced that hydrogenation activity in these catalysts. Addition of complexing agent clearly had a detrimental effect of the catalysts prepared by single-pot approach (***SP*** and ***SP-CA***) which can be attributed to their low Ni content in catalyst ***SP*** which was further reduced in ***SP-CA*** due to acidic environment.

The catalysts prepared by sequential impregnation (***SIP*** and ***SIP-CA***) benefited most by the addition of complexing agent. The $\boldsymbol{k}_{DBT}$ of ***SIP-CA*** was about 50% more than that of ***SIP*** whereas the increase in and $\boldsymbol{k}_{DMDBT}$ was about 70%. Both DDS and HYD routes contributed towards this improvement indicating that the addition of complexing agent enhanced the distribution of active metals as well as the acidic sites. These results are supported by the characterization data obtained from Raman spectroscopy and FTIR spectroscopy using pyridine adsorption. Addition of complexing agent also showed positive effect of the catalysts prepared by modified single-pot approach (***MSP*** and ***MSP-CA***). As mentioned above, the performance of catalyst ***MSP*** was the best among the catalysts prepared without complexing agent. Addition of complexing agent further improved its performance – especially for the HDS of 4,6-DMDBT. Hence, catalyst ***MSP-CA*** was the best-performing HDS catalysts among all the catalysts investigated in this study which is supported by the positive clues from the characterization data such as higher surface area, higher crystalline phase (XRD), more number of active sites (NH_3-TPD), and lower reduction temperature (TPR) compared to other catalysts.

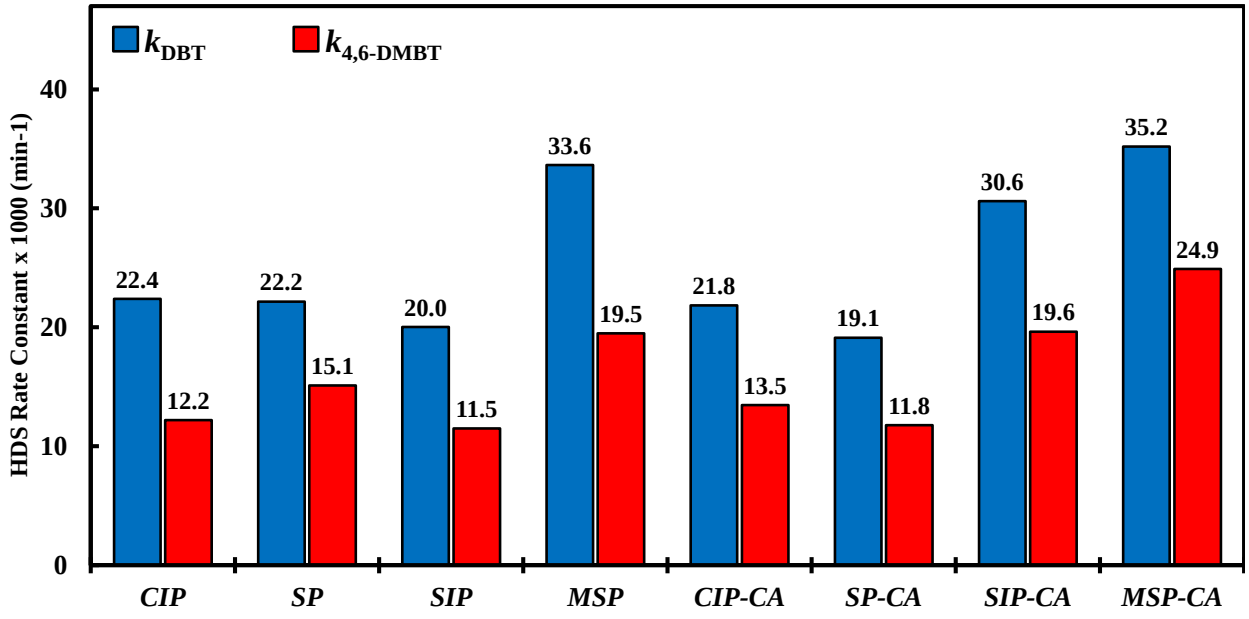

Figure 6-10 First-order rate constants for HDS of DBT and 4,6-DMDBT at 350 ºC

Table 6-6. HDS rate constants for DBT and DMDBT

Catalyst	HDS Rate Constants of DBT				HDS Rate Constants of 4,6-DMDBT			
	k_{DBT} x 10^3 (min^{-1})	k_{BP} x 10^3 (min^{-1})	k_{CHB} x 10^3 (min^{-1})	k_{BP}/k_{CHB}	k_{DMDBT} x 10^3 (min^{-1})	k_{DMBP} x 10^3 (min^{-1})	k_{DMCHB} x 10^3 (min^{-1})	k_{DMBP}/k_{DMCHB}
CIP	22.4	12.2	2.8	4.3	12.2	10.8	0.5	19.8
SP	22.2	14.1	1.9	7.5	15.1	13.3	0.5	24.3
SIP	20.0	9.3	3.3	2.8	11.5	9.3	0.8	11.1
MSP	33.6	13.0	3.9	3.4	19.5	13.8	0.9	15.1
CIP-CA	21.8	9.6	3.8	2.5	13.5	9.7	1.5	6.6
SP-CA	19.1	12.5	1.8	6.8	11.8	8.5	1.5	5.8
SIP-CA	30.6	13.8	3.4	4.1	19.6	13.3	1.6	8.1
MSP-CA	35.2	14.8	3.4	4.3	24.9	16.4	1.6	10.2

6.4 Conclusions

A series of NiMo/Ti-SBA-15 catalysts were prepared by adopting novel and conventional techniques. Detailed characterization data and activities for the simultaneous HDS of DBT and 4,6-DMDBT were systematically analyzed to get an insight into their differences. The advantages of single-pot and modified single-pot approaches were evident from the superior textural properties of these catalysts. However, the drawback of low Ni content in catalyst ***SP*** was rectified by adopting the two-step modified single-pot strategy which resulted in a much superior catalyst. Chapter 2 Despite having lower Ni content, the higher surface area and acidity of ***SP*** as compared to ***CIP*** resulted in improved DDS activity – especially for 4,6-DMDBT. The catalyst prepared by modified single-pot approach (***MSP***) grossly outperformed the catalyst prepared by successive impregnation (***SIP***) in terms of HDS rate of DBT and 4,6-DMDBT by both the routes. Such an overall enhancement in catalytic performance of ***MSP*** can be attributed to the superior textural properties and better dispersion of active metals.

Chapter 3 A significantly divergent influence of using complexing agent underscores importance of nickel loading method on catalytic behavior. The addition of citric acid as a means of aiding dispersion of active metals shows no significant effect on the performance of ***CIP*** catalyst. It had a rather detrimental effect on ***SP*** catalyst due to higher acidity of metallic salt solution which does not favor incorporation of Ni into the catalyst matrix. The catalyst prepared by sequential impregnation (***SIP***) method benefited most by the addition of complexing agent which enhanced the dispersion of active metals as well as the higher acidic sites as supported by the Raman spectroscopy and FTIR spectroscopy data. The addition of complexing agent further improved the performance of ***MSP*** – especially for the HDS of 4,6-DMDBT. Therefore, catalyst ***MSP-CA*** was found to be superior among all the catalysts investigated in this study with a great potential for deep desulfurization of diesel feedstock with minimum consumption of hydrogen.

ACKNOWLEDGMENTS

The author greatly acknowledged the financial support by King Fahd University of Petroleum & Minerals (KFUPM) for funding this work through project No. DSR NUS15105.

References

[1] Z. Đukanović, S.B. Glišić, V.J. Čobanin, M. Nićiforović, C.A. Georgiou, A.M. Orlović, Hydrotreating of straight-run gas oil blended with FCC naphtha and light cycle oil, Fuel Processing Technology, 106 (2013) 160-165.
[2] C. Botchwey, A.K. Dalai, J. Adjaye, Two-stage hydrotreating of Athabasca heavy gas oil with interstage hydrogen sulfide removal: Effect of process conditions and kinetic analyses, Industrial & engineering chemistry research, 43 (2004) 5854-5861.
[3] A. Stanislaus, A. Marafi, M.S. Rana, Recent advances in the science and technology of ultra low sulfur diesel (ULSD) production, Catalysis Today, 153 (2010) 1-68.
[4] M.Á. Calderón-Magdaleno, J.A. Mendoza-Nieto, T.E. Klimova, Effect of the amount of citric acid used in the preparation of NiMo/SBA-15 catalysts on their performance in HDS of dibenzothiophene-type compounds, Catalysis Today, 220 (2014) 78-88.
[5] P. Yuan, J. Liu, Y. Li, Y. Fan, G. Shi, H. Liu, X. Bao, Effect of pore diameter and structure of mesoporous sieve supported catalysts on hydrodesulfurization performance, Chemical Engineering Science, 111 (2014) 381-389.
[6] S. Badoga, A.K. Dalai, J. Adjaye, Y. Hu, Combined effects of EDTA and heteroatoms (Ti, Zr, and Al) on catalytic activity of SBA-15 supported NiMo catalyst for hydrotreating of heavy gas oil, Industrial & Engineering Chemistry Research, 53 (2014) 2137-2156.
[7] U.T. Turaga, C. Song, MCM-41-supported Co-Mo catalysts for deep hydrodesulfurization of light cycle oil, Catalysis Today, 86 (2003) 129-140.
[8] K. Soni, K. Mouli, A. Dalai, J. Adjaye, Influence of frame connectivity of SBA-15 and KIT-6 supported NiMo catalysts for hydrotreating of gas oil, Catalysis letters, 136 (2010) 116-125.
[9] M. Sun, D. Nicosia, R. Prins, The effects of fluorine, phosphate and chelating agents on hydrotreating catalysts and catalysis, Catalysis Today, 86 (2003) 173-189.
[10] T. Ninh, L. Massin, D. Laurenti, M. Vrinat, A new approach in the evaluation of the support effect for NiMo hydrodesulfurization catalysts, Applied Catalysis A: General, 407 (2011) 29-39.
[11] J.A. Bergwerff, M. Jansen, B. Leliveld, T. Visser, K.P. de Jong, B.M. Weckhuysen, Influence of the preparation method on the hydrotreating activity of MoS< sub> 2</sub>/Al< sub> 2</sub> O< sub> 3</sub> extrudates: A Raman microspectroscopy study on the genesis of the active phase, Journal of catalysis, 243 (2006) 292-302.
[12] S. Eijsbouts, Hydrotreating catalysts, Synthesis of solid catalysts, VILEY-VCH Verlag GmbH & Co, KGa A Weinheim2009.
[13] T. Kabe, K. Akamatsu, A. Ishihara, S. Otsuki, M. Godo, Q. Zhang, W. Qian, Deep hydrodesulfurization of light gas oil. 1. Kinetics and mechanisms of dibenzothiophene hydrodesulfurization, Industrial & engineering chemistry research, 36 (1997) 5146-5152.
[14] F. Plantenga, R. Leliveld, Sulfur in fuels: more stringent sulfur specifications for fuels are driving innovation, Applied Catalysis A: General, 248 (2003) 1-7.
[15] T. Zepeda, Comparison and performance of different sulphided Ti-loaded mesostructured silica-supported CoMo catalysts in deep HDS, Applied Catalysis A: General, 347 (2008) 148-161.
[16] C. Song, An overview of new approaches to deep desulfurization for ultra-clean gasoline, diesel fuel and jet fuel, Catalysis today, 86 (2003) 211-263.
[17] C. Song, Fuel processing for low-temperature and high-temperature fuel cells: Challenges, and opportunities for sustainable development in the 21st century, Catalysis today, 77 (2002) 17-49.
[18] M. Muzic, K. Sertic-Bionda, Z. Gomzi, Kinetic and Statistical Studies of Adsorptive Desulfurization of Diesel Fuel on Commercial Activated Carbons, Chemical Engineering & Technology, 31 (2008) 355-364.
[19] L. Qu, W. Zhang, P.J. Kooyman, R. Prins, MAS NMR, TPR, and TEM studies of the interaction of NiMo with alumina and silica–alumina supports, Journal of Catalysis, 215 (2003) 7-13.
[20] J.C.T. Duchet, M. J.; Cornet, D.; Vivier, L.; Perot, G.;, L.M. Bekakra, C.; Szabo, G. Catalytic properties of nickel, molybdenum sulphide supported on zirconia. Catal. Today 1991, 579.

[21] M.A. Breysse, P.; Geantet, C.; Vrinat, M. Overview of, support effects in hydrotreating catalysts. Catal. Today 2003, 5.
[22] V. Sundaramurthy, I. Eswaramoorthi, A.K. Dalai, J. Adjaye, Hydrotreating of gas oil on SBA-15 supported NiMo catalysts, Microporous and Mesoporous Materials, 111 (2008) 560-568.
[23] T. Klimova, L. Pena, L. Lizama, C. Salcedo, O.Y. Gutiérrez, Modification of activity and selectivity of NiMo/SBA-15 HDS catalysts by grafting of different metal oxides on the support surface, Industrial & Engineering Chemistry Research, 48 (2008) 1126-1133.
[24] G.M. Kumaran, S. Garg, K. Soni, V. Prasad, L.D. Sharma, G.M. Dhar, Catalytic functionalities of H-β-zeolite-supported molybdenum hydrotreating catalysts, Energy & fuels, 20 (2006) 1784-1790.
[25] N. Prabhu, A.K. Dalai, J. Adjaye, Hydrodesulphurization and hydrodenitrogenation of light gas oil using NiMo catalyst supported on functionalized mesoporous carbon, Applied Catalysis A: General, 401 (2011) 1-11.
[26] V. Meynen, P. Cool, E. Vansant, Synthesis of siliceous materials with micro-and mesoporosity, Microporous and mesoporous materials, 104 (2007) 26-38.
[27] S. Badoga, K.C. Mouli, K.K. Soni, A. Dalai, J. Adjaye, Beneficial influence of EDTA on the structure and catalytic properties of sulfided NiMo/SBA-15 catalysts for hydrotreating of light gas oil, Applied catalysis. B, Environmental, 125 (2012) 67-84.
[28] N. Rinaldi, T. Kubota, Y. Okamoto, Effect of Citric Acid Addition on Co− Mo/B2O3/Al2O3 Catalysts Prepared by a Post-Treatment Method, Industrial & engineering chemistry research, 48 (2009) 10414-10424.
[29] G. Kishan, L. Coulier, V. De Beer, J. Van Veen, J. Niemantsverdriet, Sulfidation and thiophene hydrodesulfurization activity of nickel tungsten sulfide model catalysts, prepared without and with chelating agents, Journal of catalysis, 196 (2000) 180-189.
[30] M.S. Rana, J. Ramírez, A. Gutiérrez-Alejandre, J. Ancheyta, L. Cedeño, S. Maity, Support effects in CoMo hydrodesulfurization catalysts prepared with EDTA as a chelating agent, Journal of catalysis, 246 (2007) 100-108.
[31] M. Lélias, E. Le Guludec, L. Mariey, J. Van Gestel, A. Travert, L. Oliviero, F. Maugé, Effect of EDTA addition on the structure and activity of the active phase of cobalt–molybdenum sulfide hydrotreatment catalysts, Catalysis Today, 150 (2010) 179-185.
[32] J. Choma, S. Pikus, M. Jaroniec, Adsorption characterization of surfactant-templated ordered mesoporous silicas synthesized with and without hydrothermal treatment, Applied surface science, 252 (2005) 562-569.
[33] P.A. Russo, M.M.L. Carrott, P.J. Carrott, Effect of hydrothermal treatment on the structure, stability and acidity of Al containing MCM-41 and MCM-48 synthesised at room temperature, Colloids and Surfaces A: Physicochemical and Engineering Aspects, 310 (2007) 9-19.
[34] O.A. Dudarko, C. Gunathilake, V.V. Sliesarenko, Y.L. Zub, M. Jaroniec, Microwave-assisted and conventional hydrothermal synthesis of ordered mesoporous silicas with P-containing functionalities, Colloids and Surfaces A: Physicochemical and Engineering Aspects, 459 (2014) 4-10.
[35] R. Huirache-Acuña, R. Nava, C.L. Peza-Ledesma, J. Lara-Romero, G. Alonso-Núez, B. Pawelec, E.M. Rivera-Muñoz, SBA-15 mesoporous silica as catalytic support for hydrodesulfurization catalysts—review, Materials, 6 (2013) 4139-4167.
[36] L. Peña, D. Valencia, T. Klimova, CoMo/SBA-15 catalysts prepared with EDTA and citric acid and their performance in hydrodesulfurization of dibenzothiophene, Applied Catalysis B: Environmental, 147 (2014) 879-887.
[37] O.Y. Gutiérrez, S. Singh, E. Schachtl, J. Kim, E. Kondratieva, J. Hein, J.A. Lercher, Effects of the Support on the Performance and Promotion of (Ni) MoS2 Catalysts for Simultaneous Hydrodenitrogenation and Hydrodesulfurization, ACS Catalysis, 4 (2014) 1487-1499.
[38] Z. Liu, L. Zhang, J. Jiang, C. Bian, Z. Zhang, Z. Gao, Advancement of hydro-desulfurization catalyst and discussion of its application in coal tar, (2013).
[39] P.-Y. Wu, S.-F. Ji, L.-H. Hu, J.-Q. Zhu, C.-Y. Li, Preparation, characterization, and catalytic properties of the Mo2C/SBA-15 catalysts, Journal of Porous Materials, 15 (2008) 181-187.

[40] P. Castaño, B. Pawelec, J. Fierro, J. Arandes, J. Bilbao, Enhancement of pyrolysis gasoline hydrogenation over Pd-promoted Ni/SiO 2–Al 2 O 3 catalysts, Fuel, 86 (2007) 2262-2274.
[41] V. Sundaramurthy, I. Eswaramoorthi, A. Dalai, J. Adjaye, Hydrotreating of gas oil on SBA-15 supported NiMo catalysts, Microporous and Mesoporous Materials, 111 (2008) 560-568.
[42] J. Duchet, M. Tilliette, D. Cornet, L. Vivier, G. Perot, L. Bekakra, C. Moreau, G. Szabo, Catalytic properties of nickel molybdenum sulphide supported on zirconia, Catalysis today, 10 (1991) 579-592.
[43] G.M. Kumaran, S. Garg, K. Soni, V. Prasad, L. Sharma, G.M. Dhar, Catalytic functionalities of H-β-zeolite-supported molybdenum hydrotreating catalysts, Energy & fuels, 20 (2006) 1784-1790.
[44] M. Breysse, P. Afanasiev, C. Geantet, M. Vrinat, Overview of support effects in hydrotreating catalysts, Catalysis Today, 86 (2003) 5-16.
[45] N. Prabhu, A. Dalai, J. Adjaye, Hydrodesulphurization and hydrodenitrogenation of light gas oil using NiMo catalyst supported on functionalized mesoporous carbon, Applied Catalysis A: General, 401 (2011) 1-11.
[46] L. Pena, D. Valencia, T. Klimova, CoMo/SBA-15 catalysts prepared with EDTA and citric acid and their performance in hydrodesulfurization of dibenzothiophene, Applied Catalysis B: Environmental, 147 (2014) 879-887.
[47] D. Valencia, T. Klimova, Citric acid loading for MoS 2-based catalysts supported on SBA-15. New catalytic materials with high hydrogenolysis ability in hydrodesulfurization, Applied catalysis B: environmental, 129 (2013) 137-145.
[48] D. Zhao, J. Feng, Q. Huo, N. Melosh, G.H. Fredrickson, B.F. Chmelka, G.D. Stucky, Triblock Copolymer Syntheses of Mesoporous Silica with Periodic 50 to 300 Angstrom Pores, Science, 279 (1998) 548-552.
[49] K. Cassiers, T. Linssen, M. Mathieu, M. Benjelloun, K. Schrijnemakers, P. Van Der Voort, P. Cool, E. Vansant, A detailed study of thermal, hydrothermal, and mechanical stabilities of a wide range of surfactant assembled mesoporous silicas, Chemistry of materials, 14 (2002) 2317-2324.
[50] Z. Jin, X. Wang, X. Cui, Synthesis and morphological investigation of ordered SBA-15-type mesoporous silica with an amphiphilic triblock copolymer template under various conditions, Colloids and Surfaces A: Physicochemical and Engineering Aspects, 316 (2008) 27-36.
[51] S. Badoga, R.V. Sharma, A.K. Dalai, J. Adjaye, Hydrotreating of heavy gas oil on mesoporous zirconia supported NiMo catalyst with EDTA, Fuel, 128 (2014) 30-38.
[52] H. Sun, C. Wang, S. Pang, X. Li, Y. Tao, H. Tang, M. Liu, Photocatalytic TiO 2 films prepared by chemical vapor deposition at atmosphere pressure, Journal of Non-Crystalline Solids, 354 (2008) 1440-1443.
[53] O.Y. Gutiérrez, F. Pérez, G.A. Fuentes, X. Bokhimi, T. Klimova, Deep HDS over NiMo/Zr-SBA-15 catalysts with varying MoO 3 loading, Catalysis Today, 130 (2008) 292-301.
[54] W. Li, G.D. Meitzner, R.W. Borry, E. Iglesia, Raman and X-ray absorption studies of Mo species in Mo/H-ZSM5 catalysts for non-oxidative CH 4 reactions, Journal of Catalysis, 191 (2000) 373-383.
[55] Y.V. Plyuto, I. Babich, I. Plyuto, A. Van Langeveld, J. Moulijn, Synthesis and characterization of molybdenum (VI) oxo-species on the surface of fumed alumina and silica, Colloids and Surfaces A: Physicochemical and Engineering Aspects, 125 (1997) 225-230.
[56] G. Mestl, P. Ruiz, B. Delmon, H. Knozinger, Oxygen-exchange properties of MoO3: an in situ Raman spectroscopy study, The Journal of Physical Chemistry, 98 (1994) 11269-11275.
[57] B.C. Windom, W. Sawyer, D.W. Hahn, A Raman spectroscopic study of MoS2 and MoO3: applications to tribological systems, Tribology Letters, 42 (2011) 301-310.
[58] M. Py, P.E. Schmid, J. Vallin, Raman scattering and structural properties of MoO3, Il Nuovo Cimento B (1971-1996), 38 (1977) 271-279.
[59] M. Dieterle, G. Weinberg, G. Mestl, Raman spectroscopy of molybdenum oxides Part I. Structural characterization of oxygen defects in MoO 3− x by DR UV/VIS, Raman spectroscopy and X-ray diffraction, Physical Chemistry Chemical Physics, 4 (2002) 812-821.
[60] K. Amakawa, P. Hildebrandt, R. Schlögl, R. Schomäcker, C. Limberg, Active site for propene metathesis in silica-supported molybdenum oxide catalysts, Technische Universität Berlin, 2013.

[61] S. Braun, L.G. Appel, V.L. Camorim, M. Schmal, Thermal spreading of MoO3 onto silica supports, The Journal of Physical Chemistry B, 104 (2000) 6584-6590.
[62] S. Maity, M. Rana, S. Bej, J. Ancheyta-Juarez, G.M. Dhar, T.P. Rao, Studies on physico-chemical characterization and catalysis on high surface area titania supported molybdenum hydrotreating catalysts, Applied Catalysis A: General, 205 (2001) 215-225.
[63] L.Y. Lizama, T.E. Klimova, SBA-15 modified with Al, Ti, or Zr as supports for highly active NiW catalysts for HDS, Journal of materials science, 44 (2009) 6617-6628.
[64] Z. Han, W. Pei, J. Xie, Y. Zou, X.-M. Ren, Two {Mo 36}-containing polymolybdates: Synthesis, crystal structures, and spectral characterizations, Inorganic Chemistry Communications, 16 (2012) 61-64.
[65] A. Tuel, Modification of mesoporous silicas by incorporation of heteroelements in the framework, Microporous and Mesoporous Materials, 27 (1999) 151-169.
[66] Y. Li, D. Pan, C. Yu, Y. Fan, X. Bao, Synthesis and hydrodesulfurization properties of NiW catalyst supported on high-aluminum-content, highly ordered, and hydrothermally stable Al-SBA-15, Journal of catalysis, 286 (2012) 124-136.
[67] W. Lai, Z. Chen, J. Zhu, L. Yang, J. Zheng, X. Yi, W. Fang, A NiMoS flower-like structure with self-assembled nanosheets as high-performance hydrodesulfurization catalysts, Nanoscale, 8 (2016) 3823-3833.
[68] S.A. Ali, S. Ahmed, K.W. Ahmed, M.A. Al-Saleh, Simultaneous hydrodesulfurization of dibenzothiophene and substituted dibenzothiophenes over phosphorus modified CoMo/Al 2 O 3 catalysts, Fuel processing technology, 98 (2012) 39-44.
[69] G.M. Dhar, H. Ramakrishna, T.P. Rao, Effect of sintering on the catalytic functionalities of MOS2/Al2O3 catalysts, Catalysis letters, 22 (1993) 351-359.
[70] Y. Okamoto, A. Maezawa, T. Imanaka, Active sites of molybdenum sulfide catalysts supported on Al 2 O 3 and TiO 2 for hydrodesulfurization and hydrogenation, Journal of Catalysis, 120 (1989) 29-45.
[71] K.S. Rao, G.M. Dhar, Catalytic functionalities of supported tungsten sulfide catalysts, Journal of Catalysis, 115 (1989) 277-281.
[72] K.S. Rao, H. Ramakrishna, G.M. Dhar, Catalytic functionalities of WS2/ZrO2, Journal of Catalysis, 133 (1992) 146-152.
[73] G. Muralidhar, F. Massoth, J. Shabtai, Catalytic functionalities of supported sulfides: I. Effect of support and additives on the CoMo catalyst, Journal of Catalysis, 85 (1984) 44-52.
[74] W. Zhaobin, X. Qin, G. Xiexian, E. Sham, P. Grange, B. Delmon, Titania-modified hydrodesulphurization catalysts: I. Effect of preparation techniques on morphology and properties of TiO2—Al2O3 carrier, Applied catalysis, 63 (1990) 305-317.
[75] M.A. Al-Daous, S.A. Ali, Deep desulfurization of gas oil over NiMo catalysts supported on alumina–zirconia composites, Fuel, 97 (2012) 662-669.
[76] S.A. Ganiyu, K. Alhooshani, S.A. Ali, Single-Pot Synthesis of Ti-SBA-15-NiMo Hydrodesulfurization Catalysts: Role of Calcination Temperature on Dispersion and Activity, Applied Catalysis B: Environmental, (2016).
[77] D. Zhao, Q. Huo, J. Feng, B.F. Chmelka, G.D. Stucky, Nonionic triblock and star diblock copolymer and oligomeric surfactant syntheses of highly ordered, hydrothermally stable, mesoporous silica structures, Journal of the American Chemical Society, 120 (1998) 6024-6036.
[78] W. Cai, J. Yu, C. Anand, A. Vinu, M. Jaroniec, Facile synthesis of ordered mesoporous alumina and alumina-supported metal oxides with tailored adsorption and framework properties, Chemistry of Materials, 23 (2011) 1147-1157.
[79] C.S. Cundy, P.A. Cox, The hydrothermal synthesis of zeolites: Precursors, intermediates and reaction mechanism, Microporous and Mesoporous Materials, 82 (2005) 1-78.
[80] C.S. Cundy, P.A. Cox, The hydrothermal synthesis of zeolites: history and development from the earliest days to the present time, Chemical Reviews, 103 (2003) 663-702.
[81] X. Jiaqiang, C. Yuping, C. Daoyong, S. Jianian, Hydrothermal synthesis and gas sensing characters of ZnO nanorods, Sensors and Actuators B: Chemical, 113 (2006) 526-531.

[82] Y. Ding, G. Zhang, H. Wu, B. Hai, L. Wang, Y. Qian, Nanoscale Magnesium Hydroxide and Magnesium Oxide Powders: Control over Size, Shape, and Structure via Hydrothermal Synthesis, Chemistry of Materials, 13 (2001) 435-440.
[83] X.W. Lou, H.C. Zeng, Hydrothermal synthesis of α-MoO3 nanorods via acidification of ammonium heptamolybdate tetrahydrate, Chemistry of materials, 14 (2002) 4781-4789.
[84] X.C. Song, Y.F. Zheng, E. Yang, Y. Wang, Large-scale hydrothermal synthesis of WO 3 nanowires in the presence of K 2 SO 4, Materials Letters, 61 (2007) 3904-3908.
[85] H. Cheng, J. Ma, Z. Zhao, L. Qi, Hydrothermal preparation of uniform nanosize rutile and anatase particles, Chemistry of Materials, 7 (1995) 663-671.
[86] M. Xu, L. Kong, W. Zhou, H. Li, Hydrothermal synthesis and pseudocapacitance properties of α-MnO2 hollow spheres and hollow urchins, The Journal of Physical Chemistry C, 111 (2007) 19141-19147.
[87] H. Zhang, H. Lin, Y. Zheng, Y. Hu, A. MacLennan, Understanding of the effect of synthesis temperature on the crystallization and activity of nano-MoS 2 catalyst, Applied Catalysis B: Environmental, 165 (2015) 537-546.
[88] A. Karlsson, M. Stöcker, R. Schmidt, Composites of micro-and mesoporous materials: simultaneous syntheses of MFI/MCM-41 like phases by a mixed template approach, Microporous and Mesoporous Materials, 27 (1999) 181-192.
[89] P. Van Der Voort, P.I. Ravikovitch, K.P. De Jong, M. Benjelloun, E. Van Bavel, A.H. Janssen, A.V. Neimark, B.M. Weckhuysen, E.F. Vansant, A New Templated Ordered Structure with Combined Micro- and Mesopores and Internal Silica Nanocapsules, The Journal of Physical Chemistry B, 106 (2002) 5873-5877.
[90] E. Devers, P. Afanasiev, B. Jouguet, M. Vrinat, Hydrothermal syntheses and catalytic properties of dispersed molybdenum sulfides, Catalysis letters, 82 (2002) 13-17.
[91] B. Yoosuk, C. Song, J.H. Kim, C. Ngamcharussrivichai, P. Prasassarakich, Effects of preparation conditions in hydrothermal synthesis of highly active unsupported NiMo sulfide catalysts for simultaneous hydrodesulfurization of dibenzothiophene and 4, 6-dimethyldibenzothiophene, Catalysis Today, 149 (2010) 52-61.
[92] H. Wang, Y. Fan, G. Shi, Z. Liu, H. Liu, X. Bao, Highly dispersed NiW/γ-Al 2 O 3 catalyst prepared by hydrothermal deposition method, Catalysis today, 125 (2007) 149-154.
[93] Z. Huang, W. Bensch, W. Sigle, P.A. van Aken, L. Kienle, T. Vitoya, H. Modrow, T. Ressler, The modification of MoO3 nanoparticles supported on mesoporous SBA-15: characterization using X-ray scattering, N2 physisorption, transmission electron microscopy, high-angle annular darkfield technique, Raman and XAFS spectroscopy, Journal of materials science, 43 (2008) 244-253.
[94] Y.V. Plyuto, I.V. Babich, I.V. Plyuto, A.D. Van Langeveld, J.A. Moulijn, Synthesis and characterization of molybdenum (VI) oxo-species on the surface of fumed alumina and silica, Colloids and Surfaces A: Physicochemical and Engineering Aspects, 125 (1997) 225-230.
[95] S. Aslam, F. Subhan, Z. Yan, P. Peng, K. Qiao, W. Xing, P. Bai, R. Ullah, U.J. Etim, J. Zeng, M. Ikram, Facile fabrication of Ni-based KIT-6 for adsorptive desulfurization, Chemical Engineering Journal, 302 (2016) 239-248.
[96] S. Maity, J. Ancheyta, F. Alonso, M.S. Rana, Preparation, characterization and evaluation of Maya crude hydroprocessing catalysts, Catalysis today, 98 (2004) 193-199.
[97] R. Shafi, G.J. Hutchings, Hydrodesulfurization of hindered dibenzothiophenes: an overview, Catalysis Today, 59 (2000) 423-442.
[98] M. Egorova, R. Prins, Hydrodesulfurization of dibenzothiophene and 4, 6-dimethyldibenzothiophene over sulfided NiMo/γ-Al 2 O 3, CoMo/γ-Al 2 O 3, and Mo/γ-Al 2 O 3 catalysts, Journal of Catalysis, 225 (2004) 417-427.
[99] C.S. Hsu, P. Robinson, Practical advances in petroleum processing, Springer Science & Business Media2007.
[100] O.Y. Gutiérrez, T. Klimova, Effect of the support on the high activity of the (Ni) Mo/ZrO 2–SBA-15 catalyst in the simultaneous hydrodesulfurization of DBT and 4, 6-DMDBT, Journal of catalysis, 281 (2011) 50-62.

[101] R.Y. Parapat, O.H. Saputra, A.P. Ang, M. Schwarze, R. Schomäcker, Support effect in the preparation of supported metal catalysts via microemulsion, RSC Advances, 4 (2014) 50955-50963.
[102] S.L. Suib, New and Future Developments in Catalysis: Catalysis by Nanoparticles, Newnes2013.
[103] C.-J. Jia, F. Schüth, Colloidal metal nanoparticles as a component of designed catalyst, Physical Chemistry Chemical Physics, 13 (2011) 2457-2487.
[104] Y. Okamoto, M. Breysse, G.M. Dhar, C. Song, Effect of support in hydrotreating catalysis for ultra clean fuels, Catalysis Today, 86 (2003) 1-3.
[105] F. Dumeignil, K. Sato, M. Imamura, N. Matsubayashi, E. Payen, H. Shimada, Modification of structural and acidic properties of sol–gel-prepared alumina powders by changing the hydrolysis ratio, Applied Catalysis A: General, 241 (2003) 319-329.
[106] F. Sun, W. Wu, Z. Wu, J. Guo, Z. Wei, Y. Yang, Z. Jiang, F. Tian, C. Li, Dibenzothiophene hydrodesulfurization activity and surface sites of silica-supported MoP, Ni2P, and NiMoP catalysts, Journal of Catalysis, 228 (2004) 298-310.
[107] J.J. Lee, S. Han, H. Kim, J.H. Koh, T. Hyeon, S.H. Moon, Performance of CoMoS catalysts supported on nanoporous carbon in the hydrodesulfurization of dibenzothiophene and 4, 6-dimethyldibenzothiophene, Catalysis today, 86 (2003) 141-149.
[108] G.M. Dhar, B. Srinivas, M. Rana, M. Kumar, S. Maity, Mixed oxide supported hydrodesulfurization catalysts—a review, Catalysis Today, 86 (2003) 45-60.
[109] M.S. Rana, B.N. Srinivas, S.K. Maity, G. Murali Dhar, T.S.R. Prasada Rao, Origin of Cracking Functionality of Sulfided (Ni) CoMo/SiO2–ZrO2 Catalysts, Journal of Catalysis, 195 (2000) 31-37.
[110] A. Wang, L. Ruan, Y. Teng, X. Li, M. Lu, J. Ren, Y. Wang, Y. Hu, Hydrodesulfurization of dibenzothiophene over siliceous MCM-41-supported nickel phosphide catalysts, Journal of Catalysis, 229 (2005) 314-321.
[111] L. Lizama, T. Klimova, Highly active deep HDS catalysts prepared using Mo and W heteropolyacids supported on SBA-15, Applied Catalysis B: Environmental, 82 (2008) 139-150.
[112] H. Topsøe, The role of Co–Mo–S type structures in hydrotreating catalysts, Applied Catalysis A: General, 322 (2007) 3-8.
[113] F. Cui, G. Li, X. Li, M. Lu, M. Li, Enhancement of hydrodesulfurization of 4, 6-dimethyldibenzothiophene catalyzed by CoMo catalysts supported on carbon-covered γ-Al 2 O 3, Catalysis Science & Technology, 5 (2015) 549-555.
[114] M. Jia, P. Afanasiev, M. Vrinat, The influence of preparation method on the properties of NiMo sulfide catalysts supported on ZrO 2, Applied Catalysis A: General, 278 (2005) 213-221.
[115] O.Y. Gutiérrez, G.A. Fuentes, C. Salcedo, T. Klimova, SBA-15 supports modified by Ti and Zr grafting for NiMo hydrodesulfurization catalysts, Catalysis Today, 116 (2006) 485-497.
[116] C. Kresge, M. Leonowicz, W. Roth, J. Vartuli, J. Beck, Ordered mesoporous molecular sieves synthesized by a liquid-crystal template mechanism, nature, 359 (1992) 710-712.
[117] J. Beck, J. Vartuli, W.J. Roth, M. Leonowicz, C. Kresge, K. Schmitt, C. Chu, D.H. Olson, E. Sheppard, S. McCullen, A new family of mesoporous molecular sieves prepared with liquid crystal templates, Journal of the American Chemical Society, 114 (1992) 10834-10843.
[118] W.-H. Zhang, J. Lu, B. Han, M. Li, J. Xiu, P. Ying, C. Li, Direct synthesis and characterization of titanium-substituted mesoporous molecular sieve SBA-15, Chemistry of Materials, 14 (2002) 3413-3421.
[119] M.-J. López-Muñoz, R. van Grieken, J. Aguado, J. Marugán, Role of the support on the activity of silica-supported TiO 2 photocatalysts: structure of the TiO 2/SBA-15 photocatalysts, Catalysis Today, 101 (2005) 307-314.
[120] A. Liu, K. Hidajat, S. Kawi, D. Zhao, A new class of hybrid mesoporous materials with functionalized organic monolayers for selective adsorption of heavy metal ions, Chemical Communications, (2000) 1145-1146.
[121] Y.-J. Han, G.D. Stucky, A. Butler, Mesoporous silicate sequestration and release of proteins, Journal of the American Chemical Society, 121 (1999) 9897-9898.
[122] S.J. Bae, S.-W. Kim, T. Hyeon, B.M. Kim, New chiral heterogeneous catalysts based on mesoporous silica: asymmetric diethylzinc addition to benzaldehyde, Chemical Communications, (2000) 31-32.

[123] Y.M. Wang, Z.Y. Wu, L.Y. Shi, J.H. Zhu, Rapid Functionalization of Mesoporous Materials: Directly Dispersing Metal Oxides into As- Prepared SBA- 15 Occluded with Template, Advanced Materials, 17 (2005) 323-327.
[124] B. Tian, X. Liu, H. Yang, S. Xie, C. Yu, B. Tu, D. Zhao, General Synthesis of Ordered Crystallized Metal Oxide Nanoarrays Replicated by Microwave- Digested Mesoporous Silica, Advanced Materials, 15 (2003) 1370-1374.
[125] S. Jun, S.H. Joo, R. Ryoo, M. Kruk, M. Jaroniec, Z. Liu, T. Ohsuna, O. Terasaki, Synthesis of new, nanoporous carbon with hexagonally ordered mesostructure, Journal of the American Chemical Society, 122 (2000) 10712-10713.
[126] R. Ryoo, S.H. Joo, M. Kruk, M. Jaroniec, Ordered mesoporous carbons, Advanced Materials, 13 (2001) 677-681.
[127] L. Vradman, M.V. Landau, M. Herskowitz, V. Ezersky, M. Talianker, S. Nikitenko, Y. Koltypin, A. Gedanken, High loading of short WS2 slabs inside SBA-15: promotion with nickel and performance in hydrodesulfurization and hydrogenation, Journal of Catalysis, 213 (2003) 163-175.
[128] P. Rayo, J. Ramírez, M.S. Rana, J. Ancheyta, A. Aguilar-Elguézabal, Effect of the Incorporation of Al, Ti, and Zr on the Cracking and Hydrodesulfurization Activity of NiMo/SBA-15 Catalysts, Industrial & Engineering Chemistry Research, 48 (2009) 1242-1248.
[129] G. Muthu Kumaran, S. Garg, K. Soni, M. Kumar, L.D. Sharma, G. Murali Dhar, K.S. Rama Rao, Effect of Al-SBA-15 support on catalytic functionalities of hydrotreating catalysts: I. Effect of variation of Si/Al ratio on catalytic functionalities, Applied Catalysis A: General, 305 (2006) 123-129.
[130] T. Klimova, J. Reyes, O. Gutiérrez, L. Lizama, Novel bifunctional NiMo/Al-SBA-15 catalysts for deep hydrodesulfurization: Effect of support Si/Al ratio, Applied Catalysis A: General, 335 (2008) 159-171.
[131] S. Jiang, Y. Zhou, W. Zhou, Y. Shan, Effect of Direct Synthesis Al-SBA-15 Supports on the Morphology and Catalytic Activity of NiMoS Phase in HDS of DBT, RSC Advances, (2016).
[132] D.-W. Lee, S.-J. Park, S.-K. Ihm, K.-H. Lee, Synthesis of bimodal mesoporous titania with high thermal stability via replication of citric acid-templated mesoporous silica, Chemistry of materials, 19 (2007) 937-941.
[133] K.C. Mouli, K. Soni, A. Dalai, J. Adjaye, Effect of pore diameter of Ni–Mo/Al-SBA-15 catalysts on the hydrotreating of heavy gas oil, Applied Catalysis A: General, 404 (2011) 21-29.
[134] K.K. Soni, K.C. Mouli, A. Dalai, J. Adjaye, Effect of Ti loading on the HDS and HDN activity of KLGO on NiMo/TiSBA-15 catalysts, Microporous and Mesoporous Materials, 152 (2012) 224-234.
[135] F. Plantenga, R. Leliveld, Sulfur in fuels: more stringent sulfur specifications for fuels are driving innovation, Elsevier, 2003.
[136] A. Sampieri, S. Pronier, J. Blanchard, M. Breysse, S. Brunet, K. Fajerwerg, C. Louis, G. Pérot, Hydrodesulfurization of dibenzothiophene on MoS 2/MCM-41 and MoS 2/SBA-15 catalysts prepared by thermal spreading of MoO 3, Catalysis today, 107 (2005) 537-544.
[137] L. Vradman, M. Landau, M. Herskowitz, V. Ezersky, M. Talianker, S. Nikitenko, Y. Koltypin, A. Gedanken, High loading of short WS 2 slabs inside SBA-15: promotion with nickel and performance in hydrodesulfurization and hydrogenation, Journal of Catalysis, 213 (2003) 163-175.
[138] E. Hensen, P. Kooyman, Y. Van der Meer, A. Van der Kraan, V. De Beer, J. Van Veen, R. Van Santen, The relation between morphology and hydrotreating activity for supported MoS 2 particles, Journal of Catalysis, 199 (2001) 224-235.
[139] G.M. Dhar, G.M. Kumaran, M. Kumar, K. Rawat, L. Sharma, B.D. Raju, K.R. Rao, Physico-chemical characterization and catalysis on SBA-15 supported molybdenum hydrotreating catalysts, Catalysis Today, 99 (2005) 309-314.
[140] T.E. Klimova, D. Valencia, J.A. Mendoza-Nieto, P. Hernández-Hipólito, Behavior of NiMo/SBA-15 catalysts prepared with citric acid in simultaneous hydrodesulfurization of dibenzothiophene and 4, 6-dimethyldibenzothiophene, Journal of catalysis, 304 (2013) 29-46.

[141] S.A. Ganiyu, K. Alhooshani, S.A. Ali, Single-pot synthesis of Ti-SBA-15-NiMo hydrodesulfurization catalysts: Role of calcination temperature on dispersion and activity, Applied Catalysis B: Environmental, 203 (2017) 428-441.
[142] P. Mazoyer, C. Geantet, F. Diehl, S. Loridant, M. Lacroix, Role of chelating agent on the oxidic state of hydrotreating catalysts, Catalysis Today, 130 (2008) 75-79.
[143] B. Pawelec, T. Halachev, A. Olivas, T. Zepeda, Impact of preparation method and support modification on the activity of mesoporous hydrotreating CoMo catalysts, Applied Catalysis A: General, 348 (2008) 30-41.
[144] G. Mestl, P. Ruiz, B. Delmon, H. Knozinger, Oxygen-Exchange Properties of MoO3 an in-Situ Raman-Spectroscopy Study, Journal of Physical Chemistry, 98 (1994) 11269-11275.
[145] K. Amakawa, R. Schlögl, R. Schomäcker, C. Limberg, Active site for propene metathesis in silica-supported molybdenum oxide catalysts, Technische Universität Berlin, 2013.
[146] G. Busca, Spectroscopic characterization of the acid properties of metal oxide catalysts, Catalysis today, 41 (1998) 191-206.
[147] S. Badoga, A. Ganesan, A.K. Dalai, S. Chand, Effect of synthesis technique on the activity of CoNiMo tri-metallic catalyst for hydrotreating of heavy gas oil, Catalysis Today, (2017).
[148] V. Meynen, P. Cool, E.F. Vansant, Verified syntheses of mesoporous materials, Microporous and mesoporous materials, 125 (2009) 170-223.
[149] J.C. Morales-Ortuño, T.E. Klimova, Development of new hydrodesulfurization NiMo catalysts supported on Al 2 O 3-TiSBA-15 hybrid materials, Fuel, (2017).

Appendix A

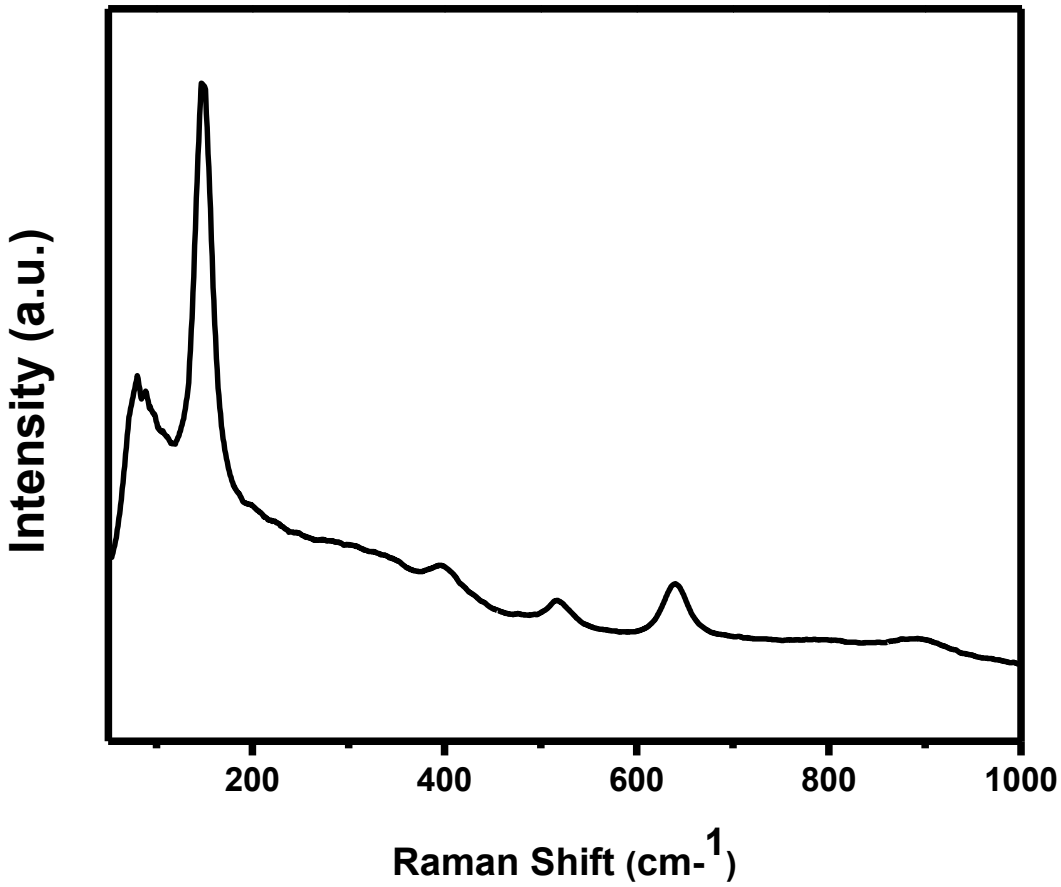

Raman analysis of Ti-SBA-15 showing anatase mode of vibrations.

Appendix B

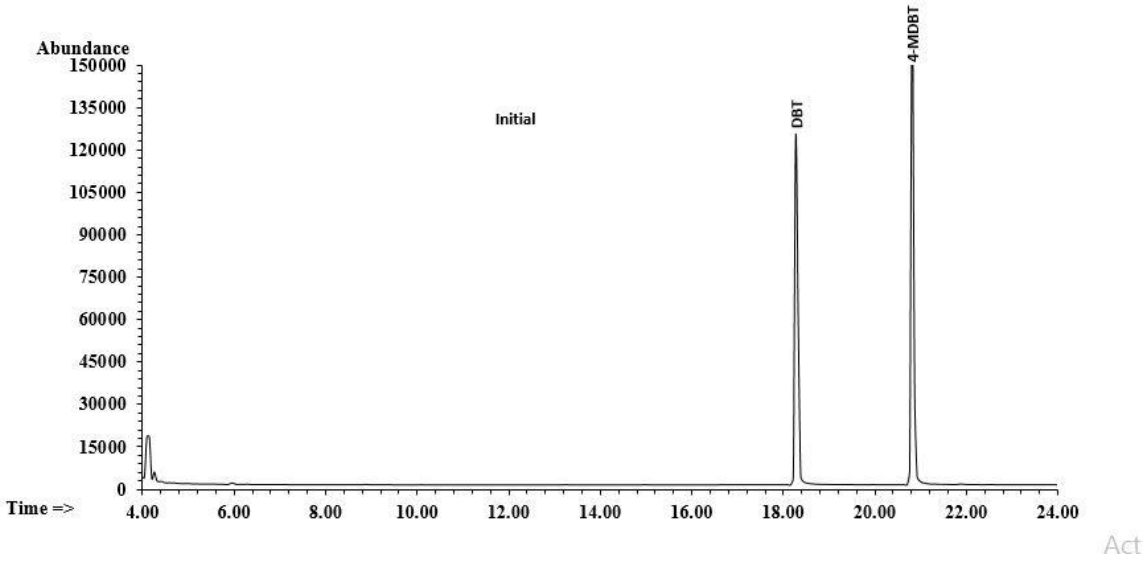

Chromatograph obtained from GC-MS for the model feedstock containing 1000 ppm-S each of dibenzothiophene (DBT) and 4-methyldibenzothiophene (4-MDBT) in dodecane.

Appendix B1

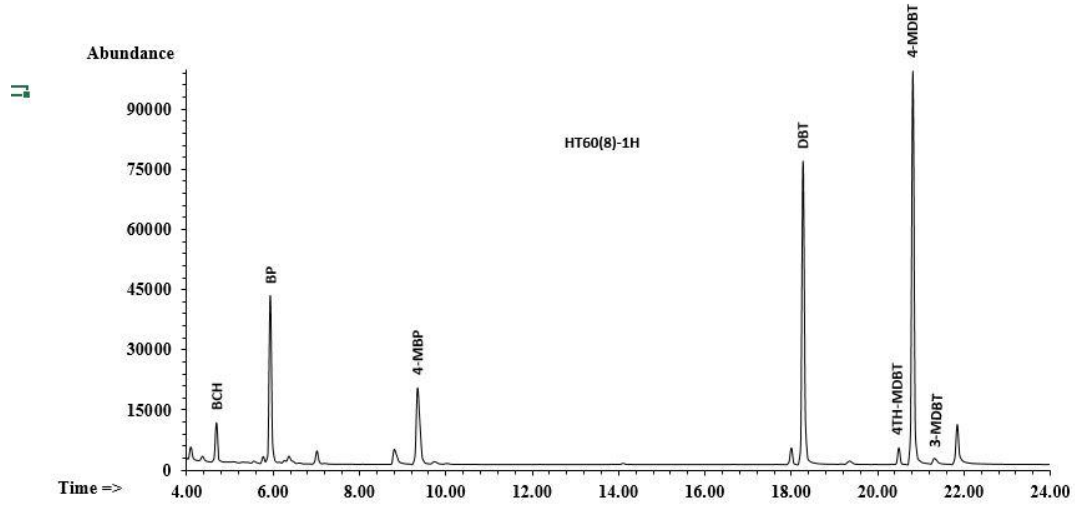

Chromatograph obtained from GC-MS for the product obtained after 1h over HT60(8) catalyst.

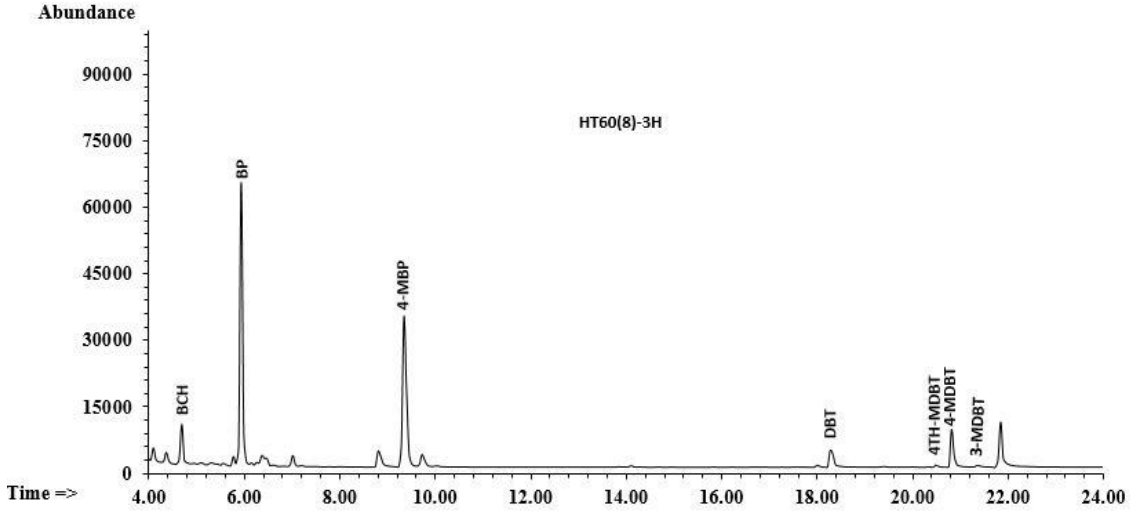

Chromatograph obtained from GC-MS for the product obtained after 3h over HT60(8) catalyst.

Appendix B2

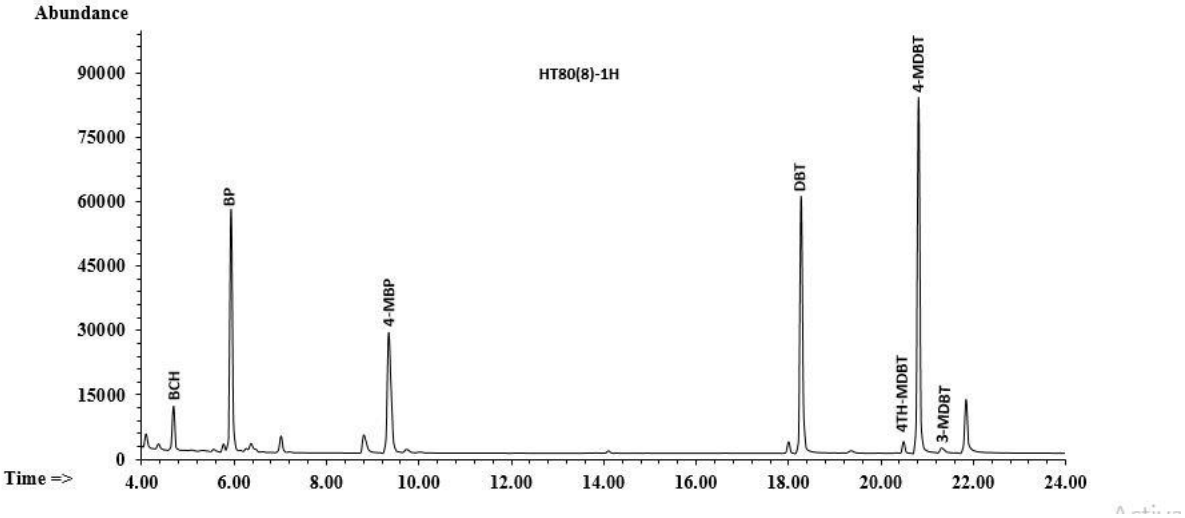

Chromatograph obtained from GC-MS for the product obtained after 1h over HT80(8) catalyst.

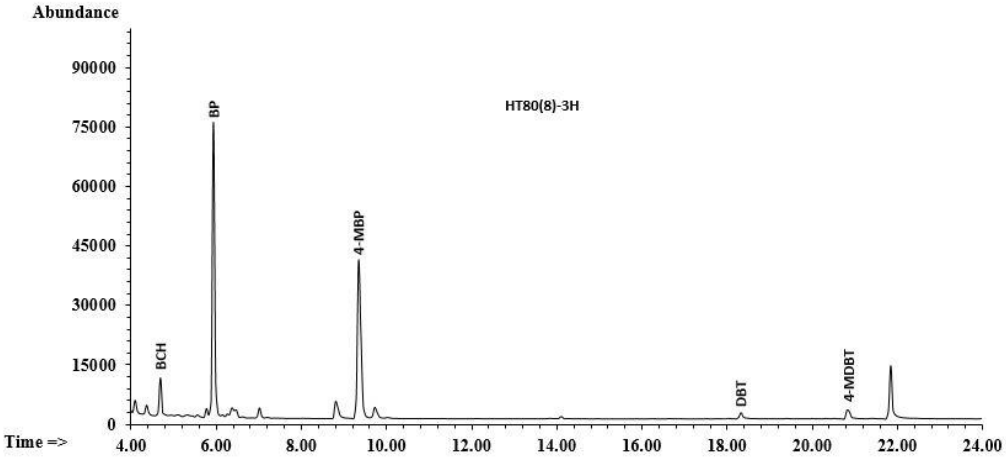

Chromatograph obtained from GC-MS for the product obtained after 3h over HT80(8) catalyst

VITAE

Name :Saheed Adewale Ganiyu

Nationality :Nigerian

Date of Birth :8/8/1981

Email :gsadewale@gmail.com

Address :Chemistry Dept. King Fahd University of petroleum and Minerals,

P.O. Box 31261, Dhahran, Saudi Arabia.

Academic Background :B.Sc. Industrial Chemistry, University of Ilorin, Ilorin Nigeria, 2005

MSc. Chemistry, King Fahd University of Petroleum & Minerals, Dhahran, Saudi Arabia, 2013.

Publications

- **Ganiyu, Saheed A**., Khalid Alhooshani, and Syed Ahmed Ali. "Single-pot synthesis of Ti-SBA-15-NiMo hydrodesulfurization catalysts: Role of calcination temperature on dispersion and activity." Applied Catalysis B: Environmental 203 (2017): 428-441. **Impact Factor: 8.328**

- **Ganiyu, Saheed A**., Syed Ahmed Ali and Khalid Alhooshani. "Simultaneous HDS of DBT and 4,6-DMDBT over single-pot Ti-SBA-15-NiMo catalysts. Influence of Si/Ti ratio on the structural properties, dispersion and catalytic activities. RSC Adv. 2017, 7, 21943. **Impact Factor: 3.289**

- **Ganiyu, Saheed A**., Syed Ahmed Ali and Khalid Alhooshani. Synthesis of Ti-SBA-15-NiMo hydrodesulfurization catalyst: The effect of hydrothermal synthesis temperature of NiMo and molybdenum loading on catalytic activity. Ind. Eng. Chem. Res. 2017. **Impact Factor: 2.567**

- **Ganiyu, Saheed A.,** Ajumobi, O., Lateef, S.A., Sulaiman, K.O., Bakare, I.A., Muhammad, Q. and Alhooshani, K. Boron-doped activated carbon as efficient and selective adsorbent for ultra-deep desulfurization of 4, 6-dimethyldibenzothiophene. Chemical Engineering Journal. 2017, 321: 651-661. **Impact Factor: 5.310**

- **Ganiyu, Saheed A.,** Khalid Alhooshani, Kazeem O. Sulaiman, Muhammad Qamaruddin, Idris A. Bakare, Abdulkadir Tanimu, and Tawfik A. Saleh. "Influence of aluminium impregnation on activated carbon for enhanced desulfurization of DBT at ambient

temperature: Role of surface acidity and textural properties." *Chemical Engineering Journal* 303 (2016): 489-500. **Impact Factor: 5.310**

- **Ganiyu, Saheed A.**, Oki Muraza, Abbas S. Hakeem, Khalid Alhooshani, Muataz A. Atieh, Carbon nanostructures grown on 3D silicon carbide foams: Role of intermediate silica layer and metal growth, **Chemical Engineering Journal**, (**2014**), 258, 110–118. **Impact Factor = 5.310**

- Odewunmi, Nurudeen A., Saviour A. Umoren, Zuhair M. Gasem, **Ganiyu Saheed A.**, and Qamaruddin Muhammad. "L-Citrulline: An active corrosion inhibitor component of watermelon rind extract for mild steel in HCl medium." *Journal of the Taiwan Institute of Chemical Engineers* 51 (2015): 177-185. **Impact Factor = 2.848**

- Bakare, Idris A., Oki Muraza, **Ganiyu Saheed A**., Abbas S. Hakeem, Zain H. Yamani, and Adnan MJ Al-Amer. "Synthesis of zeolite–magadiite composites: Effects of co-solvent and aluminum source." *Particuology* 27 (2016): 34-39. **Impact Factor = 2.280**

- Candy Li-Fen Lim, **Ganiyu, Saheed A**, Khalid R. Alhooshani, Stephan Jaenick*e* *"*Influence of the preparation conditions on textural and chemical properties of hexagonal MSU-3" *Advance porous materials (2016).*